Title
Transient Platoon Aerodynamics During Passing Maneuvers and In-line Oscillations

Authors
Tsuei, J. L.
Savas, O.
Hedrick, J. K.

Publication Date
2000-12-01

CALIFORNIA PATH PROGRAM
INSTITUTE OF TRANSPORTATION STUDIES
UNIVERSITY OF CALIFORNIA, BERKELEY

Transient Platoon Aerodynamics During Passing Maneuvers and In-line Oscillations

JL. Tsuei, Ö. Savas, J.K. Hedrick
University of California, Berkeley

California PATH Research Report
UCB-ITS-PRR-2000-26

This work was performed as part of the California PATH Program of the University of California, in cooperation with the State of California Business, Transportation, and Housing Agency, Department of Transportation; and the United States Department of Transportation, Federal Highway Administration.

Report for MOU 307

December 2000

ISSN 1055-1425

Transient Platoon Aerodynamics during Passing Maneuvers and In-Line Oscillations

L. Tsuei, Ö. Savaş, and J. K. Hedrick

Department of Mechanical Engineering
University of California at Berkeley
Berkeley, CA 94720-1740

California PATH Research Report
UCB-ITS-PRR-xx-xx
California PATH Program
Institute of Transportation Studies
University of California, Berkeley

June 2000

Transient Platoon Aerodynamics during Passing Maneuvers and In-Line Oscillations

by

L. Tsuei, Ö. Savaş, and J. K. Hedrick

Department of Mechanical Engineering

University of California at Berkeley

Berkeley, CA 94720-1740

Abstract

The transient aerodynamic effects in a four-vehicle platoon during passing maneuvers and in-line oscillations are investigated. A vehicle model is moved longitudinally parallel to a four-car platoon to simulate passing maneuvers. The drag and side forces experienced by each platoon member are measured using strain gauge balances. The resulting data are presented as dimensionless coefficients. It is shown that each car in the platoon experiences a repulsive side force when the passing vehicle is in the neighborhood of its rear half. The side force reverses its direction and becomes an attractive force when the passing vehicle moves to the neighborhood of its front half. The drag force experienced by each platoon member is increased when the passing vehicle is in its proximity. The effects of the lateral spacing and relative velocity between the platoon and the passing vehicle, as well as the shape of the passing vehicle, are also investigated. Similar trends are observed in simulations of both a vehicle passing a platoon and a platoon overtaking a vehicle.

During the in-line oscillation experiments, one of the four platoon members is forced to undergo longitudinal periodic motions. The drag force experienced by each platoon member is determined simultaneously during the oscillations. The effects of the location of the oscillating vehicle, the shape of the vehicles and the displacement and velocity amplitudes of the oscillation are examined. The results from the transient conditions are compared to those from the steady tests in the same setup. In the case of a four-car platoon, the drag variations experienced by the vehicles adjacent to the oscillating vehicle are discussed using

a cavity model. It is found that when the oscillating car moves forward and approaches its upstream neighbor, itself and its downstream neighbor experiences an increased drag, but its upstream neighbor experiences a decreased drag. Opposite results are obtained when the oscillating car moves backward and away from its front neighbor. In the case of a four-box platoon, a critical spacing of about 0.3 vehicle length is observed when the rectangular boxes are used as platoon members, where the drag force experienced by the upstream box shows a dramatic drop.

Contents

List of Tables

List of Figures

Chapter 1

Introduction

This study is motivated by an Automated Highway System (AHS) proposed by California Partners for Advanced Transit and Highways (PATH). The subject matter of this study is the transient aerodynamic effects of the platoon operations in this AHS. In this chapter, the background of California PATH and its proposed AHS is introduced. A brief review of previous research related to this study is also provided, including work regarding vehicle and platoon aerodynamics. The objective and an overview of the present work are described last.

1.1 California PATH

As the population and the number of vehicles continue to grow unabatedly, traditional methods of constructing new freeways or improving public transportation systems may not be sufficient to reduce the time wasted in traffic jams. Automated Highway System (AHS) is one of the many approaches suggested to relieve this problem. Although the concept of AHS had been around since 1930s, it did not draw attention more than a passing interest until mid 1980s, when the traffic congestion problems became serious and the technology required was mature enough to make its implementation possible [1].

California Partners for Advanced Transit and Highways (PATH), founded in 1986, has one of the most active AHS programs in the United States. A collaboration between the government, academia, and industry, PATH's purpose is to improve the operation of

the state's transportation systems, by integrating the widespread advanced technologies [2]. More specifically, this program is designed to increase California's highway capacity and safety, and to alleviate the rapidly growing problems of traffic congestion, air pollution, and energy consumption . Although PATH is a state-level program, it has received national and international attention since its demonstrations of automated vehicles in 1997 and 1998 [3].

Since California's population and its transportation demands grow so significantly, PATH focuses on long-term and high-impact solutions that can "dramatically" improve the operations of the state's surface transportation system [3]. In the PATH proposed AHS, the highway capacity (vehicles/lane/hour) can be increased by operating vehicles at closer spacing using automated control. A term *platoon* is used to describe one or more vehicles operated as a unit when they travel at the same speed with relatively small inter-vehicle spacings. In a typical case, the inter-vehicle spacing, or the intra-platoon distance is $2-4m$ for a platoon consisting of $5m$ long vehicles.

1.2 Scope of Previous Work

1.2.1 Vehicle Aerodynamics

Aerodynamics has a strong influence on the design and performance of a vehicle. The components of aerodynamic forces and moments experienced by a vehicle are shown in Figure 1.1. In characterizing the aerodynamic behavior of road vehicles, drag force is the most important factor from the point of fuel economy. From the control and stability point of view, however, the side force and yaw moment are the more crucial aerodynamic characteristics. Lift force and pitch moment are especially important to light weight, high speed vehicles (for example, racing cars) [4], and roll moment is critical in some specific circumstances that strong gusts occur [5]. Because the lift force, pitch moment, and roll moment are not significant during most of normal driving conditions, they are not discussed in this report.

A recent extensive study was given in *Aerodynamics of Road Vehicles* [6]. Older publications addressing issues related to road vehicle aerodynamics can be found in Scibor-

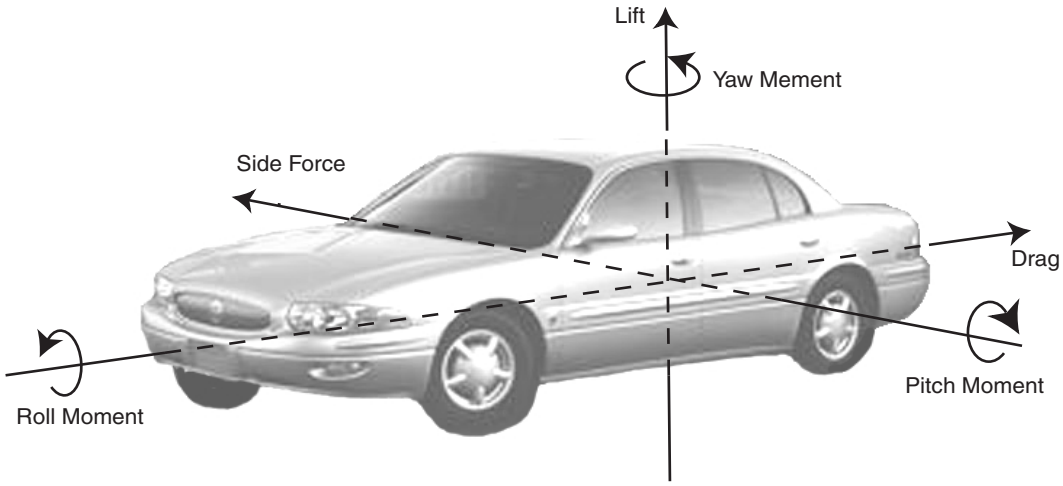

Figure 1.1: Forces and moments on a vehicle

Rylski [5], Hucho & Sovran [7], and Sovran [8]. These reviews discussed the fundamentals of fluid dynamics, experimental results, and various automobile designs which were related to vehicle aerodynamics. However, they focused mostly on the performance of a single car and covered relatively less material of the aerodynamic interactions involved with more than one vehicle. Unfortunately, vehicle stability can be affected significantly when aerodynamic interference happens between two or more road vehicles.

It is a common experience among drivers that one feels a severe aerodynamic effect when his car passes or is passed by a large truck. Several studies have discovered that a passed car experiences a significant change of drag, side force and yaw moment induced by an overtaking vehicle, which may cause the overtaken car lose control [9] [10] [11]. Abdel-Azim and Abdel-Gawad employed the flow visualization technique to clarify the flow behavior around vehicle models and the wake behind two interfering cars [12]. Although the images presented were not very clear, they did capture some interesting flow structures. They found a"flow jet" passing between two side-by-side cars, and wake interactions were observed during the overtaking process. These studies, however, emphasized the aerodynamic interaction between two cars and the work has not yet been extended to the field of platoon operations. Furthermore, most wind tunnel experiments are conducted with the assumption that the force affecting the cars has reached the equilibrium state. The

steady flow measurement describes aerodynamic forces as functions of the relative position of vehicles only, thus the approximation may not be sufficient to characterize their transient nature. This assumption, for example, implies that the forces on platoon members would be the same for a passed platoon and a passing platoon.

1.2.2 Complementary Research in PATH

From our perspective as a contribution to PATH, to study platoon aerodynamics for vehicle interactions is much more critical than to investigate isolated vehicle aerodynamics. The extremely small longitudinal spacings between vehicles in a platoon make the flow field more complicated than that around a single vehicle. In the past few years, two groups have contributed to this area. Wind tunnel and field studies at University of Southern California (USC) showed that the overall drag was significantly reduced in a uniform platoon than that measured around a single vehicle, and the reduction depended on the longitudinal separations [13] [14]. They also discovered significant changes of side force and yaw moment in a misaligned platoon due to the asymmetric flow field [15]. The works done at USC were under steady or stationary conditions.

Wind tunnel experiments conducted at University of California at Berkeley (UCB) explored the transient nature of aerodynamic effects in a uniform platoon under lane change maneuvers. Various time scales were used to simulate one vehicle merging into and moving out of a platoon with different accelerations and decelerations, and the effect of longitudinal spacings was also investigated. Chen [16][17] discovered that the change of side force was of the same order as the change of drag during a lane change maneuver, which meant that the distorted flow pattern may pose serious controllability problems in very short intervals of time and space. The quasi-steady results in Chen also confirmed the results of the steady state study obtained at USC [16]. Efforts had been made in UCB to incorporate the transient aerodynamic data into vehicle control simulation algorithms. The aerodynamic side force acting on a vehicle in a platoon that trailed a lane changing vehicle was modeled. It was found that the force exhibited a characteristic curve in lateral position of the exiting or merging vehicle. A mathematical model was built based on this observation [18]. By

implementing this model in the control simulation algorithm, it could provide the algorithm with an estimate of the aerodynamic forces for which it must compensate.

1.3 Objectives and Overview of Present Work

The subject matter of this study is the transient aerodynamic effects of the platoon operations. In order to provide PATH's platoon control algorithms with realistic estimates of the unsteady platoon aerodynamic characteristics, a series of wind tunnel experiments were conducted. These experiments include steady platoon aerodynamics, transient aerodynamics during passing maneuvers, and during in-line oscillations. Using scale models in the wind tunnel investigations allowed us to measure the aerodynamic forces in a well-controlled environment, and at low cost.

Chapter 2 describes briefly the facilities and the data acquisition system used in all wind tunnel investigations. In particular, steady force data in a two-, three-, and four-vehicle platoon are summarized in Section 2.5. Chapter 3 covers transient aerodynamic data during passing maneuvers. The results followed by a description of the experiments and an explanation of the way the data are analyzed. Chapter 4 presents transient aerodynamic data during in-line oscillations. A theoretical consideration of accelerating flows is discussed in Section 4.2, followed by the descriptions of the experiments. The results and discussions of observations are provided in Section 4.4 and 4.5. All aerodynamic forces are presented as dimensionless coefficients, and the transient data are compared with the steady results.

The last Chapter, Chapter 5, summarizes the results of the previous chapters.

Chapter 2

Steady Platoon Aerodynamics

The facilities and data acquisition system used in all wind tunnel experiments are introduced in this chapter. Steady force measurements were conducted in a two-, three-, and four-vehicle platoon. Passenger car models and similarly sized rectangular boxes were both tested as platoon members. The steady drag force experienced by the individual members of a multi-vehicle platoon was compared with that measured on a single vehicle and the results were summarized in Section 2.5.

2.1 Wind Tunnel

All platoon aerodynamic experiments presented in Chapters 2-4 were performed in a low turbulence, low speed wind tunnel, located in the Fluid Mechanics Laboratory at the University of California at Berkeley. As shown in Figure 2.1, the wind tunnel has a cross section of $81cm \times 81cm$, and the length of its test section is $3.65m$. However, only the upstream half of the test section was used in the experiments, due to the difficulty of instrumentation. A computer was used to control the wind tunnel velocity through a pressure feedback loop. All the experiments were conducted at a tunnel velocity of $20m/s$. Two ground planes were designed and constructed for the transient platoon aerodynamic tests during passing maneuvers and in-line oscillations. Those investigations will be described in Chapters 3 and 4. Up to four vehicle models can be lined up as a platoon on these ground planes, at a fixed longitudinal spacing of 2/5 of vehicle length.

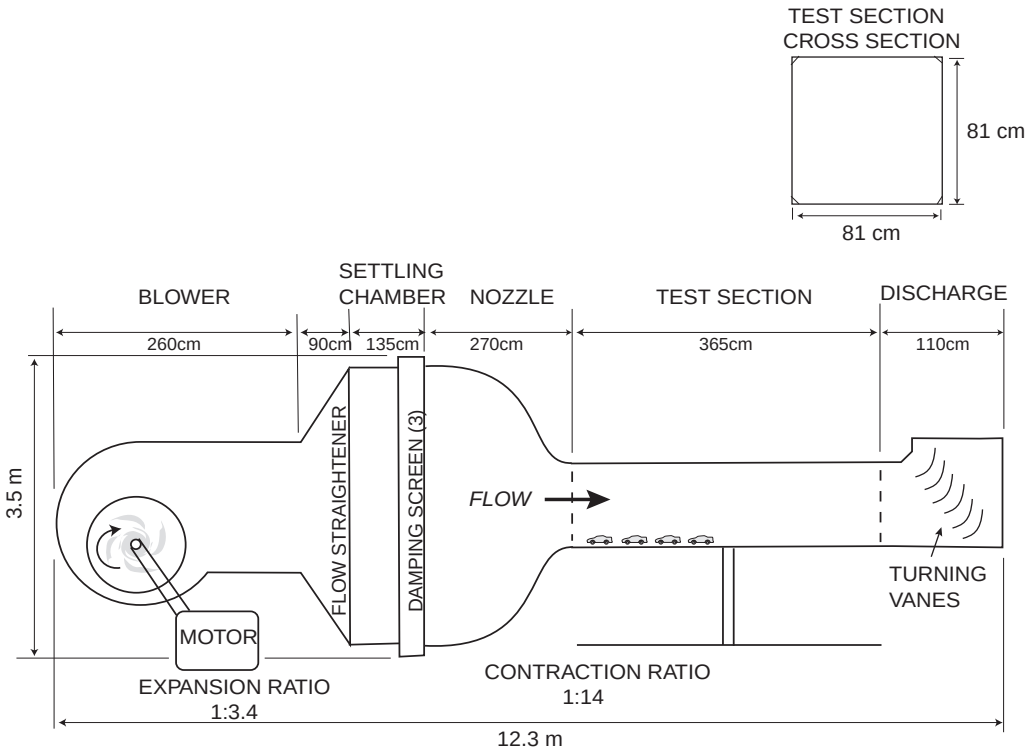

Figure 2.1: Wind tunnel diagram

Two major limitations exist for conducting road vehicle experiments in the wind tunnel. First, the blockage effects need to be corrected if the flow in the test section is disturbed too greatly by the models. The blockage ratio, φ, a factor that is usually used to determine the severity of the disturbance, is defined as

$$\varphi = \frac{A}{A_n} \tag{2.1}$$

where A is the frontal area of the vehicle model, and A_n is the cross section area of the wind tunnel nozzle. In this study, the blockage ratio measured about 1% is much lower than the well accepted limit of 5% for the aerodynamic testing of cars [7]. Therefore the blockage effects was neglected in this investigation. Second, in the wind tunnel experiments, the air flow over the ground plane generates a boundary layer that does not occur for the road vehicles, because there is no relative motion between the air and the ground in the

real case. A turbulent boundary layer tends to grow linearly along a flat plate; therefore models further downstream in the wind tunnel test section are affected more. Hucho [6] discussed the advantages and drawbacks of various methods which had been used to reduce the influence of the boundary layer. Amongst these, using a suction mechanism to reduce boundary layer thickness is relatively simple, especially when a long ground plane is required to test a platoon of vehicles. Chen et al. [16] employed a suction slot at the entrance of the test section of the wind tunnel currently used. Zabat et al. [19] removed the boundary layer through a porous ground plane in their investigation of aerodynamic performance of platoons. However, both studies have not shown significant changes in the results after suction applied. Therefore, the boundary layer was left untouched in this study, and its displacement thickness was measured about $1.9mm$ at the test section entrance and $4.4mm$ at $108cm$ downstream [16].

2.2 Flow Models and Force Balance

In the platoon aerodynamic testings, several identical 1997 Buick LeSabre vehicle models were used as platoon members in the experiments. Each car model was constructed in 1/20-scale with its mold created by stereolithography from surface data of the full-scale vehicle [20].

In addition to the vehicle models, similarly sized rectangular boxes were also used in the experiments to study the influence of the model shape. Figure 2.2 shows a photograph of the rectangular box and scale car model. Compared with the streamlined front and rear ends of the vehicle model, both ends of the rectangular box are flat with sharp corners,

Dimensions(cm)	**1997 Buick LeSabre**	**Vehicle Model**	**Box Model**
Length(L)	510	25.4	25.4
Width(W)	190	9.4	10.2
Height(H)	140	7.1	8.9
Ground clearance(h)	26	1.3	1.3

Table 2.1: Dimensions of 1997 Buick LeSabre and models used in the experiments

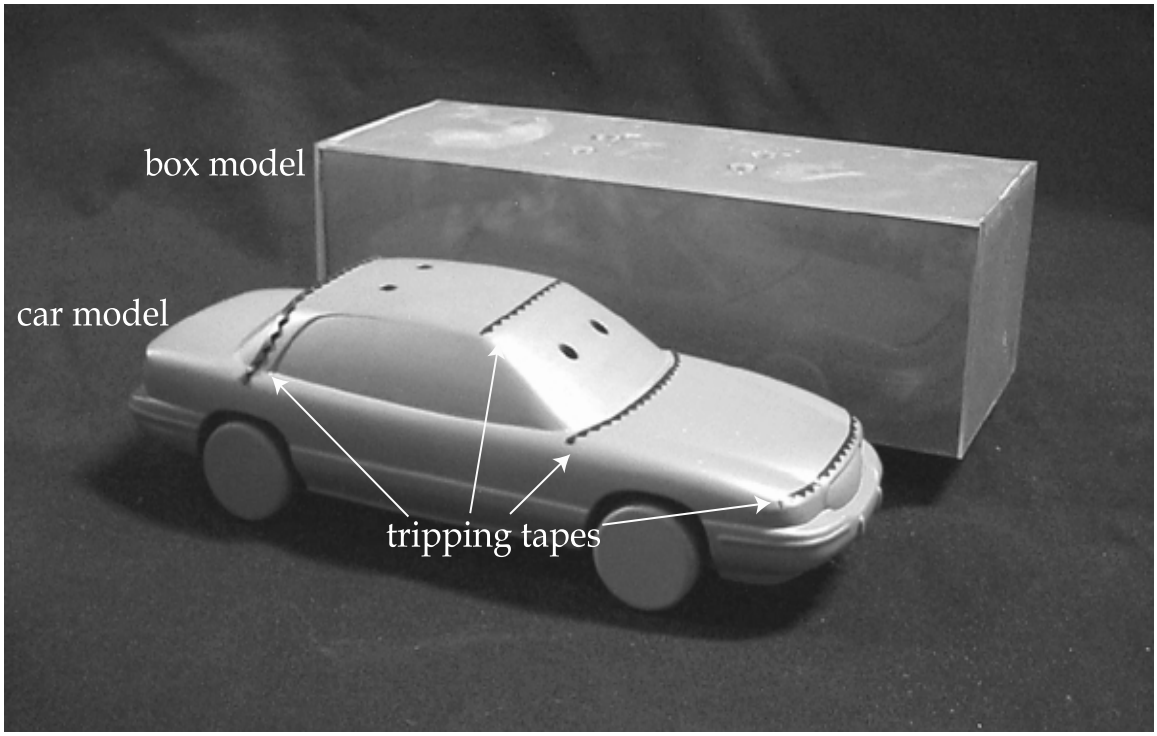

Figure 2.2: Rectangular box and scale car model

which provides a reasonable simulation of a mini-van or a bus. The dimensions of the full scale 1997 Buick LeSabre, the scale vehicle model, and the rectangular box model are shown in Table 2.1.

Figure 2.3 shows a photograph and a diagram of the strain gauge force balance used in the experiments. It has dimensions of $7.0cm \times 7.0cm \times 1.27cm (2.75in \times 2.75in \times 0.5in)$, allowing it to fit completely inside a cavity at the bottom of the scale vehicle or rectangular box model. The force balance is capable of measuring the drag, side force, and yaw moment simultaneously. On each force balance, a total of sixteen strain gauges are mounted and wired into three independent Wheatstone bridges. Four gauges measure strain caused by drag on the arms of each force balance, four gauges obtain the strain caused by side force, and another eight gauges collect the information caused by yaw moment.

These gauges were calibrated before and after the experiments to check for drift. By applying known forces to each balance, a linear calibration curve was obtained, for each of

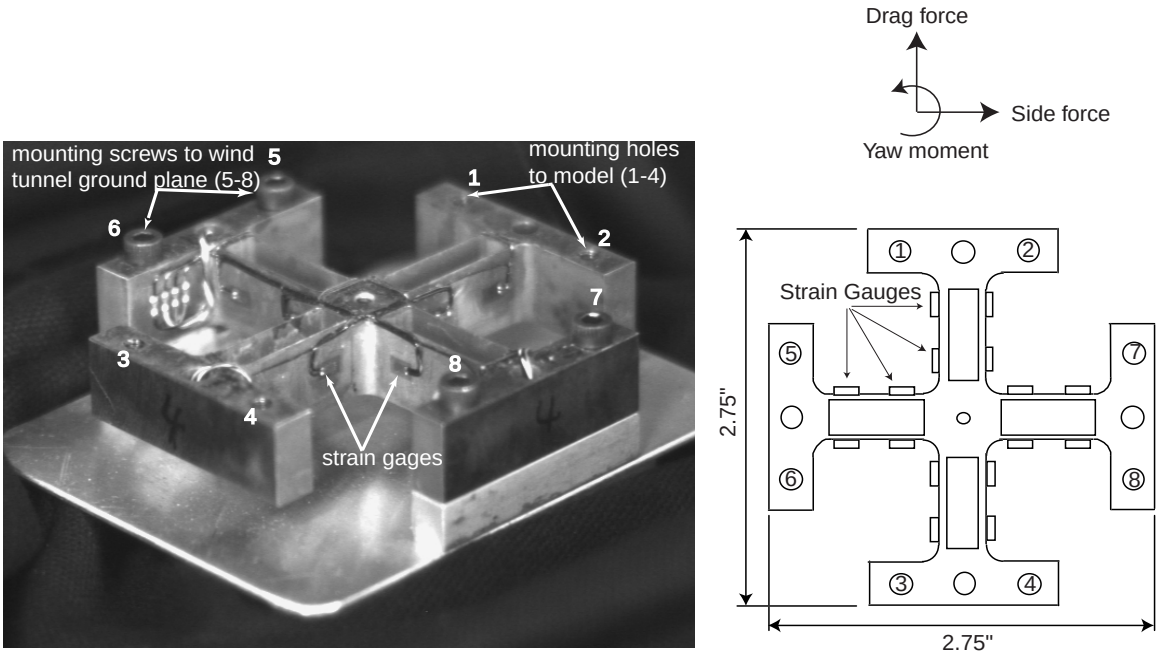

Figure 2.3: Force balance (photo courtesy of Chen [20])

the drag, side force and yaw moment. Therefore, the aerodynamic loads experienced by the vehicle models were determined from the outputs of the balances and their calibration curves.

Figure 2.4 shows sample calibration curves for one of the force balances. Frames (a)-(c) in this figure represent the measured side force, drag force, and yaw moment, respectively, when a lateral force is applied. Similarly, the second and third column show the strain gauge outputs after individually applying a known drag force and yaw moment to the force balance. As can be seen from this figure, the diagonal frames present the results of the forces and moment in interest. The high degree of linearity of these three curves provides the reliability of the aerodynamic information obtained in the experiments. The low dependence on particular force or moment shown on the remaining frames, implies that only very little electrical and mechanical cross-talk between the force balance exists in the system. The details about the constructions of the scale models and force balances can be found in Chen [20].

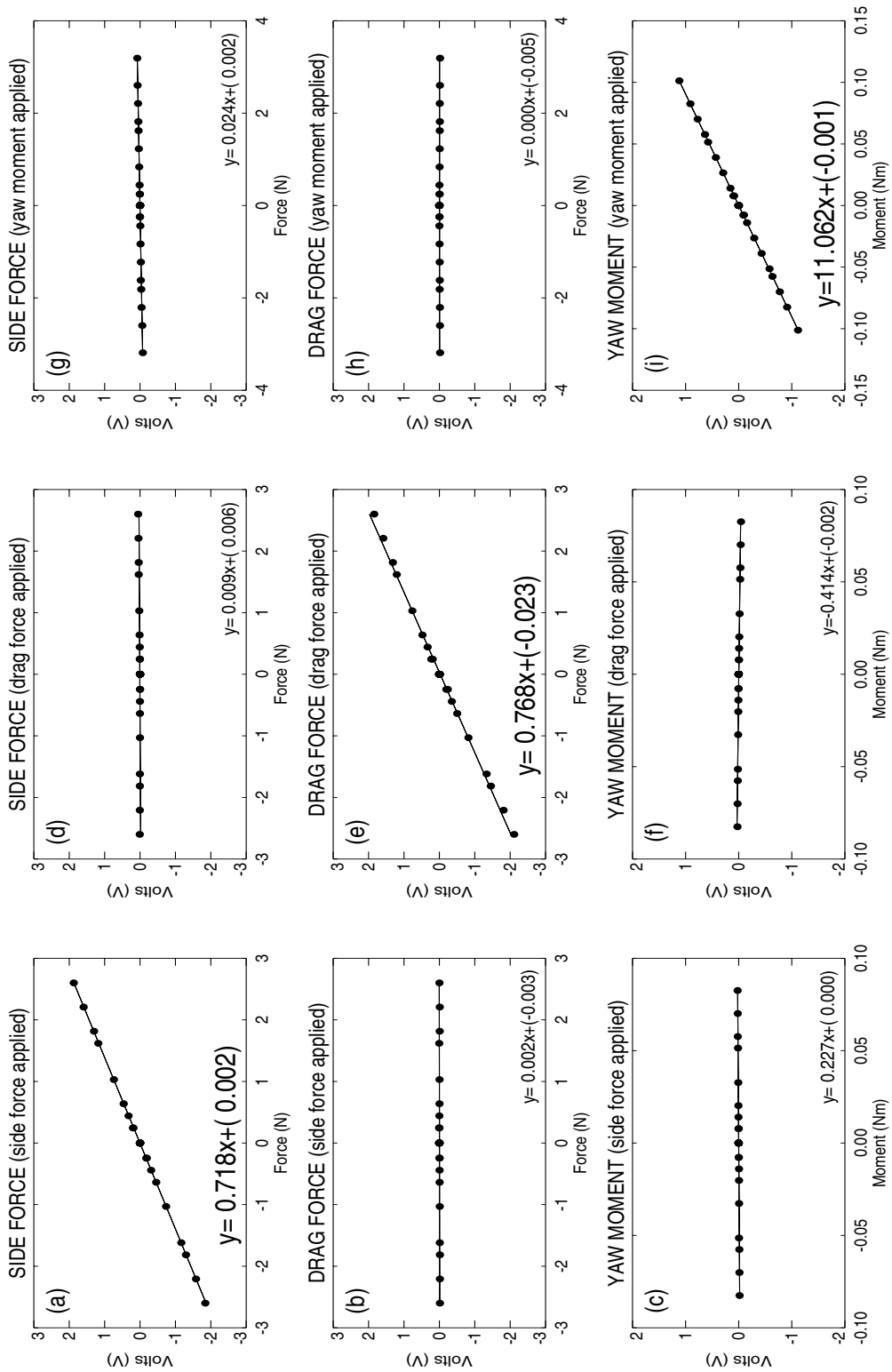

Figure 2.4: Sample force balance calibration curves

2.3 Incomplete Reynolds Number Similarity

To simulate road vehicles in wind tunnel experiments, the geometric similarity between the scale model and the full size vehicle must first be satisfied. In addition, true dynamic similarity also requires matched Reynolds numbers Re,

$$Re = \frac{UL}{\nu} \tag{2.2}$$

where U is the flow velocity, L is the vehicle's length, and ν is the kinematic viscosity of air. The flow conditions and Reynolds numbers in full scale and those used in the experiments are listed in Table 2.2. The Reynolds number in the experiments based on the model length, $Re_{exp} \sim 3.3 \times 10^5$, is much lower than the full scale flow, where $Re_{real} \sim 9.1 \times 10^6$ (see Table 2.1 for dimension L).

	$U(m/s)$	$L(m)$	$\nu(m^2/s)$	Re
Real Flow	26.7	5.10	1.5×10^{-5}	9.1×10^6
Experimental Flow	20.0	0.25	1.5×10^{-5}	3.3×10^5

Table 2.2: Incomplete Reynolds number similarity

Despite the mismatch, the experimental flow field can still provide sufficient information about the real flow because Reynolds numbers in both cases are high enough that the inertia forces dominate the viscous forces, except in boundary layers. Serrated tape was applied to each vehicle model, as shown in Figure 2.2, to trip the boundary layers on the model surface. The tape ensured a turbulent boundary layer to keep the flow attached for a greater length over the model surface. Therefore, the aerodynamic forces experienced by the models were mainly a result of pressure differences (known as "form drag"), as in the full scale case.

To compare the force data for different flows, the measured transient aerodynamic forces are non-dimensionalized by defining force coefficients. By scaling the drag force with the dynamic head, the drag coefficient is defined as

$$C_D = \frac{D}{\frac{1}{2}\rho U^2 A} \tag{2.3}$$

where D is the measured drag force and A is again the frontal area of the vehicle exposed to the oncoming flow. In this case, by assuming a rectangular frontal area,

$$A = W(H - h) \tag{2.4}$$

where W is the width, H is the height, and h is the ground clearance of the vehicle model as defined in Table 2.1. Similarly, the side force coefficient, C_S, is defined as

$$C_S = \frac{S}{\frac{1}{2}\rho U^2 A} \tag{2.5}$$

where S is the measured side force. The frontal area is used to normalize the side force coefficient so that the magnitudes of drag and side force coefficients can be compared. A yaw moment coefficient C_M is defined as

$$C_M = \frac{M}{\frac{1}{2}\rho U^2 V} \tag{2.6}$$

where M is the measured yaw moment, and the volume V, defined as

$$V = AL \tag{2.7}$$

and L, again, is the length of the model. These nondimensional coefficients will be utilized hereafter to characterize the aerodynamic forces and moment measured in different flows.

2.4 Data Acquisition System and Data Analysis

A high-resolution data acquisition system was used to collect the aerodynamic data. It employed a 16-bit analog-to-digital (A/D) board (Analogic DVX-2502) in tandem with a 16-channel, 200 kHz simultaneous-sample-and-hold multiplexer (Analogic DVX-2601). This system was designed to collect real time transient aerodynamic data in passing maneuvers and under in-line oscillating conditions (Chapter 3 and 4). In the case of steady measurements, 8000 samples were taken at a 1.9 kHz rate in each run, and their mean value was used to represent the static output.

All strain gauge data were digitally filtered in lieu of viscous damping at the hardware level. The filtering was done in the frequency domain using Fast Fourier Transform (FFT) algorithms [21]. Following numerous tests, a Gaussian filter kernel of width of 8.0 Hz was chosen to filter all the aerodynamic signals [20].

The errors caused by electronic drift and the mechanical mechanism of the force balances may change the zero force reference point whenever a balance is repositioned. To overcome these uncertainties, a "zero-reading" data file was recorded whenever a force balance was installed to a new position. The zero-reading file was taken while all the devices were powered on, but with no wind-tunnel flow or model motion. All aerodynamic data were corrected for these zero-reading values. Additional details about the data acquisition system and signal filtering can be found in Chen [20] and Snyder [18].

2.5 Single Vehicle and Multi-Vehicle Platoon

To demonstrate the influence of platooning, the drag, side force and yaw moment coefficients of a single vehicle and each member in a two-, a three-, and a four-vehicle platoon were measured and compared with the single vehicle value. The side force and yaw moment coefficient all appeared small because of their symmetric configurations. However, the drag coefficients changed dramatically after platooning the vehicle models. In the case of a single vehicle, the drag coefficient measured 0.297 for the car model, and 0.995 for the box model. The sharp corners of the box model, and thus the extensive flow separation, caused more than three times higher drag coefficient than the measurement done in the streamlined passenger car model.

For all the platoon configurations, the intra-platoon spacings were fixed as 2/5 of vehicle length or $10.2cm$. The effect of longitudinal spacings to the force and moment coefficients were not investigated here, but have been studied extensively by Chen et al. [16], Zabat et al. [13][22] and Hong et al. [14].

In Figure 2.5(a), the ratio of the drag coefficient for each car as a platoon member to that of a single car is plotted with the location of the car in the platoon. $C_{D_{platoon}}$ was used

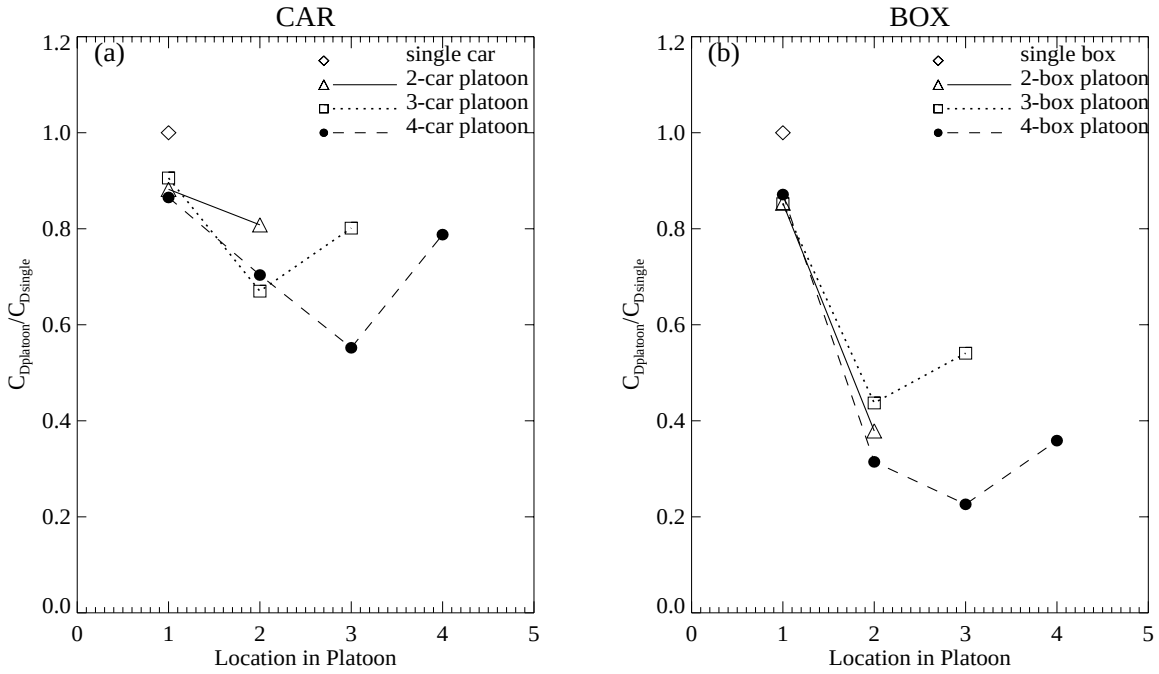

Figure 2.5: Drag reduction for a multi-vehicle platoon

to represent the drag coefficient experienced by each member in the platoon. In all cases and for each platoon member, $C_{D_{platoon}}/C_{D_{single}}$ was less than 1, which meant all platoon members benefit from platooning by experiencing a drag reduction, as compared with a single car. In the multi-car platoon, the leading car had the highest drag and shielded the rest of the members which had lower drags. A 10% decrease of drag for the first car and 20% decrease for the last car have been found in all three cases (two-, three-, and four-car platoons), compared with the drag experienced by a single car. The drag reduction for the interior platoon members were more pronounced. Reductions of about 30% in drag were achieved for the middle vehicle in a three-car platoon, and for the second vehicle in a four-car platoon. The third vehicle in a four-car platoon experienced the lowest drag in this study; its coefficient had fallen to about 55% of the single car value.

A similar behavior was observed when the rectangular boxes were used as platoon members. The results are shown in Figure 2.5(b) as the drag coefficient of each platoon member divided by that of a single box. An 15% drag reduction was discovered for the first

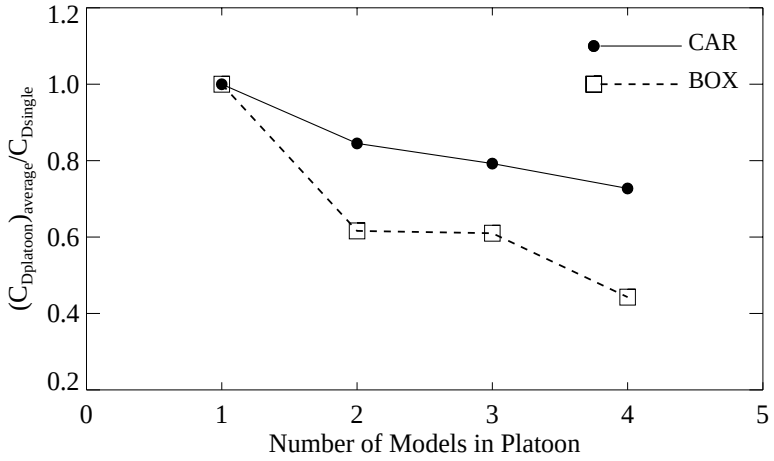

Figure 2.6: Average drag of a multi-vehicle platoon

box model in all three platoon cases. In a two-box platoon, a decrease of 60% in drag was observed for the rear box. In a three-box platoon, the last box experienced a 45% reduction, and the middle box had an even lower value, compared with the drag coefficient of a single box. In the case of a four-box platoon, a 70% and 65% drag reduction was found for the second and the last platoon member, respectively. The third box in a four-box platoon, again, experienced the lowest drag in all cases. The value has been found to be only 23% of the single box drag coefficient.

The overall drag reduction achieved in a platoon can best be presented in terms of an average platoon drag coefficient, $(C_{D_{platoon}})_{average}$ [13]. Using the drag coefficient for a single vehicle to normalize the average platoon drag coefficient, we have,

$$\frac{(C_{D_{platoon}})_{average}}{C_{D_{single}}} = \frac{1}{n}\sum_{i=1}^{n}(\frac{C_{D_i}}{C_{D_{single}}}) \tag{2.8}$$

where i represents the ith platoon member.

In Figure 2.6, $(C_{D_{platoon}})_{average}/C_{D_{single}}$ is plotted as a function of the size of the platoon. It shows the more the members in the platoon, the more drag reduction found in terms of the average. Since a single box model originally had a higher drag coefficient than an single car, a larger reduction was achieved from platooning for the box platoon.

One thing that should be noted is that the results were analyzed under the assumption

Coefficients	**Drag** C_{D_C}	**Side Force** C_{S_C}	**Yaw Moment** C_{M_C}
CAR 1	0.257	0.025	-0.001
CAR 2	0.209	0.008	0.001
CAR 3	0.164	0.002	-0.004
CAR 4	0.234	0.003	0.000

Table 2.3: Force and moment coefficients measured in a four-car platoon

of the uniformity of the wind tunnel flow. The measurements done for each platoon member did not necessarily occur at the same location of the isolated model in the wind tunnel. However, the uncertainty caused by the non-uniform flow has been reduced because the values shown in Figure 2.5 and 2.6 were averaged from numerous runs at various locations.

The coefficients measured in a four-car platoon, are provided in Table 2.3. As expected, the side force and yaw moment coefficients nearly vanish. The side force coefficient for the leading car had a slightly high value, which was perhaps due to a slight misalignment of the model with the airflow. These values, nevertheless, were sufficiently small to assume that all members of the platoon experienced only the drag force.

In Chapters 3 and 4, these results will be compared with the data collected in the transient investigations. The values shown in Table 2.3 will henceforth be referred to as coefficients of a "clean" four-car platoon, which means no mobile model is presented in or near the platoon. Note that the force and moment coefficients shown in Table 2.3 are slightly different from previous investigations [23][24]. The data shown here should be more reliable because they were averaged from more testing runs, conducted after Tsuei et al. [23] and Tsuei & Savaş [24] were published.

Coefficients	**Drag** C_{D_C}	**Side Force** C_{S_C}	**Yaw Moment** C_{M_C}
BOX 1	0.867	0.016	0.001
BOX 2	0.313	0.006	0.001
BOX 3	0.225	0.001	-0.001
BOX 4	0.357	0.019	0.002

Table 2.4: Force and moment coefficients measured in a four-box platoon

The coefficients measured in a four-box platoon are shown in Table 2.4. These data will also be used in Chapter 4 as "clean" four-box platoon results.

Chapter 3

Transient Aerodynamics in Passing Maneuvers

To understand transient aerodynamic effects on a four-car platoon during passing maneuvers, experiments were performed in the wind tunnel. Having reported in the details of the models, force balances, and the data acquisition system in Chapter 2, this chapter describes the integration of them to the current experiments. Representative results are provided in Section 3.4. The factors tested in the experiments were the lateral spacing and relative velocity between the passing vehicle and the platoon, and the shape of the passing vehicle. The effects of a vehicle passing a platoon and a vehicle overtaken by a platoon were also examined.

3.1 Description of Experiments

The apparatus used in experiments regarding to the passing maneuvers is described in this section. Four identical car models were used as platoon members, and the intra-platoon spacing was $10.2cm$, equivalent to $2m$ or 2/5 car length in full scale. As presented in Figure 3.1, during the experiments, the wind tunnel flow entered from the top of the photo. A four-car platoon is shown with a fixed inter-vehicle spacing and a single car shown to its left is movable along a rail parallel to the platoon. The separation distance between the platoon and the passing model can be adjusted by laterally repositioning the platoon members and the force balances.

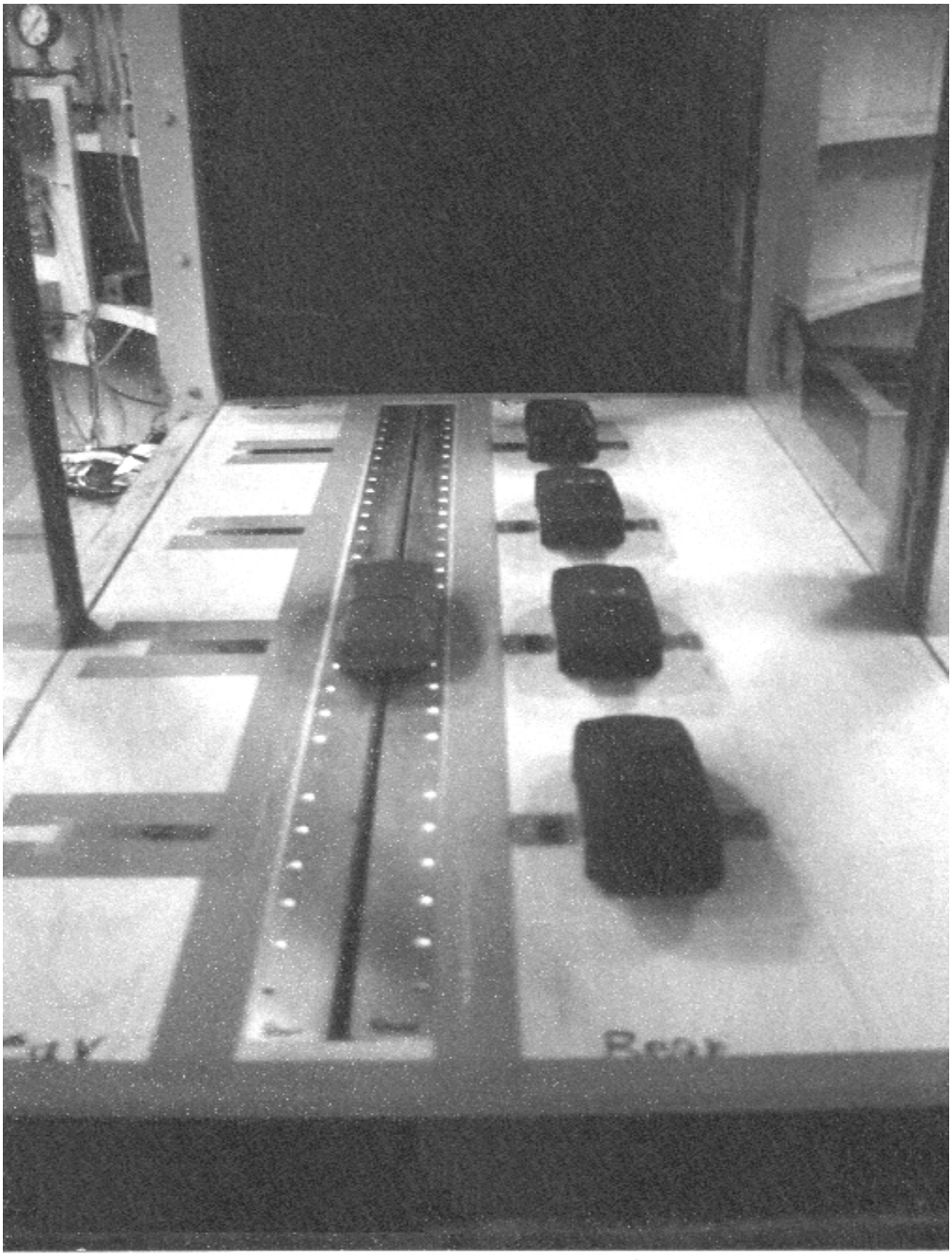

Figure 3.1: Passing maneuver in wind tunnel

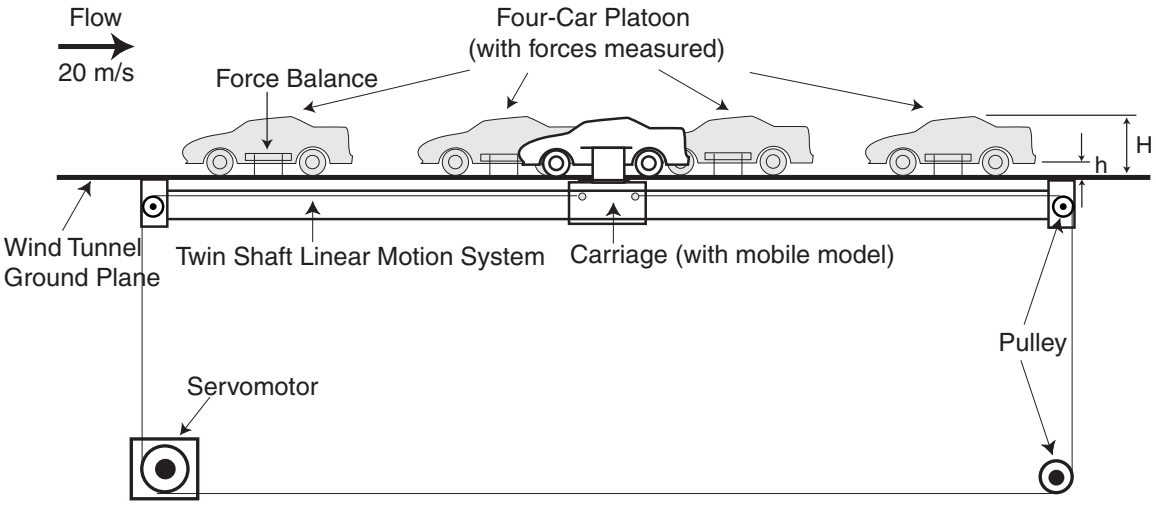

Figure 3.2: Driving mechanism for the mobile model

The experimental apparatus is sketched in Figure 3.2. Each car in the platoon was connected to a force balance, and the drag, side force, and yaw moment acting on the car were measured. A servomotor (Compumotor APEX 620) and a pulley system were used to pull the mobile model as the passing vehicle longitudinally along the twin shaft linear motion rail (Thomson 2CA Quickslide). The forces and the moment experienced by the mobile model were not measured in this study.

Figure 3.3 shows the top view of the layout of the platoon on the wind tunnel test section floor. The platoon (car 1-4) was fixed during each experimental run. When the mobile model was pulled forward (positive v in Figure 3.3), a vehicle passing the platoon was represented. The traveling distance of the mobile model was $1.2m$, starting from $6.7cm$ behind the front end of the fourth car in the platoon, and ending at $6.7cm$ ahead of the front end of the first platoon member. When it was moved backward (negative u in Figure 3.3), a vehicle overtaken by a platoon was simulated. The relative velocities between the mobile model and the platoon were ranging from 0 to $3.75m/s$. The zero relative velocity corresponded to the case while a single vehicle moved at the same speed as the platoon and would be provided as steady-state measurements. These steady measurements were conducted by manually placing the mobile model in seven different locations along the rail.

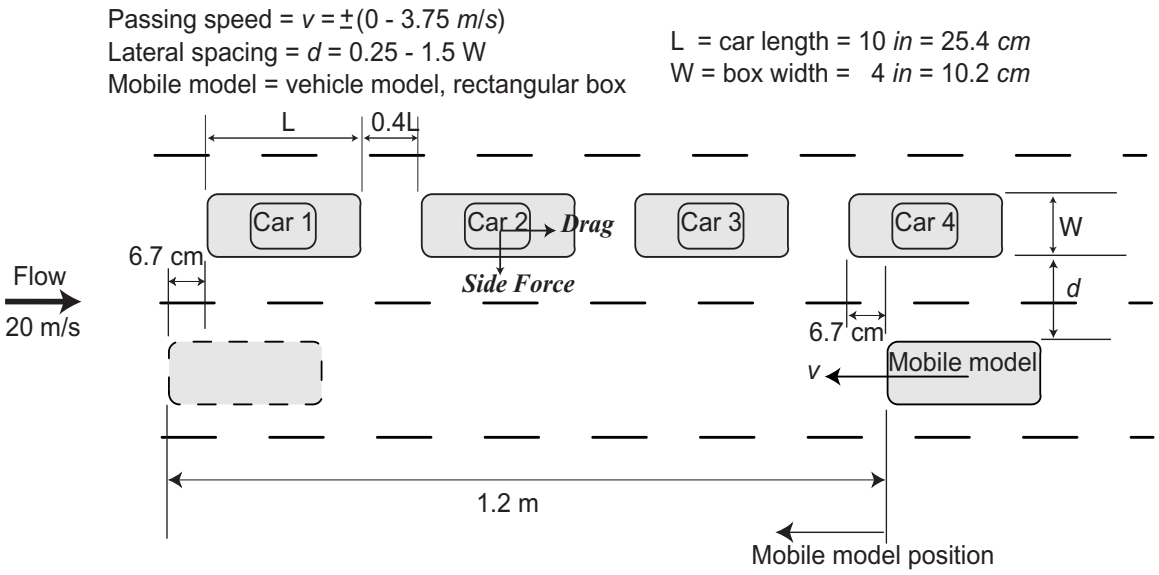

Figure 3.3: Configuration of the platoon and the mobile model

The mean values from 8000 samples taken at a 1.9 kHz rate were used as the steady results.

To determine the influence of the passing vehicle's shape on the platoon, a passenger car model (identical to the platoon members) and a similarly sized rectangular box which was described in Chapter 2 were examined separately. Four lateral spacings ($1in$, $2in$, $4in$, and $6in$) between the platoon and the mobile model were tested during the investigations. The separation distances corresponded to $\frac{1}{4}$, $\frac{1}{2}$, 1, and $\frac{3}{2}$ of the width of the box model. The experimental conditions were summarized in Table 3.1.

Mobile model	d/W_{box}	Mobile model velocity $v(m/s)$	Comments
Vehicle model / Rectangular box	1/4	3.75	forward motion
	1/2	2.50	
	1	1.25	
	3/2	0	steady-state
		-1.25	backward motion
		-2.50	
		-3.75	

Table 3.1: Test conditions of passing maneuvers

3.2 Data Analysis and Transient Time Scaling

3.2.1 Data Analysis

The data acquisition system introduced in Chapter 2 was used in the transient aerodynamic study in a similar manner, except that the signals from strain gauges and the tunnel velocity were sampled at a higher rate of 5.2 kHz to capture the transient events. The mobile model's position was sampled at 72.8 kHz.

A "zero-reading" data file was recorded whenever a force balance was installed at a new position or a new mobile model was used, as described Chapter 2. Additionally, the aerodynamic force coefficients in a "clean" four-car platoon were measured immediately after the zero-reading file was recorded. Ideally, the clean platoon data of all runs should read the same values after subtracting the corresponding zero-reading offsets, as long as there was no interference from the mobile model. Therefore, an average force coefficient of each channel in the data acquisition system was calculated from values obtained in numerous runs, and the averaged results were presented in Table 2.3. After obtaining the differences between the averaged values and the clean platoon data under each specific test condition, all of the coefficients taken under this condition were shifted based on these differences.

By doing so, the force coefficients measured in different conditions could be compared on the same basis. For example, the original force coefficient of component i (i can be drag force, side force or yaw moment) obtained on the jth ($j = 1-4$) platoon member under test condition k ($k = 1 - k_f$), changes whenever a new mobile model or a new lateral spacing is applied and is written as F_{ijk}. Its zero-reading and clean platoon values under this specific condition are Z_{ijk} and R_{ijk}, respectively. An averaged clean platoon value, M_{ij}, of ith force coefficient on jth car can be calculated as

$$M_{ij} = \frac{\sum_{k=1}^{k_f} R_{ijk}}{k_f} \tag{3.1}$$

Then the force coefficient after adjustment is

$$F^*_{ijk} = F_{ijk} - Z_{ijk} - (R_{ijk} - M_{ij}) \tag{3.2}$$

Two runs of data were conducted for each of the experimental conditions. In most measurements, the two runs under identical testing conditions agreed well with each other. However in some cases, they shifted upward or downward due to reasons discussed in Section 2.4.

The averaged error of the amplitude of force change for using the rectangular box as a passing model was about 5%. Higher averaged errors of about 10% were found when using the car model as a passing model, for the denominator (the amplitude of force change) had a much smaller value.

3.2.2 Transient Time Scaling

Because the focus of this study is on the transient nature of aerodynamic changes, the time scale of the transient events must be considered. The transient time scale t of the flow is taken as the time it takes for the flow to pass a characteristic length of the object,

$$t = \frac{L}{v} \tag{3.3}$$

where L is the vehicle length in this case and v is the relative velocity between the passing vehicle and the platoon. To simulate transient effects, the duration of the events must be scaled with this time scale. Using L/U to nondimensionalize equation (3.3) (where U is the platoon or the wind tunnel flow velocity), the relationship of the time scales of real and experimental flows becomes,

$$t^* = \left(\frac{L/v}{L/U}\right)_{real} = \left(\frac{L/v}{L/U}\right)_{exp} \tag{3.4}$$

or, equivalently,

$$\frac{v_{real}}{U_{real}} = \frac{v_{exp}}{U_{exp}} \tag{3.5}$$

The wind tunnel velocity was chosen as $U_{exp} = 20m/s$ to achieve the highest Reynolds number feasible. The time scaling in equation (3.5) was used to simulate a highway platoon velocity of $U_{real} = 60mph$ or $26.7m/s$. The relative velocities between the mobile model and the platoon in the experiments ranged from $v_{exp} = 0 - 3.75m/s$, where the zero relative velocity corresponded to the case when a single vehicle moved at the same speed as the platoon. When the passing model moves forward at $3.75m/s$ in the wind tunnel, according

to equation (3.5), it is equivalent to a single car at $71.25mph(31.7m/s)$ overtaking a platoon traveling at $60mph(26.7m/s)$.

3.3 Position, Velocity, and Acceleration

This study was designed to investigate aerodynamic effects on a platoon during "constant-speed" passing maneuvers. However, due to the acceleration and deceleration at the beginning and end of the motion, the mobile velocity v was not constant during the whole process. The real and desired motion profiles are compared in this section.

The position history of the mobile model was determined using the resolver integrated into the servomotor. The resolver, which provides positional feedback to the motor controller, has a resolution of 1024 counts/revolution. The signal generated by the resolver is a pulse train where the resolver produces a pulse with a time mark on it whenever the motor rotor crosses a certain angle. Therefore more pulses are produced in a certain period if the motor rotates faster. By knowing the perimeter of the driving wheel attached to the motor rotor, and the number of revolutions being completed, the mobile model's position could be determined.

Using the indexed time collected from the resolver pulses, the velocity and acceleration were obtained by taking first and second derivatives of the position data in the Fourier domain, respectively. However, the signals appeared noisy after the differentiations. To retain only the physical information, a Gaussian digital filter was introduced to filter the signals as it was done for the aerodynamic information (Section 2.4).

In Figure 3.4, the position, filtered velocity and acceleration profiles are presented for cases of the mobile model in both forward and backward motions. The first row (a,d) shows the position of the front end of the mobile model as a function of time for the assigned velocity. The second (b,e) and third (c,f) rows are the real velocity and acceleration the mobile model has achieved and they are plotted with respect to position. The four thick line segments shown at the bottom of the frame in the centered row (b,e) mark the positions of the four platoon members, car 1 to car 4 in order from right to left. Only part of car 4

is shown on the plots because the mobile model was starting from $6.7cm$ behind the front end of this platoon member.

As shown in Figure 3.4, the second and third platoon members were overtaking (overtaken by) a constant-speed vehicle while the first and the fourth cars might be influenced by the changing-speed of the vehicle. The acceleration and deceleration, which are expected to affect the results somewhat, need further study to quantify their effects. However, the magnitude of acceleration/deceleration was not a controlled parameter in this study.

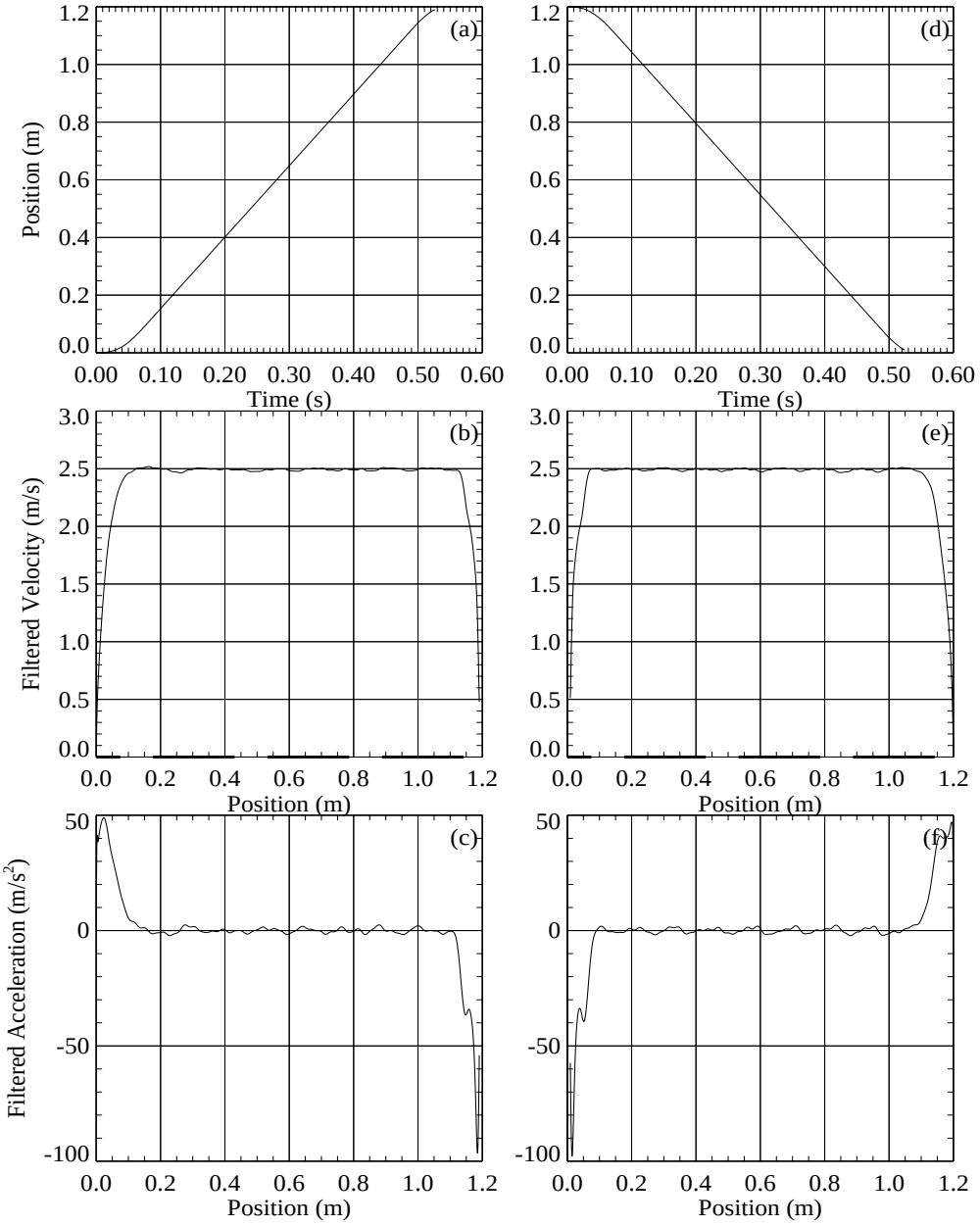

Figure 3.4: Position, velocity, and acceleration profiles in passing maneuvers The mobile model in forward [frames (a)-(c)], and backward motion [frames (d)-(f)] ($v = \pm 2.50 m/s$)

3.4 Results

The transient aerodynamic effects on a four-car platoon during passing maneuvers are discussed, and the four factors considered in the experiments are presented separately in four subsections. Since very small yaw moment data are recorded, only drag and side force data are provided. The reason the yaw moment measurements are so small is discussed in Section 3.5.

3.4.1 Effect of Lateral Spacing

In this section, aerodynamic forces experienced by every platoon member are compared for various lateral spacings between the mobile model and the platoon. Transient data in four lateral spacings ($d/W_{box} = \frac{1}{4}, \frac{1}{2}, 1$, and $\frac{3}{2}$) were recorded. Note that the curves appear on the figures in the current and following sections are all true measurements collected in real time when the passing model is traveling, so they are not drawn by curve-fitting. All the data were digitally filtered as described in Section 2.4.

Figure 3.5 and 3.6 show the force coefficients on each of the four cars in the platoon using the car model and box model as the passing vehicle, respectively. In both cases the relative velocity was $v = 2.5m/s$. These coefficients were presented with respect to the position of the front end of the passing model. The trends of force change were similar for all the four platoon members. In both figures, each platoon member experienced a significantly increased drag force when the passing vehicle moved to its proximity. The drag force decreased after reaching its maximum value and tended to overshoot slightly before returning to the non-perturbed clean platoon value. When the overtaking vehicle was in the neighborhood of the rear half of a platoon member, the side force on the platoon member was found to be directed away from the passing car (repulsive, negative in the figures). The side force reversed its direction and pointed toward the passing car (attractive) when it was in the proximity of the front half of the platoon member. These findings are in agreement with studies conducted for aerodynamic interactions between two cars during passing maneuvers [10][11].

To summarize the effect of varying lateral spacings, the difference between the maxi-

mum and minimum values of each curve were calculated. These values were shown as ΔC_D for drag coefficient measurements and ΔC_S for side force coefficient measurements on the upper left corner of each frame. The results showed that the closer the passing car to the platoon, the more severe aerodynamic forces the platoon members experienced . In the case of a box model passing a platoon at relative velocity $2.50 m/s$ (Figure 3.6), up to 120% and 80% increases in drag change, and 45% and 40% increases in side force change were noted for the conditions of $d = \frac{1}{4} W_{box}$ and $d = \frac{1}{2} W_{box}$, respectively, when they were compared with the data of $d = W_{box}$. Similarly, in comparison with the condition of $d = W_{box}$, reductions up to 50% in drag and 40% in side force change were found for the case of $d = \frac{3}{2} W_{box}$.

3.4.2 Effect of Relative Velocity

The effect of the varying relative velocities between the mobile model and the platoon is discussed in this section. Transient data were measured under three velocities ($v = 1.25, 2.50$, and $3.75 m/s$) of the mobile model. Steady data which represent the case of the mobile model moving at the same speed as the platoon were also presented. Figure 3.7 represents the case of a car model passing a platoon with a lateral spacing of $d = \frac{1}{4} W_{box}$. ΔC_D and ΔC_S in these figures are defined as in the previous section, except for steady measurements which are determined by using the difference of the maximum and minimum of seven measured points. Therefore, ΔC_D and ΔC_S for steady-state measurements may not represent the largest possible difference in force change like the transient measurements.

It was found that lower relative velocities generated higher force coefficients on each member of the platoon. In Figure 3.7, comparing with the condition of $v = 3.75 m/s$, up to a 70% increase in the drag coefficient and a 60% increase in side force coefficient were recorded for $v = 1.25 m/s$. Similar trends were observed while a box model was overtaking a platoon as shown in Figure 3.8. The changes in the steady force coefficients in Figure 3.8 were more pronounced; up to a 100% increase in the drag coefficient and a 140% in side force coefficient were recorded under the steady-state measurements, compared with the condition of $v = 3.75 m/s$. These findings may be against our intuition, but they were echoed by research conducted by Sano et al. [10]. They studied the change of lateral

displacement and yawing angle of a small car when it was passed by another vehicle for two different velocities and concluded that the changes became smaller for a higher relative speed. Sano et al. also suggested the time-lag for the disturbed car to return to the non-perturbed state would be longer for a higher relative velocity than a lower one. We found the similar phenomenon in some of our investigations (for example, Figure 3.7) but not all of them, so our results were not conclusive in terms of this argument. In both Figure 3.7 and Figure 3.8, the transient data agreed well with steady state measurements. Since the results suggested that forces on platoon members were greater at lower relative speeds in a passing maneuver, investigation under steady state conditions may work as a good estimation of an upper bound for the transient changes.

Note that the passing velocities mentioned in this chapter were those assigned to the mobile model without considering the acceleration and deceleration in the beginning or at the end of the motion, as discussed in Section 3.3.

3.4.3 Effect of Passing Model Shape

In this section, the effect of the overtaking or overtaken model's shape during passing maneuvers are investigated. A passenger car model and a similarly sized rectangular box were tested separately as the passing or passed vehicle.

Experimental results of both models driven forward and backward are shown in Figure 3.9 and Figure 3.10, respectively. In both figures, the relative velocity is $v = 1.25 m/s$ and lateral spacing is $d = W_{box}$. Instead of calculating the amplitude of force changes, the peak values of drag and side force coefficients for each platoon members were shown, and the locations of the front end of the mobile model in which the peak values occurred were determined.

As shown in Figure 3.9 and Figure 3.10, the box model generated a larger increase in drag and side force coefficients on the platoon members than the vehicle model did. The magnitude of drag force was increased by about 20% when the vehicle was replaced with the box as the mobile model, due to the box's sharp corners and larger frontal area. More significant influence of model shape was shown in the side force. Compared with

the negative and positive peaks in frames (e)-(h) in Figure 3.9 and Figure 3.10, it showed that the box mobile model created larger side force to the platoon member when it was approaching the platoon member than when it was leaving it. In the case of repulsive side force, more than three times magnitude of the value the mobile car model generated was observed, when using the rectangular box as the mobile model.

The locations of peaks varied between the mobile box and car model. The maximum values of drag coefficient occurred near the center of each platoon member with the curve reaching its maximum earlier when the box was used as the mobile model. When the passing model's front end moved into the proximity of the platoon member, the streamline-shaped vehicle had only part of its projection area contributing to the drag increase of the platoon member, unlike the rectangular box which generated higher impact due to its full frontal plane. For the same reason, the side force coefficients reached their first (negative) peaks earlier if the mobile model was a box. The positive bumps in side force coefficient were caused by the low pressure zone from the wake behind the passing model. The second (positive) peaks occurred at about 80% of car length ahead of the platoon member regardless of the model shape.

3.4.4 Effect of Passing Direction

Figure 3.12 shows the comparison of the force changes on the platoon members when a car passes a platoon and when a platoon passes a car. In this figure, the relative velocity is $v = 3.75m/s$ and lateral spacing is $d = \frac{1}{2}W_{box}$. The trend of the force changes was similar in both cases, but a greater change was observed when the mobile model was in forward motion.

The reason why smaller force coefficients were recorded when the mobile model was in backward motion is not clear. One possible explanation for the change of drag coefficient is that, when the mobile model moves backward, as the gap between the platoon member and the mobile model becomes narrower, the local flow around the platoon member is accelerated. The accelerated local flow, caused by the approaching mobile model with the same direction of the tunnel flow, tends to "close" the wake region behind the platoon

member, hence reduce the pressure difference that leads to the drag. Conversely, the local flow around the platoon member is decelerated when the mobile model moves forward (against the wind-tunnel flow). The decelerated local flow "opens" the wake region behind the platoon member and results in a greater pressure difference. This observation provided an interesting result that could not be duplicated in the steady flow measurements although the explanation should be checked with flow visualization experiments.

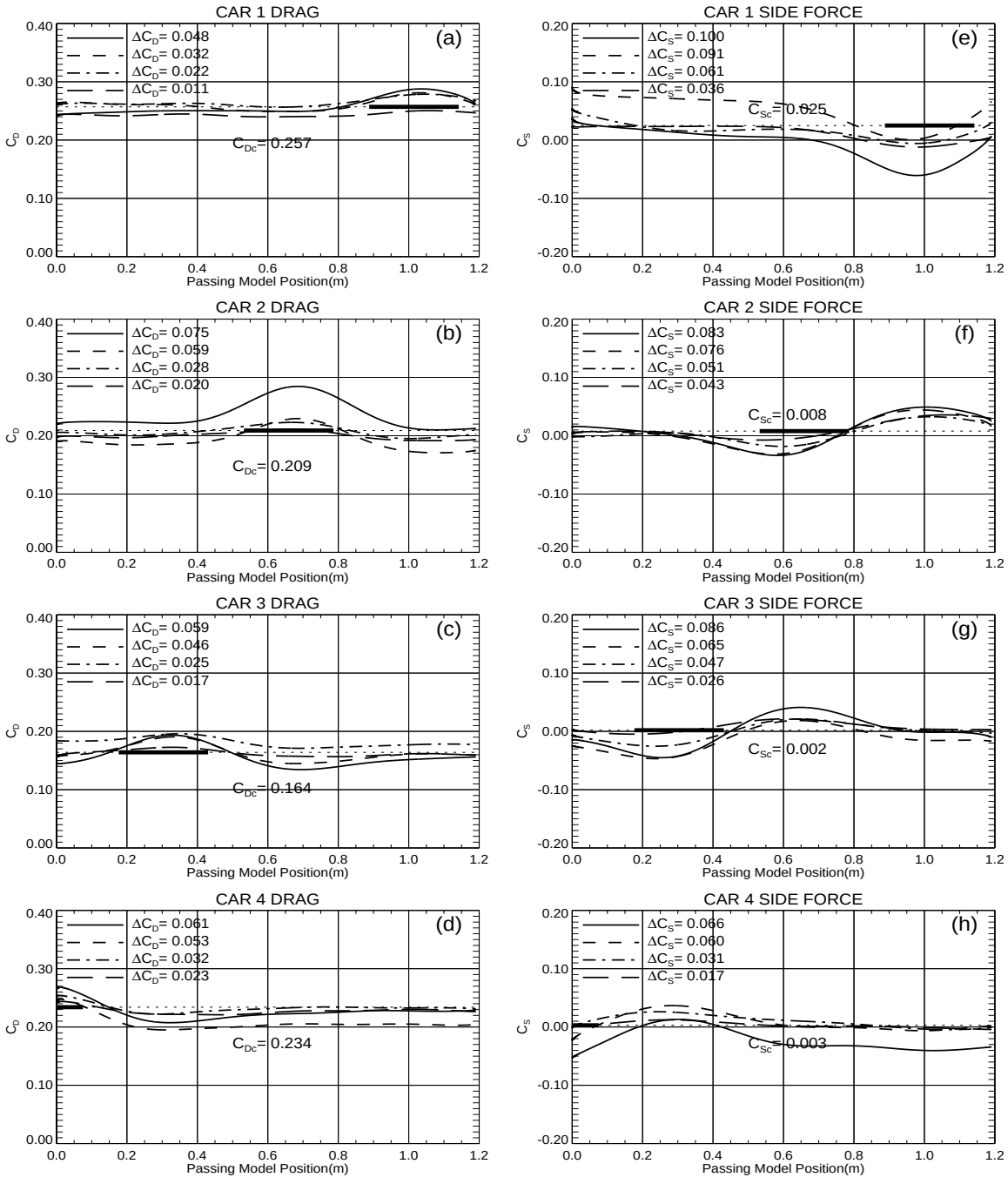

Figure 3.5: Effect of lateral spacing - a car model passing a platoon ($v = 2.50m/s$) The drag [frames (a)-(d)] and side force [frames (e)-(h)] coefficients on each car in the platoon are shown with respect to the position of mobile model.

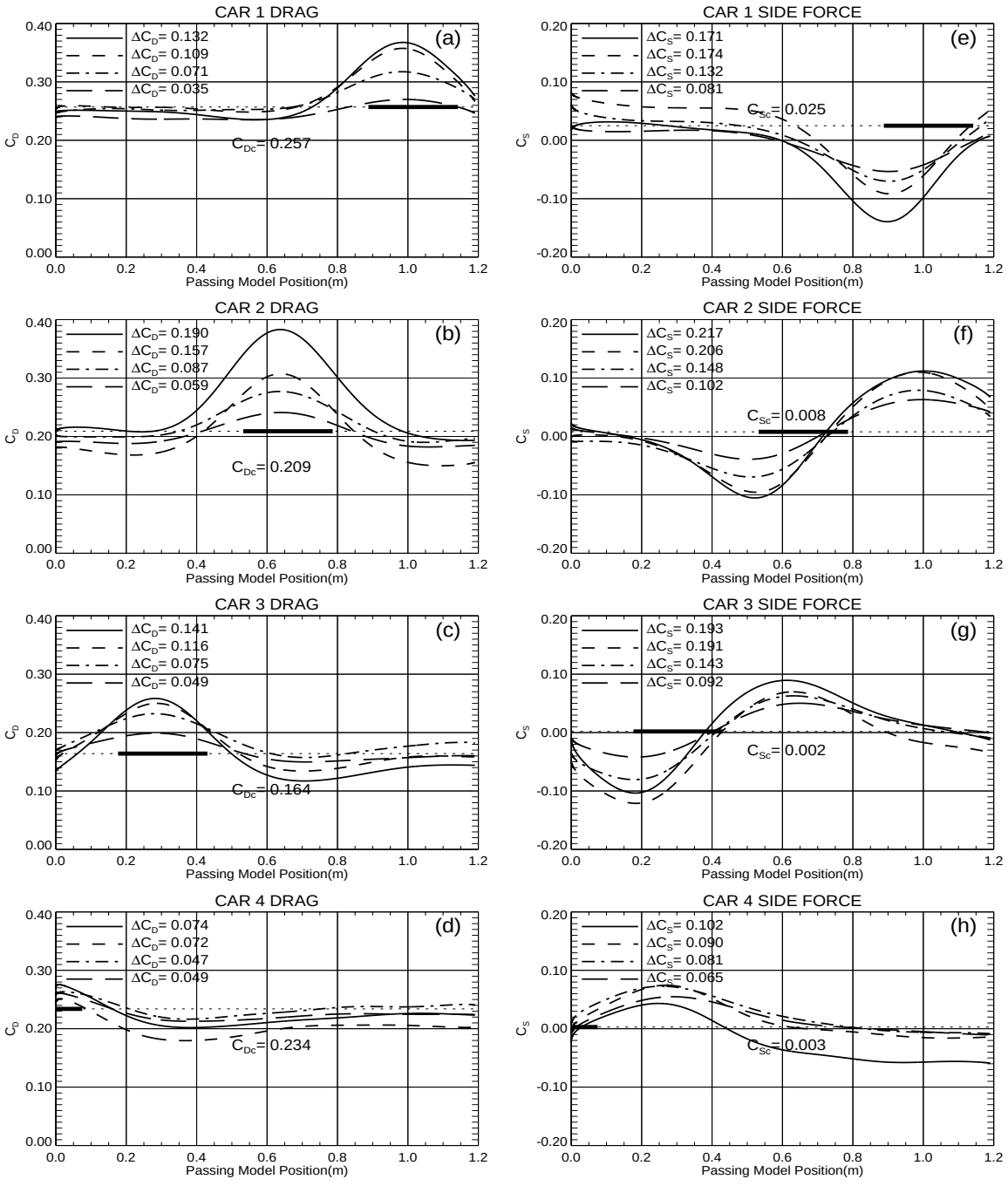

Figure 3.6: Effect of lateral spacing - a box model passing a platoon ($v = 2.50m/s$) The drag [frames (a)-(d)] and side force [frames (e)-(h)] coefficients on each car in the platoon are shown with respect to the position of mobile model.

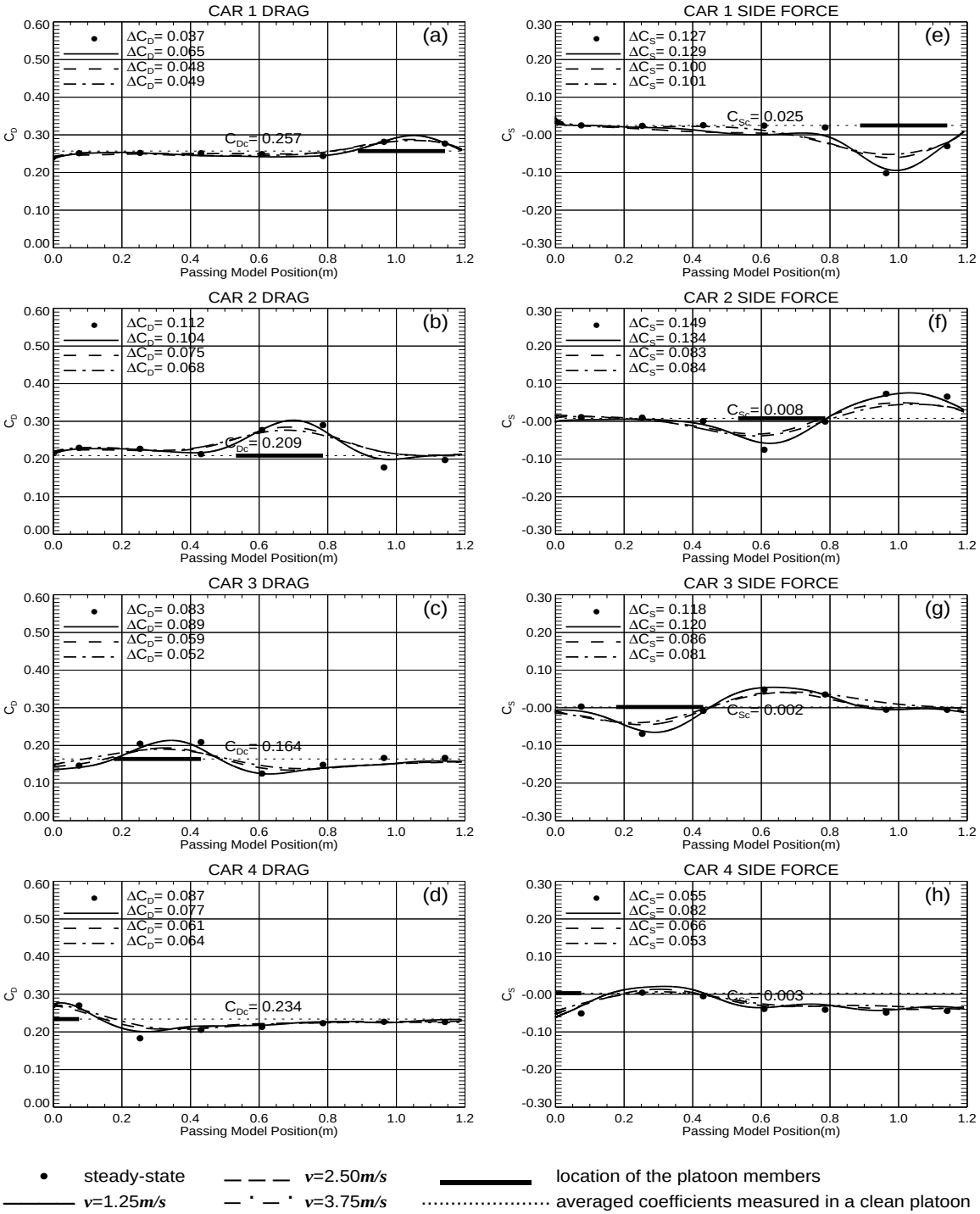

Figure 3.7: Effect of relative velocity - a car model passing a platoon ($d = \frac{1}{4}W_{box}$) The drag [frames (a)-(d)] and side force [frames (e)-(h)] coefficients on each car in the platoon are shown with respect to the position of mobile model.

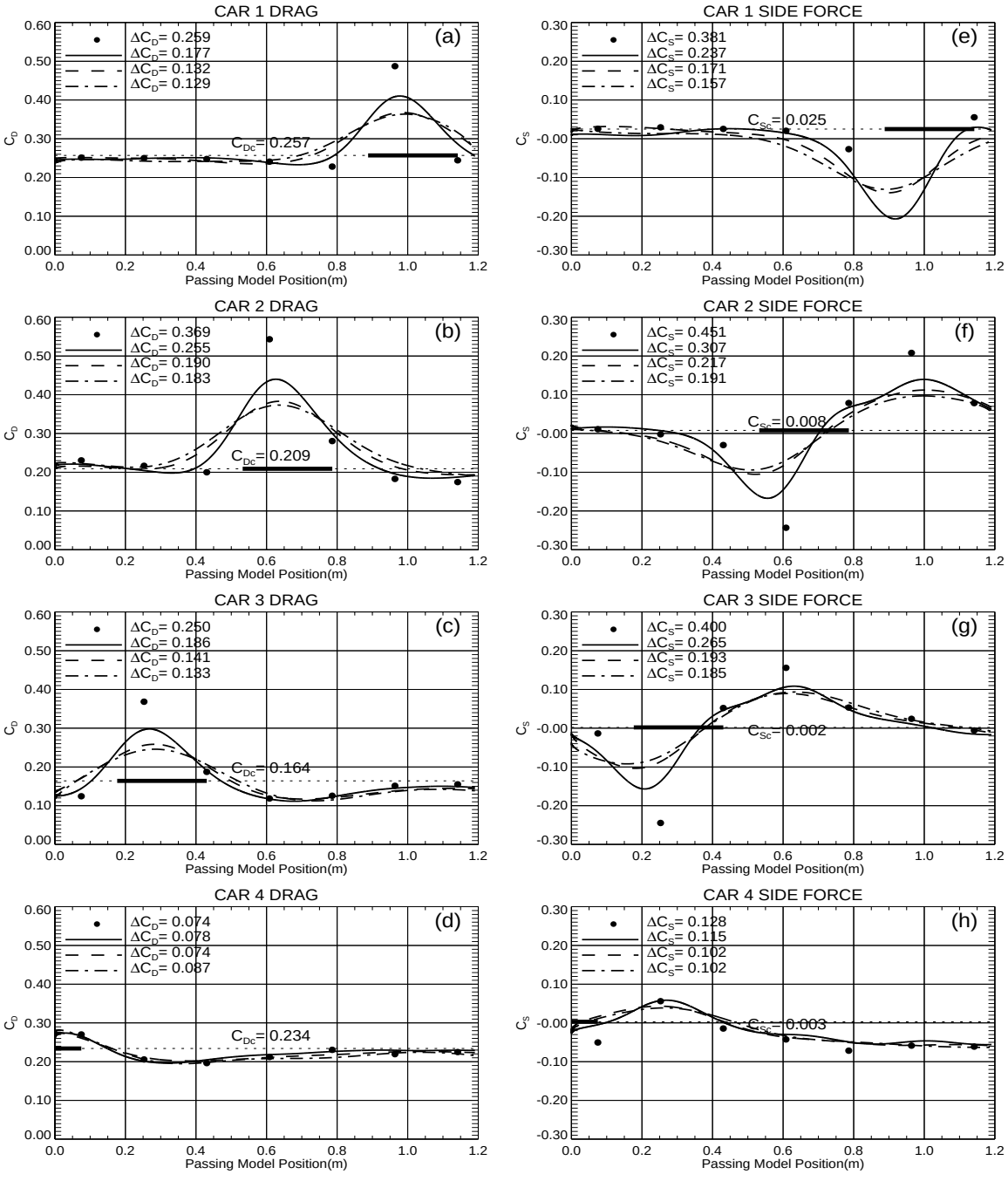

Figure 3.8: Effect of relative velocity - a box model passing a platoon ($d = \frac{1}{4}W_{box}$) The drag [frames (a)-(d)] and side force [frames (e)-(h)] coefficients on each car in the platoon are shown with respect to the position of mobile model.

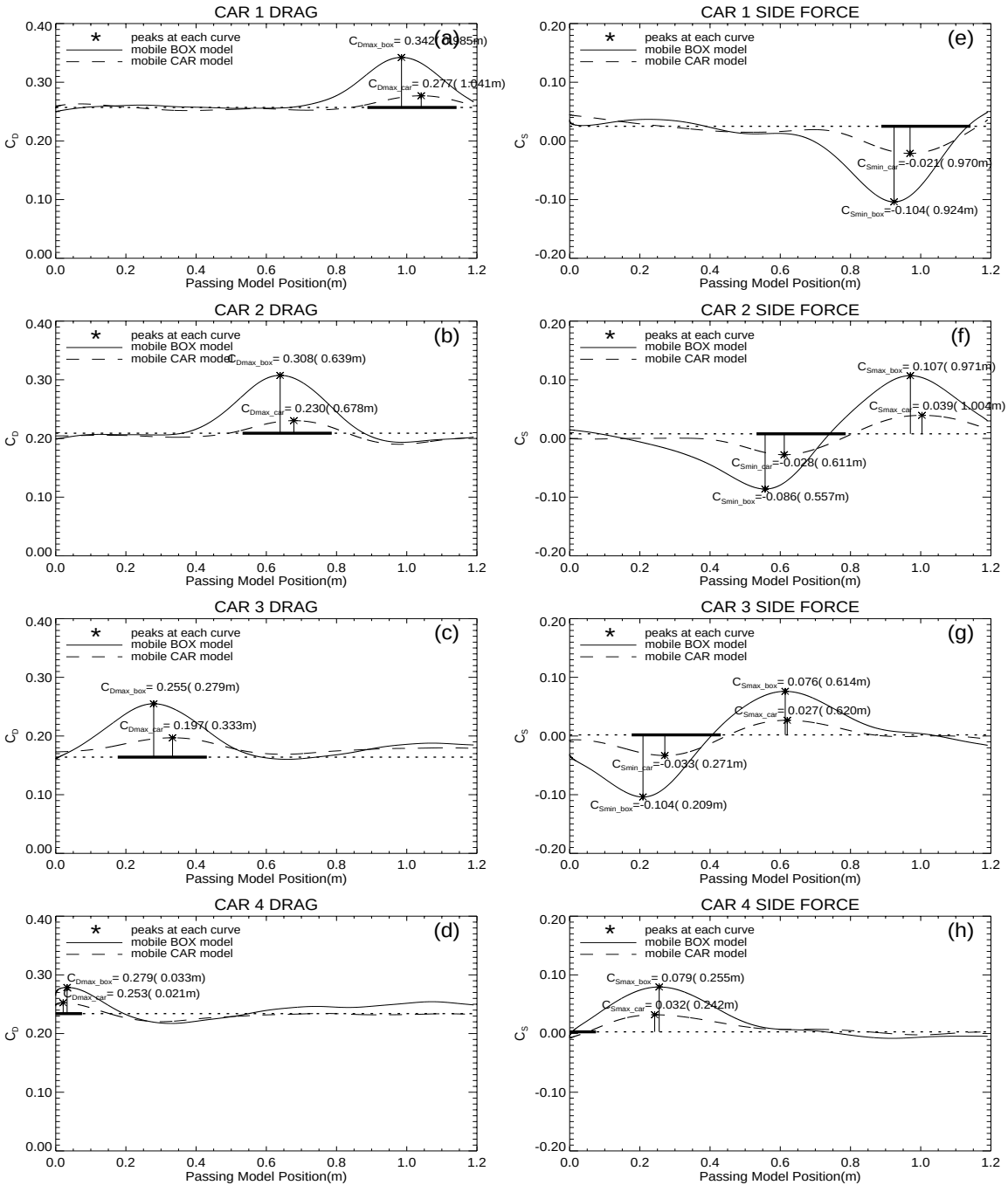

Figure 3.9: Effect of passing model shape - forward motion ($d = 1W_{box}, v = 1.25m/s$) The drag [frames (a)-(d)] and side force [frames (e)-(h)] coefficients on each car in the platoon are shown with respect to the position of mobile model.

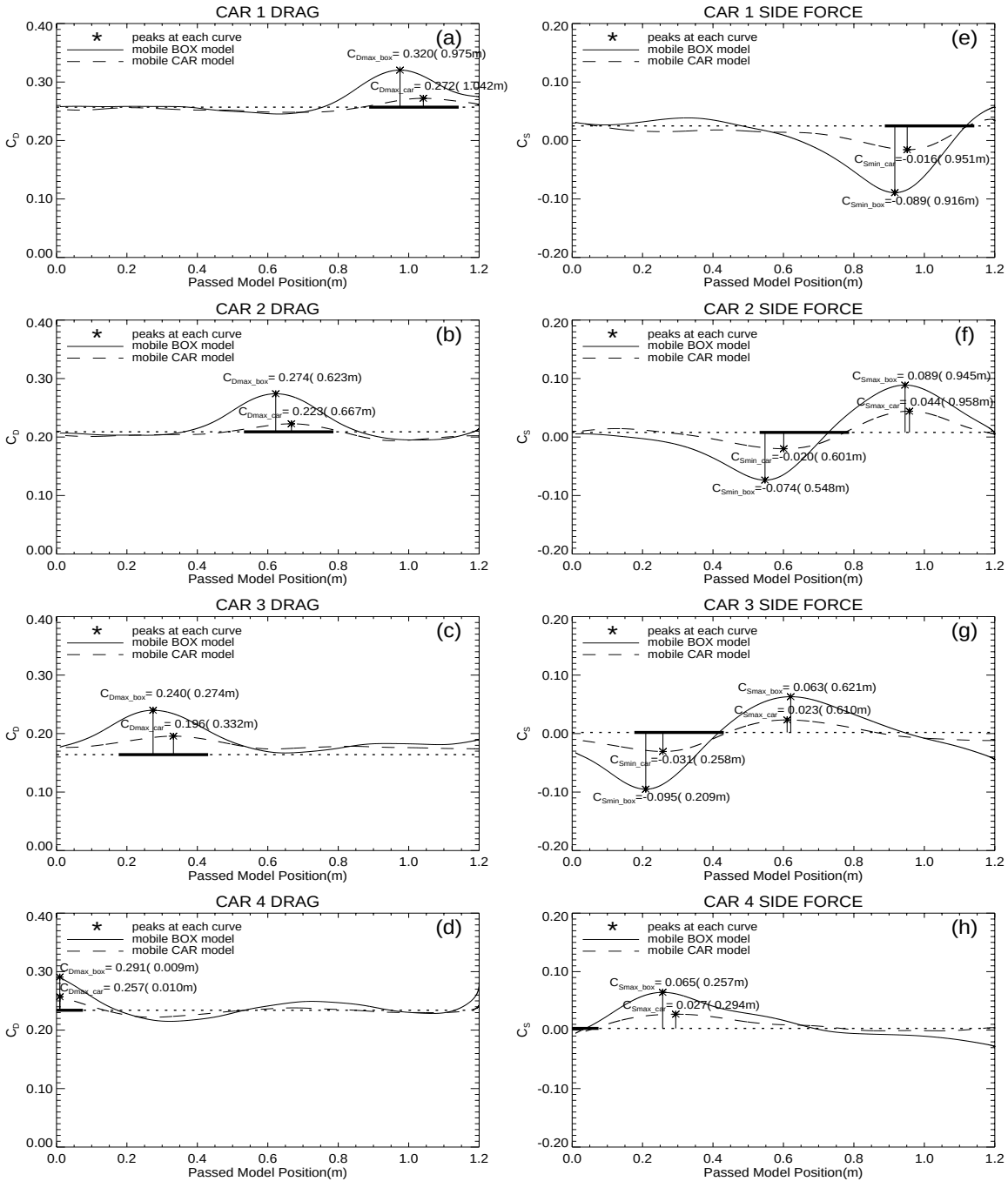

Figure 3.10: Effect of passing model shape - backward motion ($d = 1W_{box}, v = -1.25m/s$) The drag [frames (a)-(d)] and side force [frames (e)-(h)] coefficients on each car in the platoon are shown with respect to the position of mobile model.

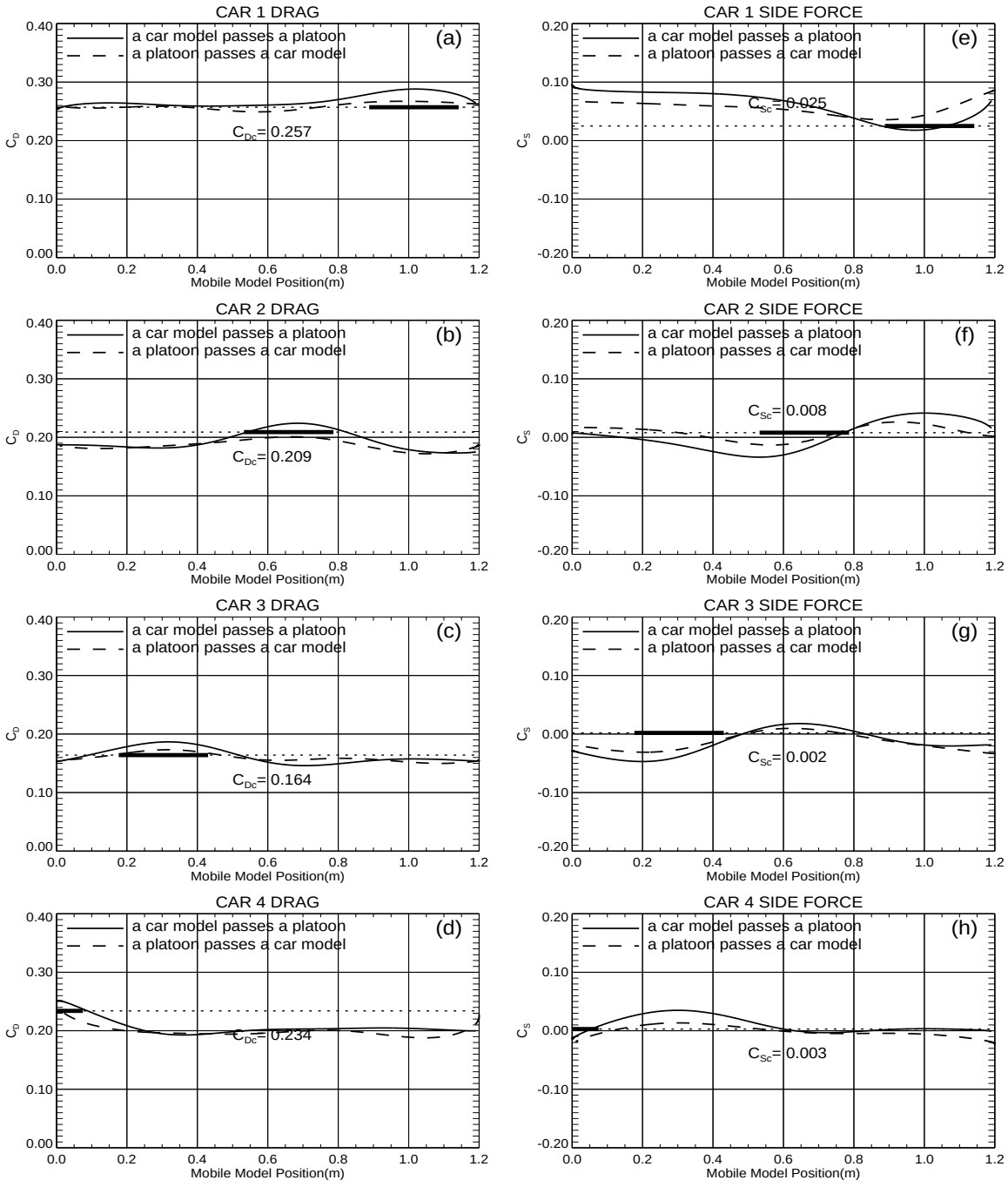

Figure 3.11: Effect of passing direction - car model ($d = \frac{1}{2}W_{box}, v = 3.75m/s$)
The drag [frames (a)-(d)] and side force [frames (e)-(h)] coefficients on each car in the platoon are shown with respect to the position of mobile model.

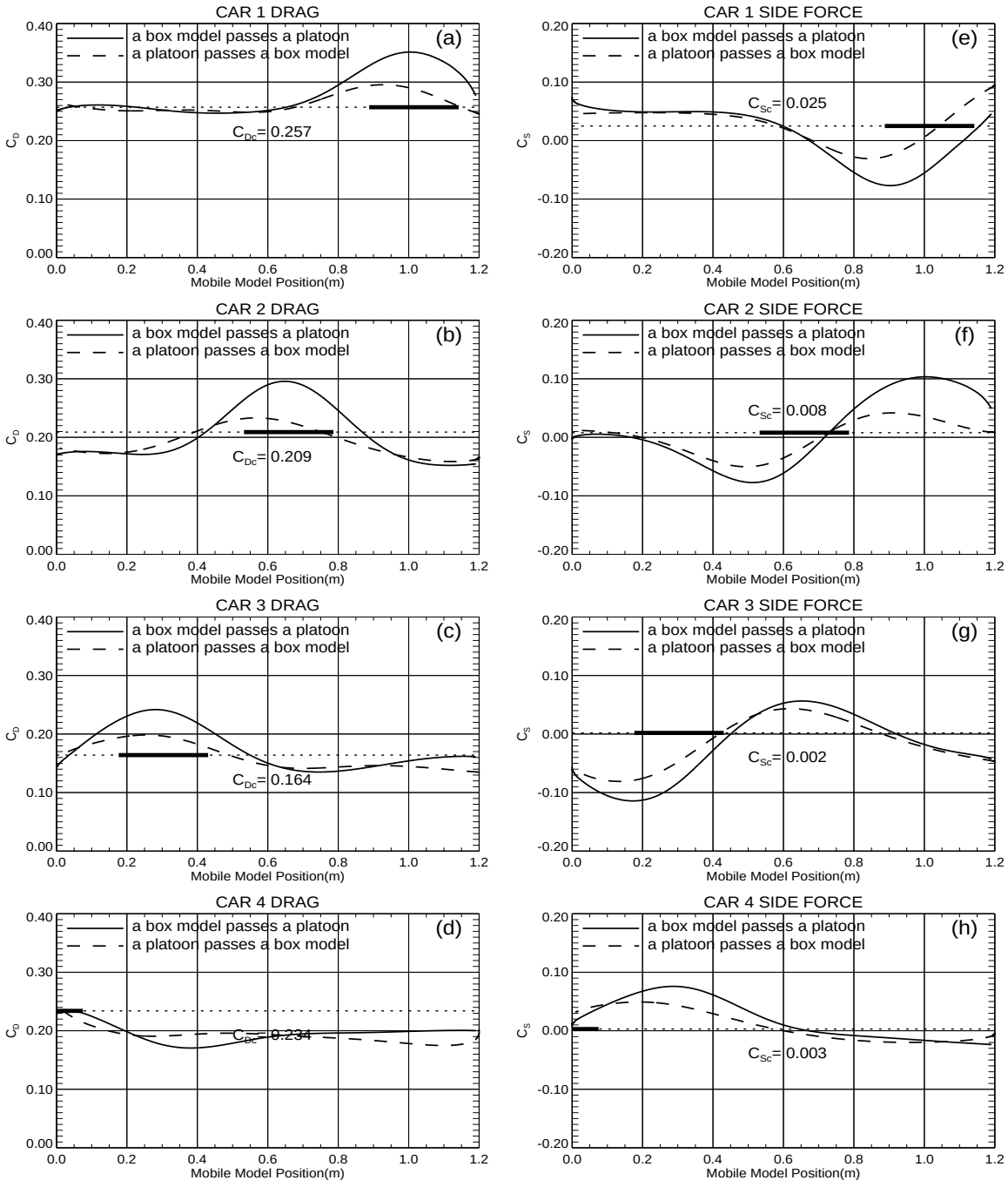

Figure 3.12: Effect of passing direction - box model ($d = \frac{1}{2}W_{box}, v = 3.75m/s$)
The drag [frames (a)-(d)] and side force [frames (e)-(h)] coefficients on each car in the platoon are shown with respect to the position of mobile model.

3.5 Discussion of Yaw Moment

The aerodynamic interactions between a single vehicle and a four-car platoon during passing process was investigated in the previous sections. Significant changes in drag and side force experienced by the platoon members were observed while the interaction was taking place, but the collected yaw moment data appeared very small.

In all figures in Section 3.4, the side force reversed direction (from repulsive to attractive) when the passing model moved from the proximity of the rear half to the front half of the platoon member. A counterclockwise yaw moment was then expected to be experienced by the platoon member. However, the yaw moment measurements in this study showed negligible values [23]. This finding was not only beyond our expectation, but also against the results of previous research in similar topics [10] [25] [26].

By inspecting the measuring facilities carefully, we discovered that the error was caused by a mistake made in the original design of the force balances. As shown in Figure 2.3, the balance is attached to an aluminum plate which is mounted in the interior of each scale vehicle model. Figure 3.13 (a) shows the original design of the force balance that the aluminum plate is connected to the balance by four mounting screws (1-4 in figure). The rigidity of the aluminum plate prevents the force balance from bending after shear force acting on it, therefore the readings from the balance do the reflect the real yaw moment it has experienced.

A better design is shown in Figure 3.13 (b). Only two mounting screws (1 and 2 in figure) are used here to connect the aluminum plate and the force balance. The modified design allows the flexures of the force balance deforming freely with the aluminum plate, which rotates a certain angle due to an acting moment. Therefore, the deformation of the balance flexures corresponding to moment should be correct, and hence the yaw moment readings are accurate.

Although the force balances can not provide accurate information of yaw moment, we believe the drag and side force measurements are reliable. The dramatic change in side force discovered in this chapter suggests that, a significant yaw moment is also expected to

act on each platoon member during passing maneuvers.

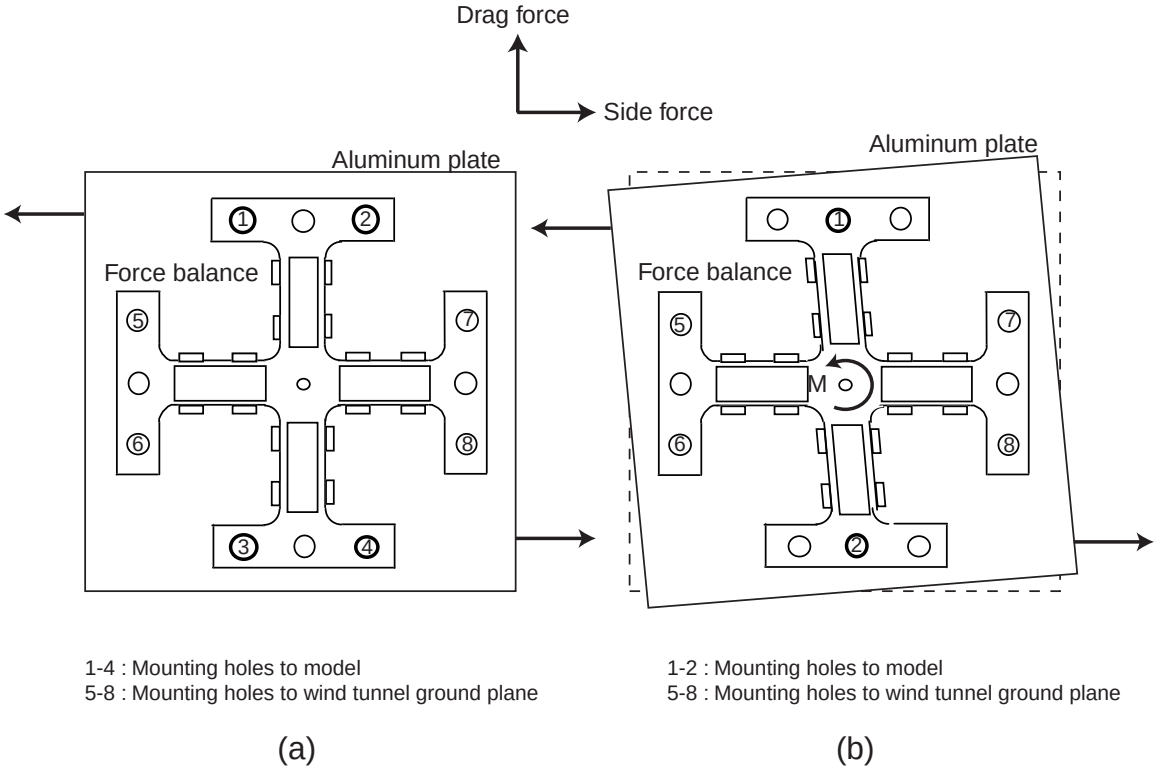

Figure 3.13: Balance under shear force
frame(a)-current design; frame(b)-modified design

3.6 Summary

Figure 3.14 presents a summary data for the third car in the platoon. The figure shows the effects on the aerodynamic characteristics of the factors discussed in this chapter. Because similar trends of force change were observed for all four cars in the platoon, as shown in Section 3.4, this figure can represent the summary for all platoon members.

The total changes (differences between the maximum and the minimum observed values) in drag and side force coefficients are plotted as a function of the lateral spacing between the platoon and the mobile model. Data taken under different relative velocities and mobile models are presented in each frame. It was observed that the excursions in force coefficients decreased as the lateral spacing or relative velocity increased. Using the box as the mobile model generated higher drag and side force on the platoon member. Comparing frames (a)(c) and frames (b)(d) in the figure, greater force changes were observed when the mobile model was in forward motion than when it was in backward motion.

In summary, the major observations and discoveries in this chapter are:

1. Each platoon member experiences a repulsive side force when the mobile vehicle is in the neighborhood of its rear half. The side force reverses its direction and becomes an attractive force when it is in the proximity of the front half of the platoon member. Each platoon member experiences significantly increased drag when in the proximity of the mobile model.

2. The trends of force change are similar for all the four cars in the platoon, in terms of the relative position of the platoon member and the mobile model.

3. Forces experienced by the cars in the platoon increase with decreasing separation between the platoon and the mobile model.

4. Reducing the relative velocity between the platoon and the mobile model increases the forces experienced by the platoon members.

5. The platoon members experience greater forces when a rectangular box is used as the

mobile model. The locations of the force coefficients' peak values vary for the box model and vehicle model.

6. Similar trends of forces change are observed in both cases of a car passing a platoon and a car overtaken by a platoon. Smaller force coefficients are recorded when the mobile model is in backward motion.

7. The acceleration and deceleration of the mobile model, which are unknown factors for the aerodynamic force changes on the platoon during passing maneuvers, need further study to quantify their effects. However, according to the data collected in this study, the force coefficients have not shown significant dependence on acceleration or deceleration during passing maneuvers.

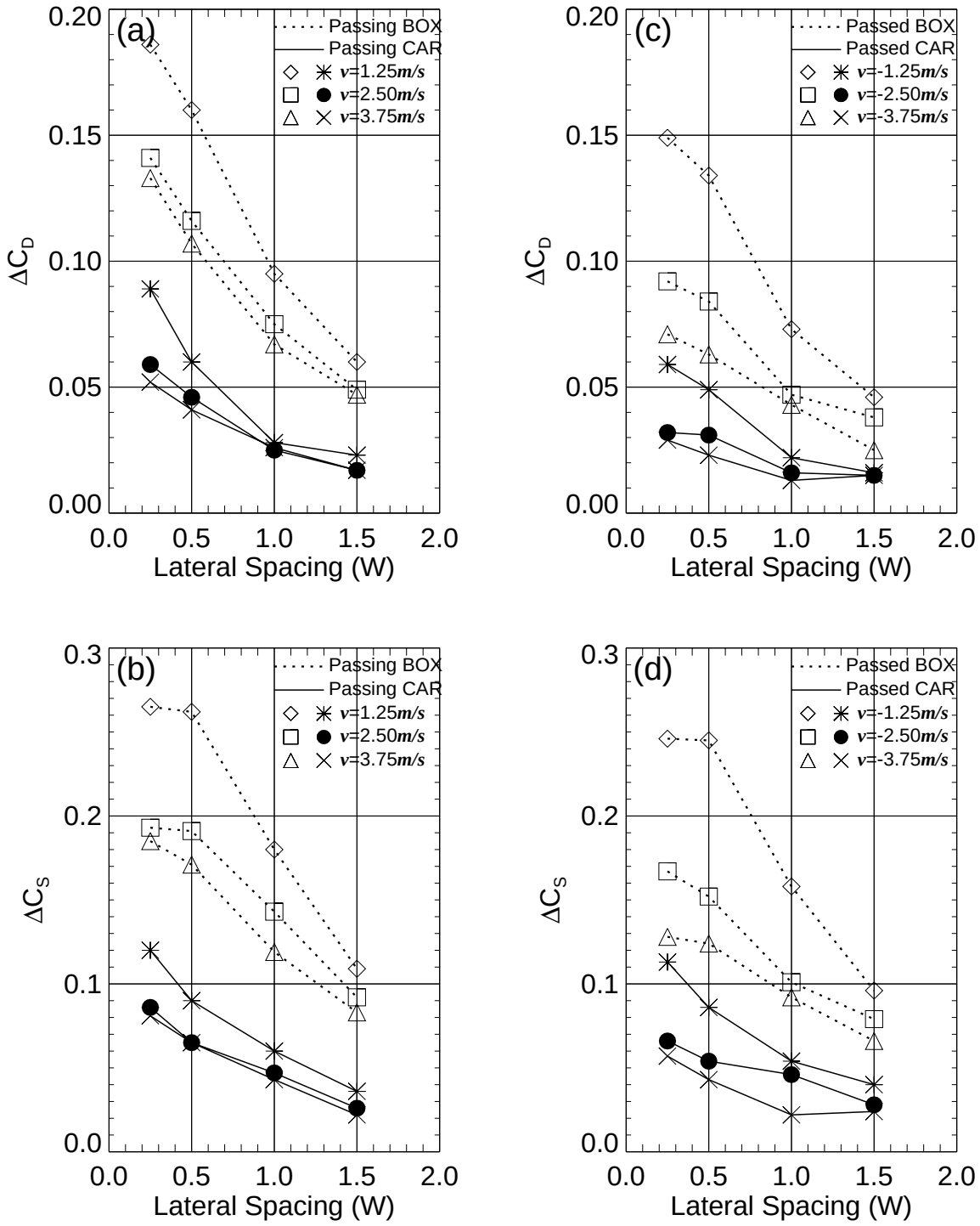

Figure 3.14: Summary plots - representative data from the third car in the platoon frames (a)(b) represent the case of the mobile model in forward motion, and frames (c)(d) represent the case of the mobile model in backward motion.

Chapter 4

Transient Aerodynamics during In-Line Oscillations

Transient platoon aerodynamics during in-line oscillations are studied in this chapter. By in-line oscillation, we mean one of the platoon members is moving periodically in its streamwise direction with specified velocity and displacement amplitudes. The oscillating condition can occur in any one of the four platoon members in the experiments.

Platoon operations may have advantages in terms of increasing highway capacity and decreasing fuel consumption. However, it is a challenge to guarantee the safety and stability of all vehicles. To prevent collisions from occurring, the extremely small inter-vehicle spacing must be kept constant to provide a buffer zone between adjacent vehicles. To meet this requirement, each platoon member detects the separation between itself and its upstream neighbor, and adjusts its velocity accordingly. Therefore, frequent accelerating and decelerating motions are common for individual vehicles during platoon operations. In this study, the vehicle's accelerating-decelerating motions were simulated as harmonic in-line oscillations. Considering a bluff body oscillating in a fluid periodically, the induced unsteady flow acting on the body is also periodic. The issue is, then, whether the excited force is resonant with the bodies' natural frequency. By investigating the aerodynamic forces experienced by all platoon members, the influence of the oscillations are studied in this chapter.

4.1 Description of Experiments

Wind tunnel experiments were conducted to study transient aerodynamic effects on a four-vehicle platoon during in-line oscillations. As before, four identical 1997 Buick LeSabre vehicle models or similarly-sized rectangular boxes were employed as platoon members. The intra-platoon spacing was $10.2cm$, which was equivalent to $2m$ or $2/5$ car length in full scale. Each member of the platoon was connected to a force balance as described in the previous chapters.

The experimental apparatus used for oscillating tests is shown in Figure 4.1. The wind tunnel actuator (WTA), with a $81.3cm$ length and $12.7cm$ width, fitted underneath the wind tunnel test section and was aligned with the platoon. The WTA used a servomotor (Compumotor APEX 620) to drive the main drum where a steel ribbon was attached. The steel ribbon was also attached to a pallet that traveled linearly along guide rails. Any one of the platoon members could be mounted longitudinally on the carriage and mobilized back and forth periodically by the actuator with specified velocity and displacement amplitudes. The drag force of all four models in the platoon were measured simultaneously. This was done by using force balances during the oscillations to characterize the transient effects. Chen et al. [16] provided more details about the construction of the WTA, and had utilized the actuator to study transient aerodynamic effects during lane change maneuvers.

Figure 4.2 shows the top view of the experimental setup. The wind tunnel flow was set as $20m/s$. A harmonic motion, in terms of the position and velocity profiles, was executed for the oscillating model. About 15 oscillation cycles were exercised in each run. The data-collecting process was manually triggered after the first five cycles and was terminated before the last five cycles. The number of cycles recorded depended on the oscillation frequency and recording time of the data acquisition system. The motion's velocity amplitudes (v_{amp}) ranged from 0.5 to $2m/s$ and displacement amplitudes (d_{amp}) were set to be 7.6 and $15.2cm$. To determine the influence of the shapes of the models in the platoon, both a four-car and a four-box platoon were tested. In addition to the transient results, for each platoon member, steady data were also collected at nine different locations ($d = 0, \pm 1.9, \pm 3.8, \pm 5.7, \pm 7.6cm$)

within its oscillating range of $15.2cm$. When d was zero, it represented the case of a clean platoon with a uniform inter-vehicle spacing. Positive d meant that the oscillating model was positioned ahead of its original position, and when d was negative, the model was positioned downstream of its original one.

The experimental conditions are summarized in Table 4.1. All the signals were processed similar to that in Chapter 2 and 3. That is, steady measurements were sampled at a 1.9 kHz rate and transient data were measured at a 5.2 kHz rate, and the signals were digitally filtered in the frequency domain to eliminate noise. Three runs of data were conducted for each of the experimental conditions. Zero-reading files and clean platoon data were obtained as in Section 3.2 to reduce the error caused by electronic drift and the mechanical mechanism of the force balances.

Model	Oscillating member's location in platoon	Velocity amplitude $v_{amp}(m/s)$	Displacement amplitude $d_{amp}(cm)$
Car model	1	0*	
- or -	2	0.5	7.6
Rectangular box	3	1.0	15.2
	4	2.0	

Table 4.1: Test conditions of oscillating investigations
* steady-state measurements at nine locations

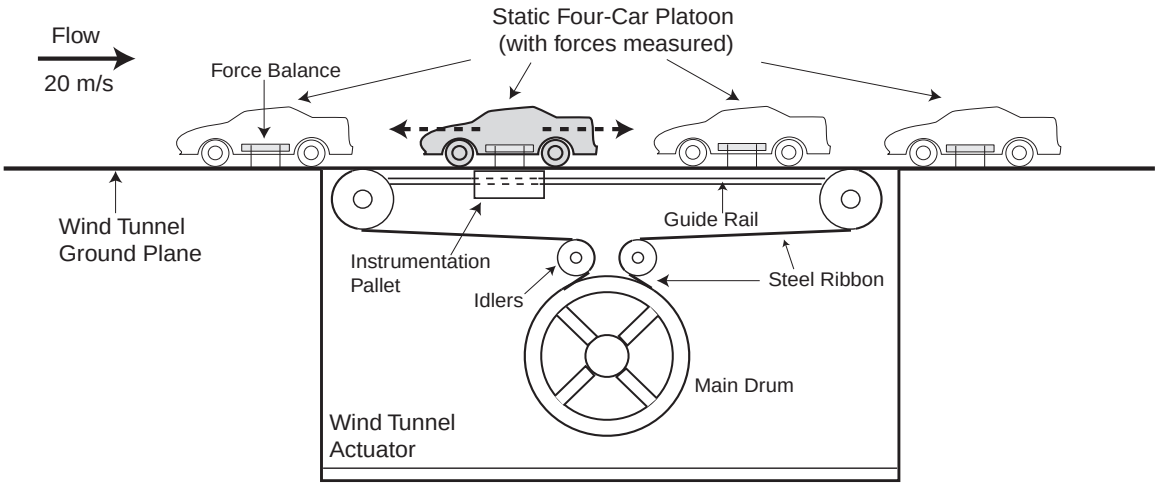

Figure 4.1: Driving mechanism for the mobile model

d = Oscillating model's position; L = Length of model = 25.4 *cm*
d_{amp} = Displacement amplitude of oscillation = (7.6, 15.2 *cm*)
v_{amp} = Velocity amplitude of oscillation = (0.5, 1.0, 2.0 *m/s*)

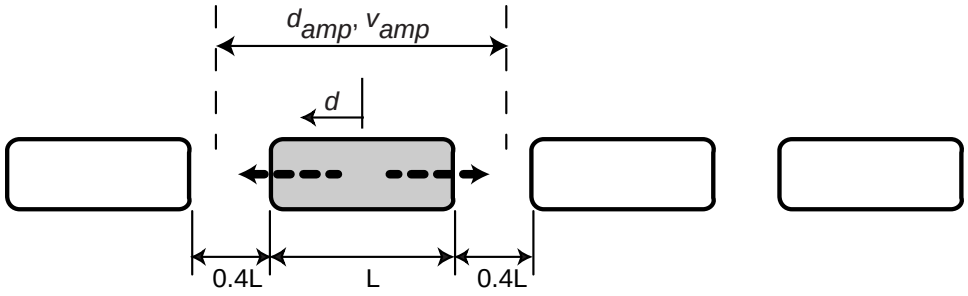

Figure 4.2: Configuration of the platoon and the mobile model

4.2 Consideration of Accelerating Flows

In the transient measurements, not only the equilibrium static forces apply on the platoon members, but also the accelerated flow plays a role. Consider that the flow is ideal and the oscillating model moves at a velocity that is a function of time, $v(t)$. Apparently when a body moves through a fluid, a certain mass of the fluid is induced to move. To balance the work carried by the oscillating model, the rate of kinetic energy of the fluid has to change as,

$$\mathbf{K} = v_i F_i = \frac{d}{dt} \int \frac{1}{2} \rho u_i u_i dV \tag{4.1}$$

where F is the force that is required to generate the flow motion, u is the flow velocity and ρ is the density of the fluid. It is noted that when the body is in a periodic motion, there is no net work done by the body, thus the mean value of $\mathbf{K}$ over one cycle is zero [27].

Because the model moves in pure translation, the i component of the force F can be determined by the pressure distribution acting on the body surface,

$$F_i = -\int_S p\, n_i dS \tag{4.2}$$

where n is the local normal vector on the surface. Assuming the flow is irrotational, the unsteady Bernoulli equation states

$$\frac{\partial \phi}{\partial t} + \frac{1}{2} u_i u_i + \frac{p}{\rho} = \frac{p_\infty}{\rho} \tag{4.3}$$

where p_∞ is pressure in far field and in potential flow $\mathbf{u} = \bigtriangledown \phi$, and $\bigtriangledown^2 \phi = 0$.

The force F can be solved by combining equations (4.1) (4.2) and (4.3). In the case when the body is a sphere, the force is reduced to

$$F = -\frac{2}{3} \pi r^3 \rho \frac{dv}{dt} \tag{4.4}$$

where r is the radius of the sphere. Note the magnitude of the force is proportional to the acceleration, and its direction is opposite to the acceleration. Equation (4.4) states that the force acting on the sphere is equivalent to accelerating the sphere by "adding a certain mass" of fluid (in this case, one-half the volume of the sphere) to its real mass. This effect is called *added mass* or *virtual mass* [28].

The above concept can also apply to the force on a body in accelerating fluid. Suppose the fluid has a velocity of $u_f(t)$ and an acceleration of a, a coordinate system is then chosen such that the flow velocity far from the body remains zero. By choosing the moving axes, the acceleration of the body relative to the fluid at infinity is $\frac{dv_i}{dt} - a_i$ and the flow velocity becomes $u_i - (u_f)_i$. By replacing the acceleration and velocity in equations (4.1) - (4.3) with the ones in the new coordinates, following similar procedures the force can be solved. If the body is fixed relative to the ground-based system, then it experiences a force in the same direction to the flow's acceleration.

4.3 Simulation of Harmonic Motion

In the experiments, the mobile model was forced to oscillate in line with the oncoming flow. The periodic position-versus-time profile and its time derivatives, ideally, should be in sinusoidal forms. Unfortunately, the motor controller (Compumotor, APEX 6154) is designed to achieve a "target" constant distance and velocity by providing parameters such as proportional and integral feedback gains, velocity feedback and feedforward gains, and acceleration feedforward gain, along with the user-assigned distance, velocity and acceleration. This feature does not allow us to generate a pure harmonic motion with time dependent variables.

To simulate a sinusoidal motion by the current facilities, a series of trial-and-error procedures were proceeded by changing gains and damping parameters of the motor. A successful simulation should meet the following requirements: (1) periodic motion; (2) smooth profiles at least in position and velocity information; (3) satisfying the desired displacement amplitudes; and (4) satisfying desired velocity amplitudes. After numerous tests, satisfactory outputs were reached and would be shown later in this section.

The displacement and velocity amplitudes were assigned to the motor controller via a software package called Motion Architect (developed by Parker Hannifin Corporation) which provided a programming environment for the servomotor. The position history of the oscillating model was determined by using an external encoder and a resolver that was

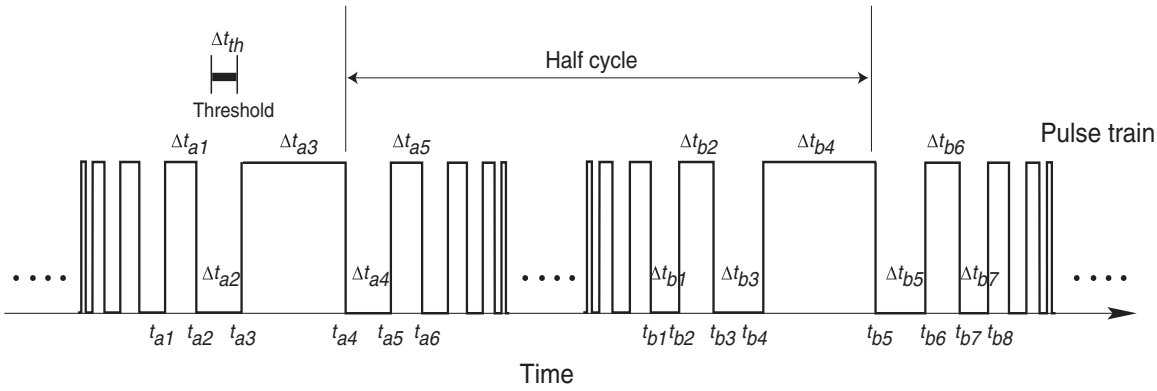

Figure 4.3: Sample encoder pulse train in a periodic motion

integrated into the servomotor. The optical encoder (Renco RM21) has a higher resolution of 2048 counts/revolution compared with the 1024 counts/revolution provided by resolver.

Both resolver and encoder signals were sampled at a rate of 72.8 kHz by the data acquisition system, and digitally filtered as done in Section 3.3. The encoder produced a pulse train as an output like the motor resolver. Their outputs, however, did not carry information about the direction of travel, which was crucial to accurately determine the position of the oscillating model. An algorithm was then developed to solve this problem. The idea was that, before the oscillating model reversed its traveling direction, the model was decelerated until its velocity became zero at the turnaround point. Therefore, the resolver and encoder outputs must have the largest time interval at or very close to the turning point.

Figure 4.3 shows a sample pulse train in a periodic motion. Since the velocity is a function of time, the intervals ($\Delta t_i's$) in the pulse train are also changing with time. The algorithm sets a threshold (Δt_{th} in figure) that whenever the time interval exceeds the threshold its index (t_i) is marked. All consecutive marked indices are formed in a group, thus each group includes the turning points in every half cycle of the motion. Using Figure 4.3 as an example, Δt_{a1}-Δt_{a5} are all larger than Δt_{th}, thus t_{a1},t_{a2},... ,t_{a5} are recorded in group "a". Later another group "b" is detected that Δt_{b1}-Δt_{b7} are all greater than Δt_{th}, so t_{b1},t_{b2},...,t_{b7} are marked. Each group now contains one turnaround point in half a cycle.

The algorithm then looks for the index of the maximum interval in the first group (t_{a4} in Figure 4.3), and reverses the sign of position increments after this point until the maximum of next group (t_{b5}) is found. The process repeats every half a cycle. By doing this, the complete position profiles can be recovered correctly, and the velocity and acceleration are obtained by taking first and second derivatives of the position data in the Fourier domain, respectively.

Figure 4.4 is an example of the position, velocity and acceleration profile. In this case, d_{amp} is $15.2cm$ and v_{amp} is $2.0m/s$. Note that the position and velocity of the model were determined by feedback of the servomotor, therefore real d_{amp} and v_{amp} were not exactly equal to $0.5, 1$, and $2m/s$. However, we still refer to these numbers later in this chapter for convenience.

The first and second column of Figure 4.4 present the position, filtered velocity, and filtered acceleration data from the optical encoder and motor resolver, respectively. Comparing frames (a)-(c) with (d)-(f), they were nearly identical because the encoder and the resolver produced similar outputs. Averaged position, velocity, and acceleration profiles were shown in frames (g)-(i) in Figure 4.4. They were obtained by linearly interpolating and averaging the resolver and encoder information at each time point that aerodynamic forces were measured.

By examining position and velocity profiles in Figure 4.4, it showed a smooth, harmonic motion was successfully simulated. To generate a motion of $2.0m/s$ velocity amplitude within a short distance, the inertia force was too significant, so it required a heavy damper to smooth out the strong jerk. Therefore, only minor jagged curves appeared on the acceleration profiles. However, the trade-off was that the real amplitudes of displacement (about $14cm$) and velocity ($1.9m/s$) were a little bit short of the desired values.

Figure 4.5 shows another example with $v_{amp} = 0.5m/s$ and $d_{amp} = 7.6cm$. As in the previous plot, the travel trajectories obtained by the encoder, resolver, and their average were shown in the first row. The filtered velocities and accelerations were then obtained by taking first and second derivatives with respect to time of the position data, and shown in the second and third rows, respectively.

Oscillation frequency $f(1/s)$	$v_{amp}(m/s)$	$d_{amp}(cm)$
0.5	0.5	15.2
1.0	0.5	7.6
	1.0	15.2
2.0	1.0	7.6
	2.0	15.2
4.0	2.0	7.6

Table 4.2: Test conditions in terms of oscillation frequencies

The lower velocity and smaller inertia force allowed v_{amp} and d_{amp} to be satisfied very well. However, due to less damping being used in this case, the velocity curves were less blunt and less similar to real sine curves. The acceleration profiles were very noisy because differentiation was a noise-amplifying process, and the damper and digital filter were not sufficient to eliminate all the noise after taking derivatives twice.

The frequency f of the oscillating model is related to its velocity and displacement amplitudes, and can be determined by the inspecting the position profiles. In Figure 4.4, the motion takes about $0.5sec$ to finish a cycle, which results in a frequence of 2 $(1/sec)$. Similarly, in Figure 4.5, the frequency is, $f \sim 1$. The relation between oscillating frequency f, and oscillation amplitudes d_{amp} and v_{amp} are listed in Table 4.2.

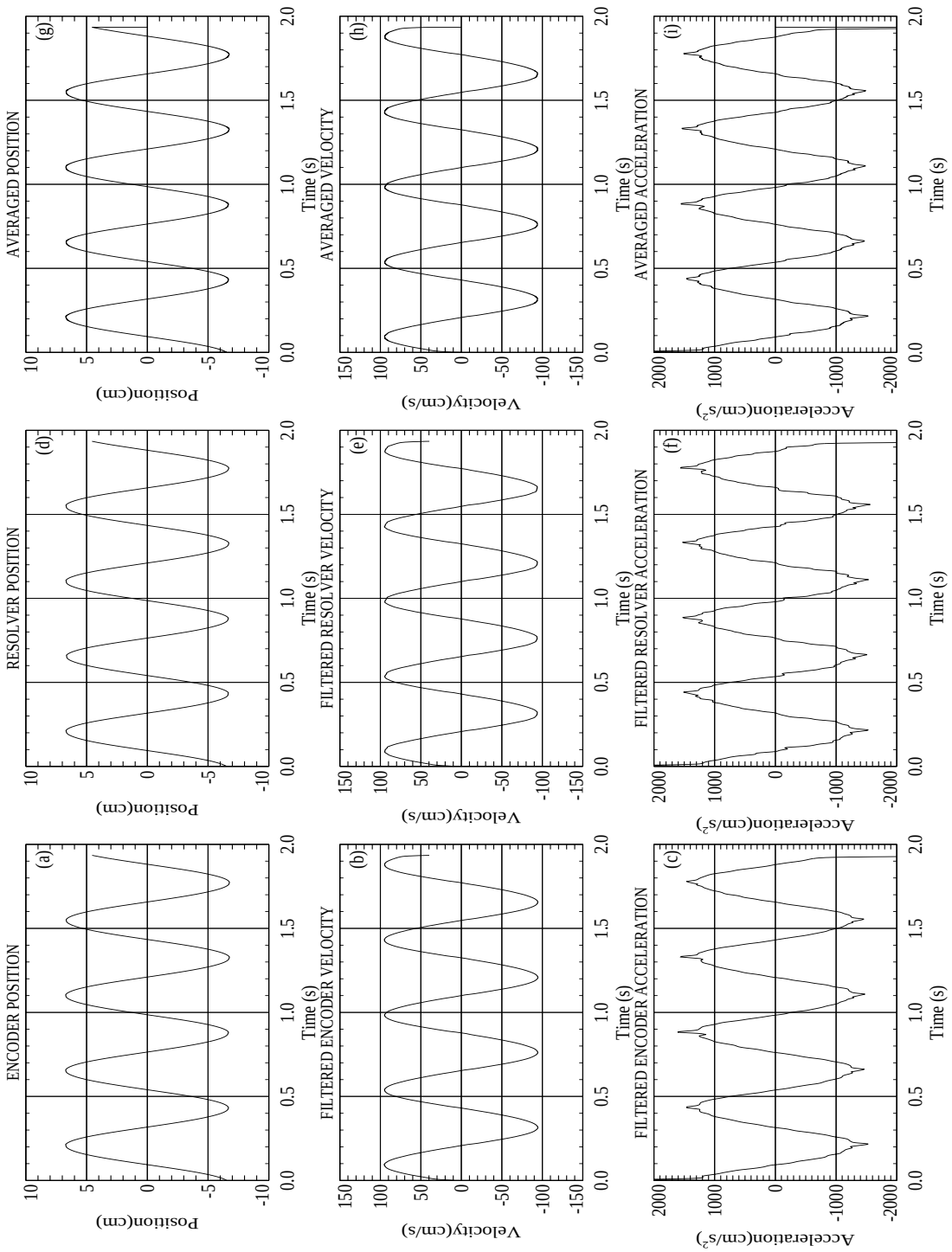

Figure 4.4: Motion profiles in oscillations ($d_{amp} = 15.2cm, v_{amp} = 2.0m/s$)
Frames (a),(d),(g) show the position profile from the encoder, resolver, and their average, respectively. The velocity (frames (b)(e)(h)) and acceleration (frames (c)(f)(i)) profiles are obtained by taking first and second derivatives of the position data before being digitally filtered.

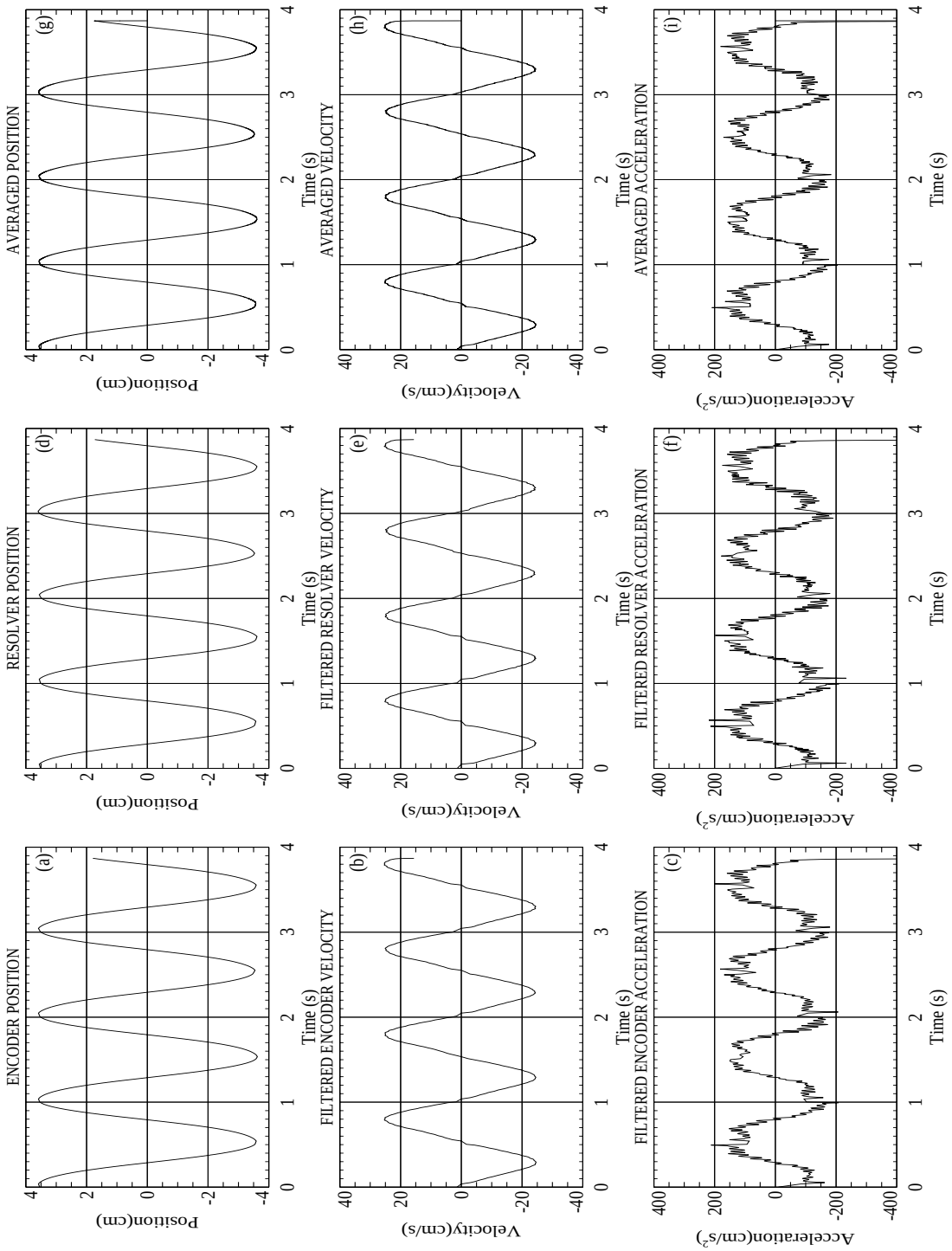

Figure 4.5: Motion profiles in oscillations ($d_{amp} = 7.6cm, v_{amp} = 0.5m/s$)
Frames (a),(d),(g) show the position profile from the encoder, resolver, and their average, respectively. The velocity (frames (b)(e)(h)) and acceleration (frames (c)(f)(i)) profiles are obtained by taking first and second derivatives of the position data before being digitally filtered.

4.4 Results

The results obtained from the transient platoon aerodynamic investigations during in-line oscillations are presented in this section. Due to the symmetric configuration of the experimental setup, only drag force is expected to be significant in a longitudinal periodic motion. Therefore, the side force and yaw moment data are not discussed in this section. Four factors were investigated, including the effects of oscillation location, the shape of models, the displacement and velocity amplitudes. A comparison of transient and static results is provided.

4.4.1 Effect of Oscillation Location and Shape of the Models

Figure 4.6 - 4.9 are a series of plots demonstrating the effects of the location of the oscillating model in the four-car and four-box platoons. The experimental condition is $d_{amp} = 15.2cm$ and $v_{amp} = 2.0m/s$. The oscillating member is the first, second, third, and fourth in Figures 4.6,4.7, 4.8, and 4.9, respectively. In these figures, frames (a)-(d) (left column) show the force coefficients measured in each member in a *car* platoon, and frames (e)-(h) show those in a *box* platoon. The force measured in the oscillating model is mostly caused by its inertia motion rather than aerodynamic drag force, thus a coefficient similar to C_D is defined

$$C_F = \frac{F_o}{\frac{1}{2}\rho U^2 A} \tag{4.5}$$

and used for the oscillatory model. In equation (4.5), F_o is the force measured by the force balance on the oscillating car.

Data in these frames are shown in the order of the platoon member that the top row (frames (a) and (e)) represents the leading model in the platoon and the bottom row (frames (d) and (h)) the trailing platoon member. The force coefficients are plotted as functions of time for 2.5 oscillation cycles. The averaged drag coefficients measured in a clean platoon are drawn as dotted lines for comparisons. All the curves that appear in this section are real measurements as described in Section 3.4, rather than drawn by curve-fitting.

To quantify the aerodynamic force of the oscillating model acting on the other platoon

members, the difference between the maximum and minimum values on each curve was calculated and labeled as ΔC_D or ΔC_F. Unfortunately, we discovered one of the force balances had some defects after all the experiments were finished. The calibration curve, which determined the relationship between the output voltages from the force balance and the known masses, were supposed to be linear and have a "constant" slope. Nevertheless, the slopes we obtained for this specific defective balance before and after the experiments were not consistent, though both curves were linear. This caused inconclusive results because their quantities may be incorrect. All problematic data are marked in Figures 4.6 - 4.15. However, we are confident about the rest of the data collected by the other force balances, and we also believe at least the "qualitative" trends shown by this defective balance are true.

In Figure 4.6, the oscillating (first) car and box (frames (a) and (e)) showed very high ΔC_F readings caused by their strong inertia motions. The rest of the members in the four-car platoon did not show significant aerodynamic force changes according to frames (b)-(d). However, more pronounced force changes were observed in a four-box platoon. The following, i.e. second, box model in the platoon (frame (f)) showed a harmonic drag behavior that was clearly caused by the oscillating model. The amplitudes of the drag coefficient for the third and fourth model decayed since they were shielded from the direct influence of the vibrating model.

More interesting results were shown in Figure 4.7 and Figure 4.8. The oscillatory model, in both figures, excited the flow fields around it. For the platoon members adjacent to the oscillatory model, it was seen that the amplitude and the phase of their drag coefficients strongly depended on the relative location with the oscillating model.

In the case of a four-car platoon, the vehicle ahead of the vibrating car experienced an almost perfect in-phase force variation with the oscillation, (frame (a) in Figure 4.7 and frame (b) in Figure 4.8), and the member behind it showed an out-of-phase drag change by about a half cycle (frame (c) in Figure 4.7 and frame (d) in Figure 4.8). Comparing ΔC_D values with the clean platoon coefficients, drag variations of about 20% and 10% have been observed for the oscillating car's upstream and downstream neighbors, respectively.

In a four-box platoon, the magnitudes of force fluctuation for the static models were much larger, as expected, due to the models' bigger front and rear surfaces and their sharp edges and corners. Up to 75% of the drag change compared with its clean platoon value was found (frame (g) in Figure 4.7). The box immediately behind the oscillating model, as in a four-car platoon, experienced an out-of-phase drag variation by about a half cycle (frame (g) and (h) in Figure 4.7 and in Figure 4.8, respectively). However, the periodic changes of aerodynamic drag observed previously in a car-platoon were no longer observable in the box in front of the oscillatory model in a box-platoon. A comparison of frames (a) and (e) in Figure 4.7, or (b) and (f) in Figure 4.8, suggested that the flow in the gap between the oscillating box and the model ahead showed strong hysteresis.

This phenomenon was also confirmed by Figure 4.9. In the left column of this figure, the oscillating (fourth) car resulted in synchronized drag variations on the car in front of it. However, the force change in the third box model fluctuated chaotically in the case of a four-box platoon (right column).

In all cases, the member farthest to the oscillating model had only minor force changes.

4.4.2 Effect of Displacement Amplitude

The effects of displacement amplitude during one model's oscillation motion are demonstrated in Figures 4.10 and 4.11. The experimental condition shown in this section is $v_{amp} = 1.0 m/s$ and the oscillating model is the third platoon member. In these two figures, the solid lines represent the case of $d_{amp} = 15.2 cm$ and dotted lines the case of $d_{amp} = 7.6 cm$. The drag coefficients of each platoon member are plotted as functions of time in the left column (frames (a)-(d)). The drag coefficients obtained in a clean platoon are also shown for comparison. In the right column (frames (e)-(h)), drag coefficients are presented versus the position of the "oscillating model". As shown in the figures, the third platoon member started its oscillatory motion at position 0, and the positive (negative) position was defined when the mobile model was ahead of (behind) its original location. Each curve was divided into two parts: the thicker half represented the data collected when the oscillating model moved from its upstream extreme to downstream extreme, and

the thinner part showed the same during the other half of the oscillation cycle. In most cases, the thinner curve overlapped well with its conjugate. This indicated that the flow was quasi-steady around the platoon member. Presenting the coefficients this way is a good measurement to determine whether the flow field is locked up by the motion of the oscillatory model. The ΔC_D or ΔC_F shown on each frame were defined as in Section 4.4.1.

Measurements in the four-car platoon were presented in Figure 4.10. The oscillating (third in this case) car had high force change values due to its inertia motions, and ΔC_F for $d_{amp} = 7.6cm$ was larger than $d_{amp} = 15.2cm$ because it needed a much higher acceleration to reach the set velocity in a shorter distance. The first car in the platoon (frames (a) and (e)) had very small force changes in both cases of $d_{amp} = 7.6cm$ and $15.2cm$, indicating that the flow around it was nearly undisturbed by the oscillating vehicle. The second car in the platoon experienced an in-line force that was synchronized with the disturbing model, as observed in Section 4.4.1. The magnitudes of the force change did not show strong dependence on the displacement amplitudes. However, ΔC_D of the fourth platoon member had a significant change which was around 50% of increase after $d_{amp} = 7.6cm$ was replaced with $15.2cm$. Both curves in frame (d) showed out-of-phase fluctuations by half a cycle with the oscillation.

Frames (e)-(h) in Figure 4.10 show how the force coefficients changes with the position of the oscillating car. It can be seen that the force data collected at the backward half-cycle motion was consistent with that in the forward half-cycle. The first car showed little effect of the oscillations. For the second vehicle, the drag decreased when the oscillating car approached it, and increased when it moved away. In contrast, the fourth car in the platoon experienced an increased drag when the third car moved forward (away from it) and the drag declined when the oscillating car was driven backward (toward the fourth car).

Figure 4.11 shows the same experimental condition applied to a four-box platoon. The first box (frames (a) and (e)) were only slightly affected by the oscillating box because the disturbing flow was blocked by the box between them. Unlike the case in the four-car platoon, the synchronization of drag experienced by the second platoon member had been broken here: the variation was not periodic. This was true for both cases of $d_{amp} = 7.6$

and $15.2cm$. As shown in frame (f), the drag coefficients did not follow the same pattern in their backward half cycles, as in the forward half. The force trajectories tended to form a close loop as they completed a cycle of oscillation. The chaotic drag variation caused up to 75% of the change, compared with the clean platoon value.

For the fourth box (frame (d) and (h)), which was behind the oscillating box, the pattern of force change was more predictable, as in a four-car platoon. The drag coefficients were 180° out-of-phase with the oscillation cycle. The ΔC_D for the case of $d_{amp} = 15.2cm$ was about twice the magnitude of $d_{amp} = 7.6cm$. The results indicated that the larger the displacement amplitude of the oscillating model, the bigger the aerodynamic force applied to its downstream neighbor.

4.4.3 Effect of Velocity Amplitude

The influence of the oscillation velocity amplitude is demonstrated in Figures 4.12 and 4.13. The test condition shown in this section is $d_{amp} = 15.2cm$ and the oscillating model is the third platoon member. Similar to the figures shown in Section 4.4.2, the left column (frames (a)-(d)) in Figures 4.12 and 4.13 presents the drag coefficients of each platoon member as functions of time, while the coefficients are plotted against the oscillating model's position in the right column (frames (e)-(h)). The ΔC_D or ΔC_F shown on each frame are as defined previously. The solid lines represent the case of $v_{amp} = 0.5m/s$, dotted curves $v_{amp} = 1.0m/s$, and dashed lines are measured at $v_{amp} = 2.0m/s$. The three conditions also represent the oscillating frequencies of $f = 0.5, 1$, and 2 respectively, (Table 4.2).

Data for the four-car platoon were presented in Figure 4.12. In all three velocities, the first platoon member (frames (a) and (e)) encountered very small changes in drag. The flow around it remained nearly undisturbed. The second platoon member, however, experienced a drag fluctuation caused by the oscillating car. The in-phase force variations with the oscillation did not show significant dependence on the velocity amplitude, as the ΔC_D values shown on frame (b). The oscillating model, which was the third in the platoon (frame (c) and (g)), had the highest ΔC_F value in the case of $v_{amp} = 2.0m/s$, and the

lowest when v_{amp} was $0.5m/s$. This was because a higher acceleration, and thus, a stronger inertia force, was required to reach the larger velocity amplitude in a fixed distance. The drag coefficients of the last car in the platoon(frame (d)) was 180° out-of-phase in all three velocity amplitudes. Again, the magnitudes of the ΔC_D did not show strong dependence on the velocity amplitudes.

All frames in the right column of this figure indicated that the drag coefficients followed similar traces in the backward half cycle as in the forward half. The overlap of all curves in frame (e),(f) and (h) also suggested that the forces did not vary significantly with different oscillation frequencies. About 15% drag variations were observed for the vehicles in front of the oscillatory car, and 10 % drag variation behind the oscillating car, in comparison with their clean platoon coefficients.

The four-box platoon results were shown in Figure 4.13. Similar to the previous figure, the first box (frames (a) and (e)) experienced very little aerodynamic drag change. The second platoon member, however, was affected strongly by the oscillating box model. The drag coefficients showed unstable fluctuations, regardless of the velocity amplitude. This phenomenon was better presented in frame (f), where the drag coefficients varied in unpredictable paths in all three cases, even though they returned to the starting value after a complete oscillation cycle. A 50% of drag change was found compared with the clean platoon values.

For the fourth box (frame (h)), the force coefficients showed strong dependence on the oscillatory model's position. When the oscillating model moved forward, the drag increased. When it was driven backward, the coefficients decreased. However, the force trajectories and the magnitudes of the force changed in similar manners in all three cases. The magnitudes of ΔC_D decreased with increased velocity. In Section 4.3, it was mentioned that the real displacement amplitude was shorter than the set value for higher velocity, because a heavy damper was used to smooth out the strong jerk of the motion. Therefore the changes of ΔC_D in frame (h) were probably more a result of the difference of the displacement amplitudes than the velocity amplitudes.

4.4.4 Comparison of Transient and Steady Results

Figure 4.14 presents the results of all steady measurements during oscillating conditions. In the experiments, each of the four platoon members was repositioned at nine different locations ($d = 0, \pm 1.9, \pm 3.8, \pm 5.7, \pm 7.6cm$ in Figure 4.2) within its "oscillating range". The drag coefficients of all models in the platoon were recorded when any of the positions changed.

In the steady-state measurements, the terms "oscillating car" and "oscillating box" are used to refer to the models in the platoon which has position changed, although it is not "oscillating" in time. The force data are then plotted as a function of the "oscillating" model's position. ΔC_D values for steady measurements are defined as the difference between the maximum and minimum coefficients collected at those nine locations for each condition.

In this figure, the left column represents data obtained in a four-car platoon and the right column a four-box platoon. The frames are organized in the order of the platoon member. For example, the coefficients of the first model in the platoon are shown in the first row, the second member in the second row, and so on. All curves in each frame have the same value when d is zero, because it represents the drag coefficients measured in a clean platoon.

The trends of force change are more predictable for a four-car platoon than a box-platoon. The left column of Figure 4.14 shows that the drag coefficient of each oscillating vehicles in the platoon, except the last, increases when it is positioned toward the upstream direction; the drag decreases when it moves to a downstream position. The fourth car, however, has an opposite trend in drag change with the previous three cases; it experiences less drag when d is positive, and more drag when it moves backward.

In most cases, the position changes of any platoon member only had significant influence on its adjacent neighbors. The drag coefficient of the platoon member right in front of the position-changed vehicle tended to decrease when its downstream partner had a closer spacing (d was positive). The measured coefficients increased when the downstream vehicle was moved backward. For the vehicle right behind the "oscillating model", the trend of drag change was just opposite. The drag coefficients of car 2-4 in the platoon increased

as their upstream neighbor was moved away from it. The coefficient curve of the second platoon member turned flat as d became positive, probably because it was measured by the defective force balance.

In the event of a four-box platoon, as shown in the right column of Figure 4.14, the force changes did not seem to have a regular pattern. The drag coefficients of the leading box, when it was used as the "oscillating model", did not show strong dependence on the model's position. Furthermore, a contrary trend to what was discovered in a four-car platoon was observed when the second and third box models were repositioned. It has been found that less drag force acted on them when they were moved forward. The results for the last box in the platoon was consistent with what we obtained in a car platoon, that the drag tended to decrease as the model was moved from downstream to upstream.

On the other hand, the members adjacent to the "oscillating box" did not show the almost-monotonous changes with the oscillating model's new position like that observed in the four-car platoon. The drag measurement of the leading box in the platoon did not respond significantly to the position change of the box that followed it. In frames (f) and (g), it was found that the box that was followed by the "oscillating model" was very sensitive to the downstream model's position. In both cases, the upstream box experienced a sudden increase of drag when the "oscillating model" was moved forward from $d = -1.9cm$ to $d = 1.9cm$.

Generally speaking, ΔC_D shown in each frame indicated that the drag changes were almost negligible for platoon members not in immediate proximity of the "oscillating model". The only exception was the force experienced by the third platoon member when the leading model had its position changed. As shown by the '+' symbols in frames (f) and (g), when the first platoon member's position was changed, the second and third boxes experienced similar drag changes. Both drag curves had concave shapes when d was less than zero, with highest and second highest coefficients measured in its most downstream and zero positions. When the leading "oscillating model" was moved in a direction of away from them, the drag coefficients of both the second and the third boxes tended to decrease with the increased d. In the case of the drag force experienced by box 3 and box 4 when the

model in front of it had position changed, the results were similar to the case of a four-car platoon. The coefficients had an almost-monotonous increase with the oscillating model's position, as shown as '△' symbols in frame (g) and '•' in (h).

To compare the results obtained in the transient and steady state measurements, selected data in Figure 4.12 - 4.14 are replotted in Figure 4.15. The selected testing condition for the transient measurements is $d_{amp} = 15.2cm$ and $v_{amp} = 0.5m/s$, and the oscillatory model is the third platoon member. The left column in Figure 4.15 represents the data collected in the four-car platoon while the right column contains information of the four-box platoon. The circles show the drag coefficients of each platoon member obtained in steady state when the third model's position is changed. The solid curves show the results from transient measurements when the third platoon member is oscillating. Each transient curve is divided into two parts, and each part demonstrates the force change in half oscillating cycle, as described in Section 4.4.2 and 4.4.3. All coefficients are plotted with respect to the oscillating model's position, with their ΔC_D or ΔC_F values shown on the upper left corner in each frame.

The first member, either in the four-car or four-box platoon, experienced very little force change in both steady and transient investigations. Apparently, this was because the the model was shielded from the disturbances by the model between them. The steady and transient measurements on the oscillating model were not comparable (frames (c) and (g)), because the inertia force was dominating the aerodynamic measurements during its time-dependent motion. For the members adjacent to the oscillating model (see frames (b), (d) and (f), (h)), it was shown that the change of steady force had almost the same trend to that of the transient results. The agreements have been observed both qualitatively and quantitatively. For the second model in a four-box platoon (frame (f)), the steady-state measurement had a dramatic change, which may be explained by the curve measured in the transient state. The transient curve, showing a wild trajectory in its forward and backward half cycles, suggested that highly unstable flow existed in the gap between the second and the third box models.

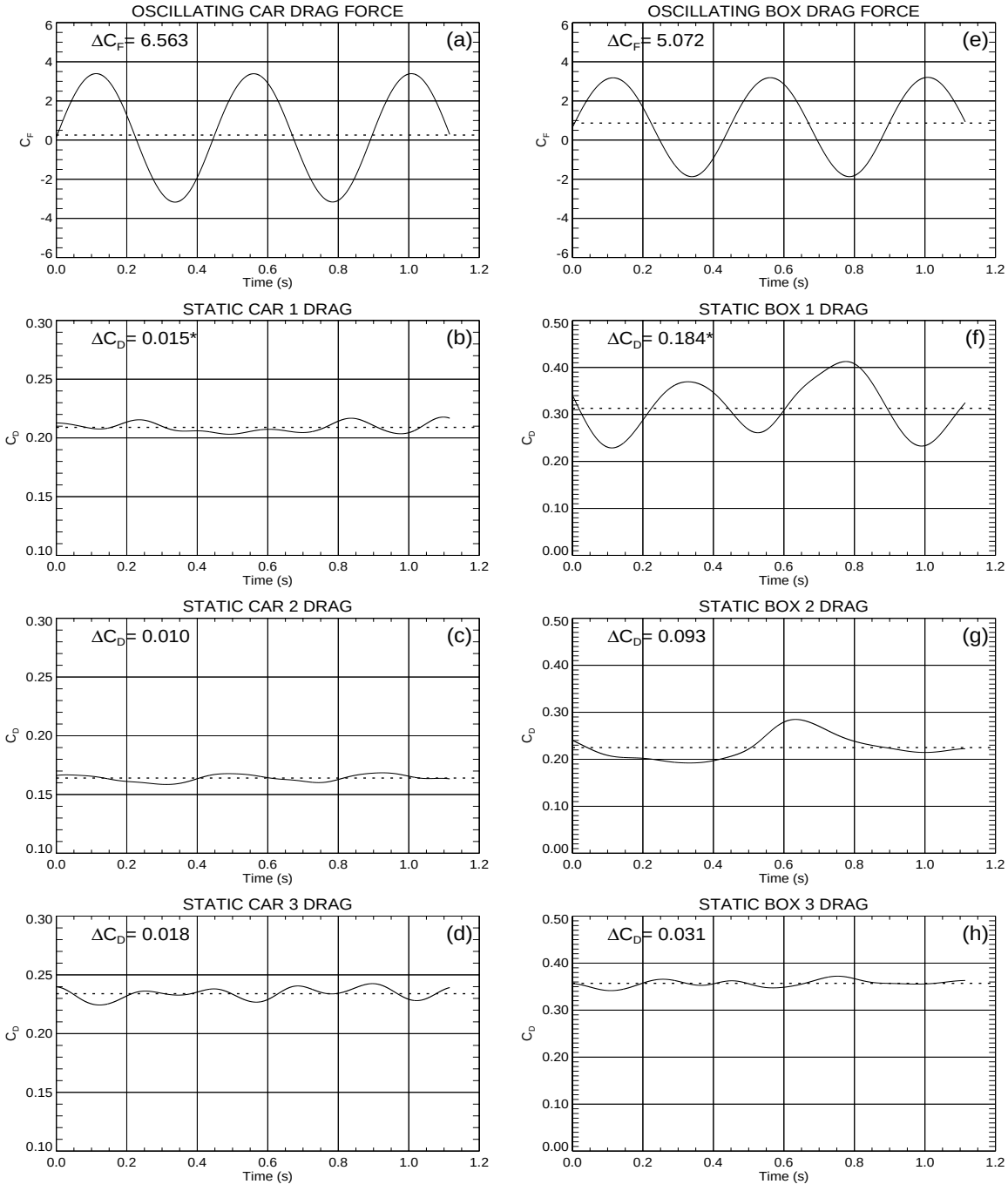

Figure 4.6: Effect of oscillation location and shape of the models — location = #1
The experimental condition is $d_{amp} = 15.2cm$ and $v_{amp} = 2.0m/s$. The drag coefficient on each member in a four-car platoon [frames (a)-(d)] and a four-box platoon [frames (e)-(h)] are shown with respect to time.

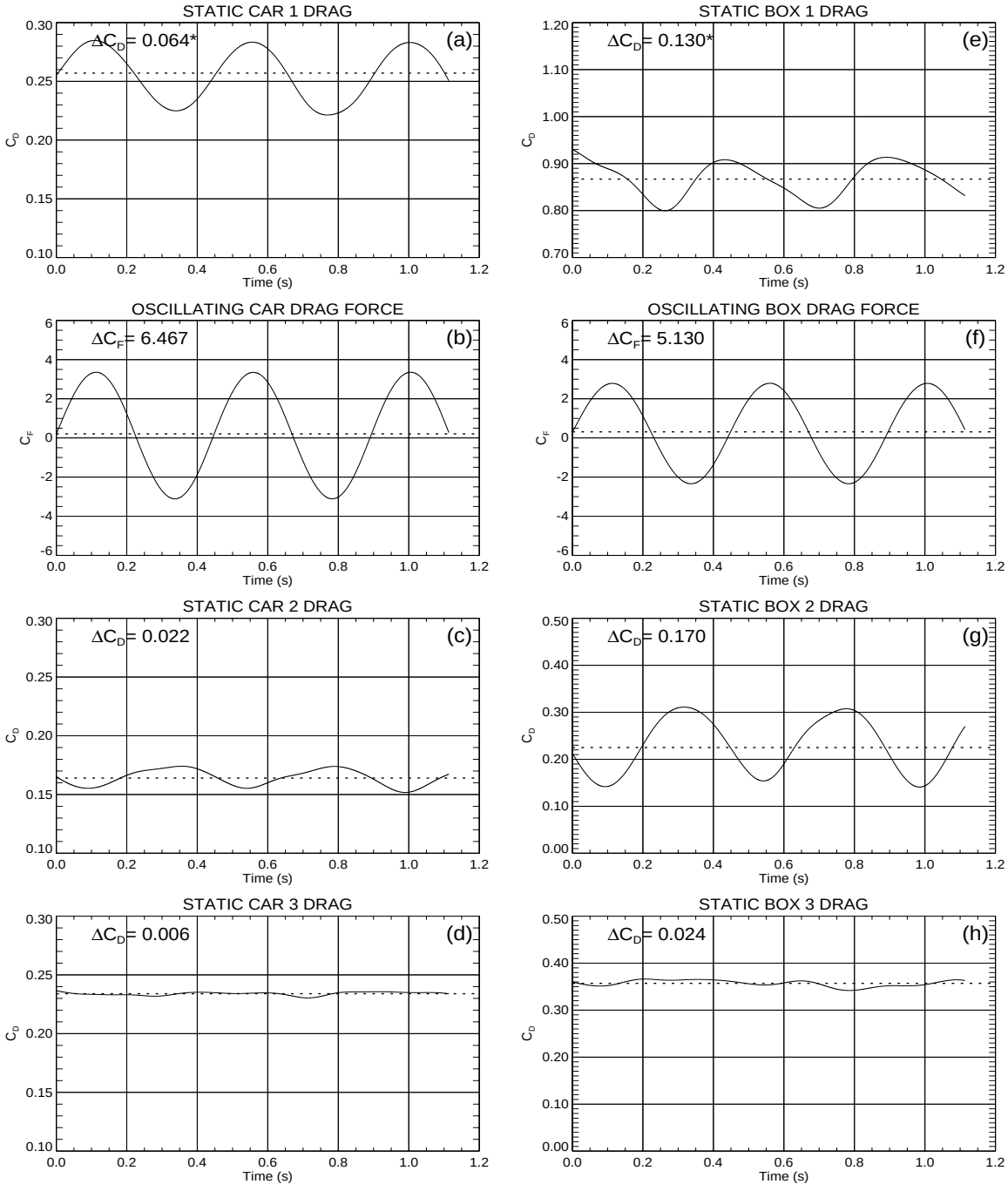

Figure 4.7: Effect of oscillation location and shape of the models — location = #2
The experimental condition is $d_{amp} = 15.2cm$ and $v_{amp} = 2.0m/s$. The drag coefficient on each member in a four-car platoon [frames (a)-(d)] and a four-box platoon [frames (e)-(h)] are shown with respect to time.

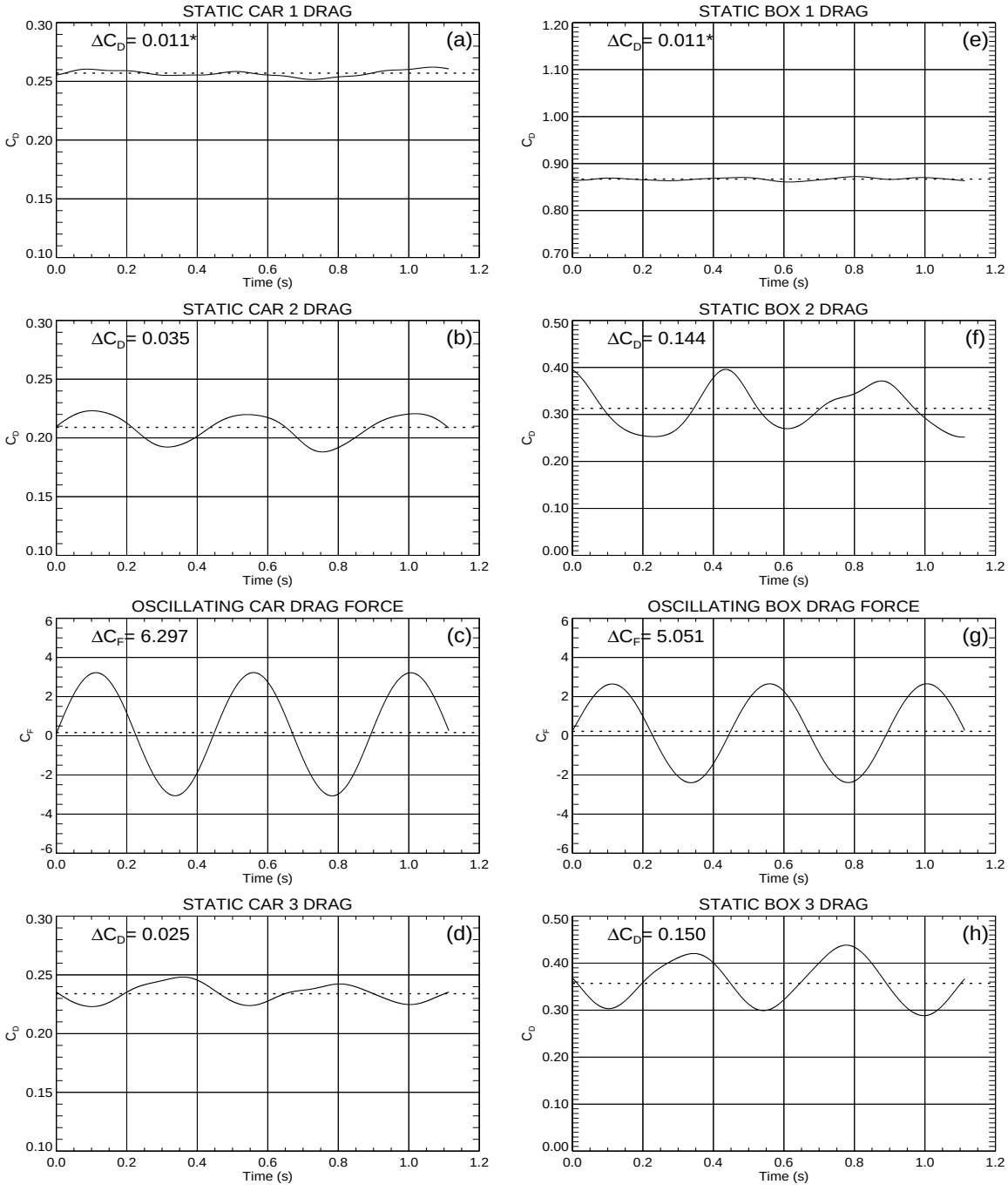

Figure 4.8: Effect of oscillation location and shape of the models — location = #3 The experimental condition is $d_{amp} = 15.2cm$ and $v_{amp} = 2.0m/s$. The drag coefficient on each member in a four-car platoon [frames (a)-(d)] and a four-box platoon [frames (e)-(h)] are shown with respect to time.

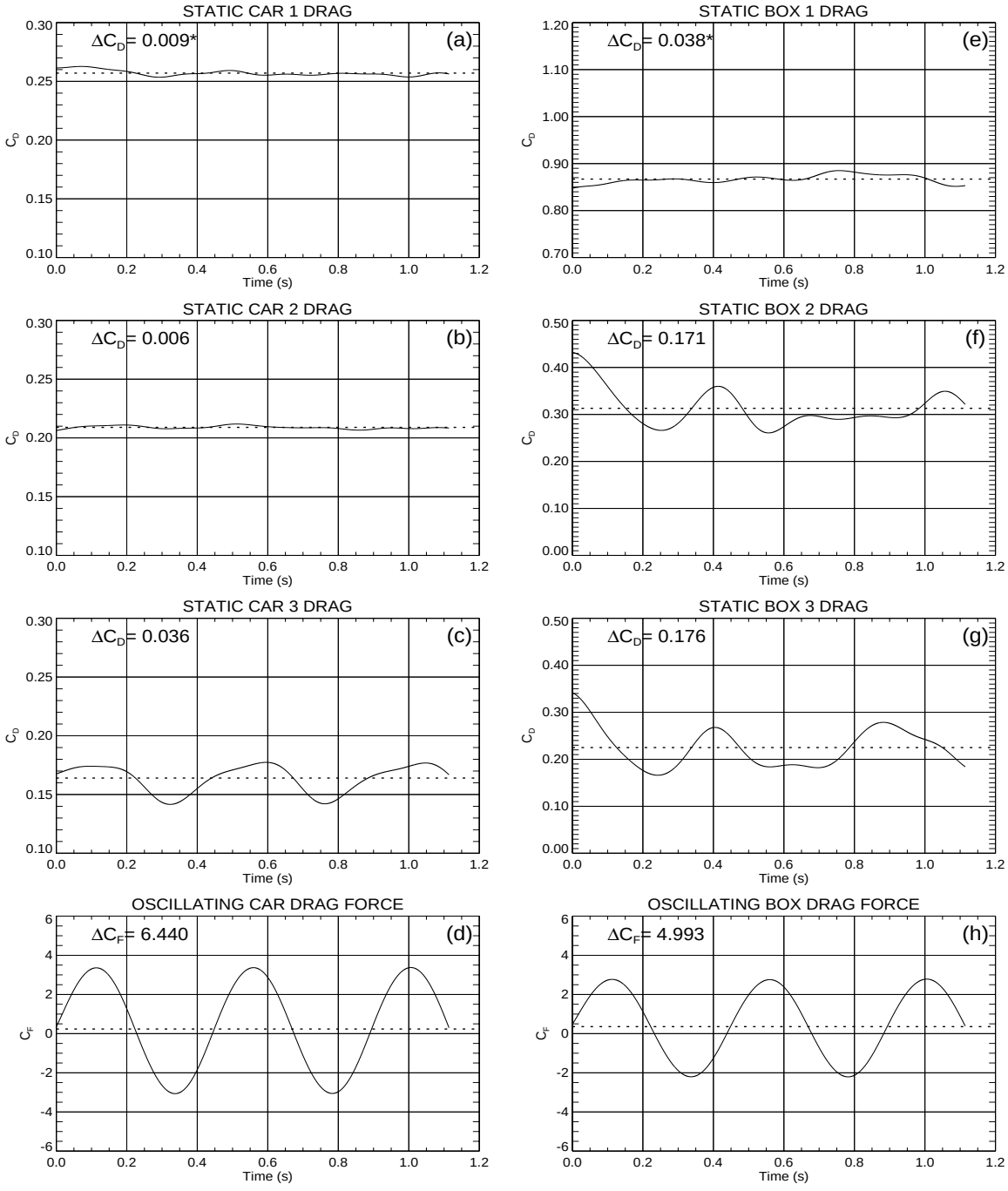

Figure 4.9: Effect of oscillation location and shape of the models — location = #4
The experimental condition is $d_{amp} = 15.2cm$ and $v_{amp} = 2.0m/s$. The drag coefficient on each member in a four-car platoon [frames (a)-(d)] and a four-box platoon [frames (e)-(h)] are shown with respect to time.

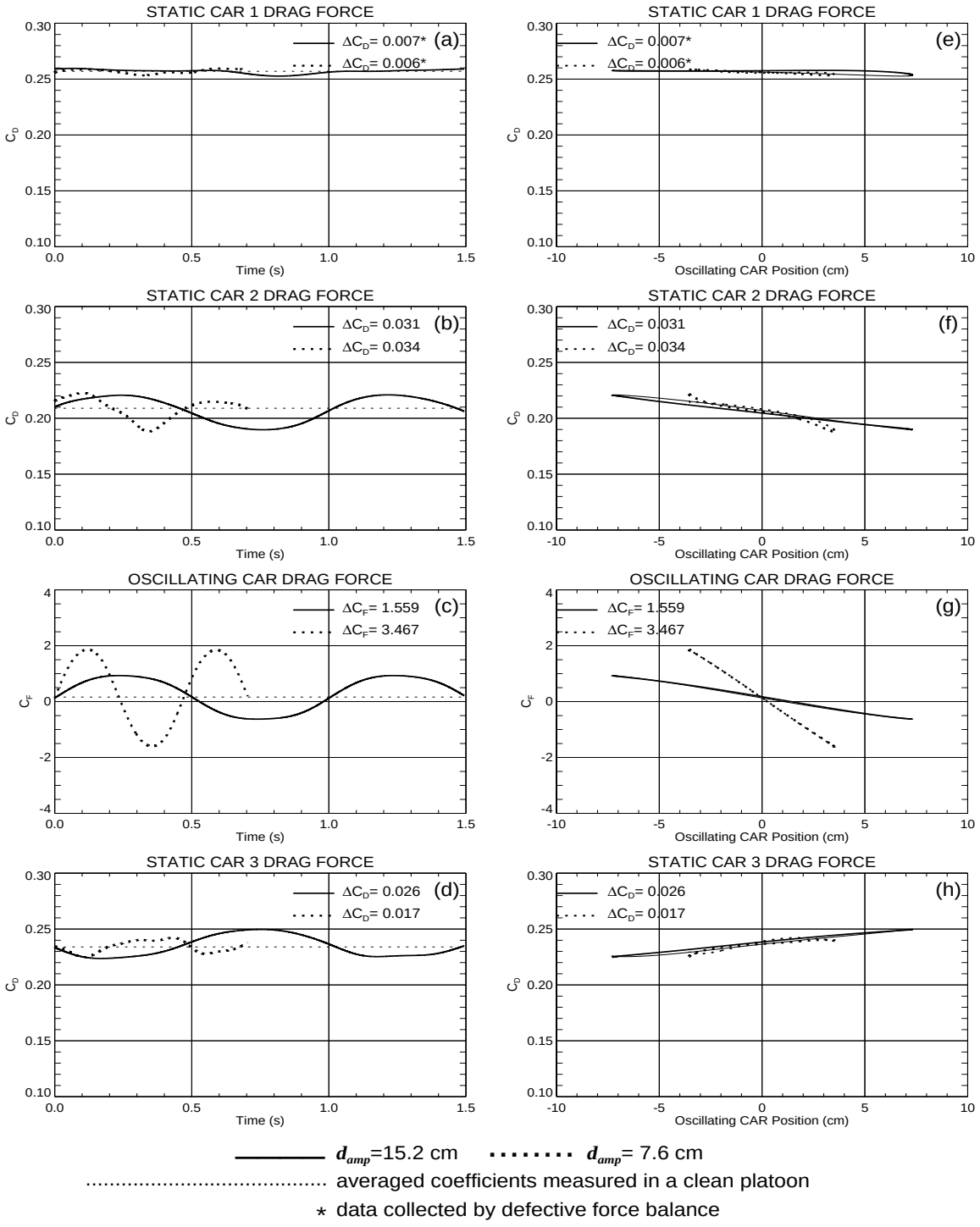

Figure 4.10: Effect of displacement amplitude — a four-car platoon ($v_{amp} = 1.0 m/s$) The drag coefficient on each platoon member are shown with respect to time [frames (a)-(d)] and the oscillating car position [frames (e)-(h)].

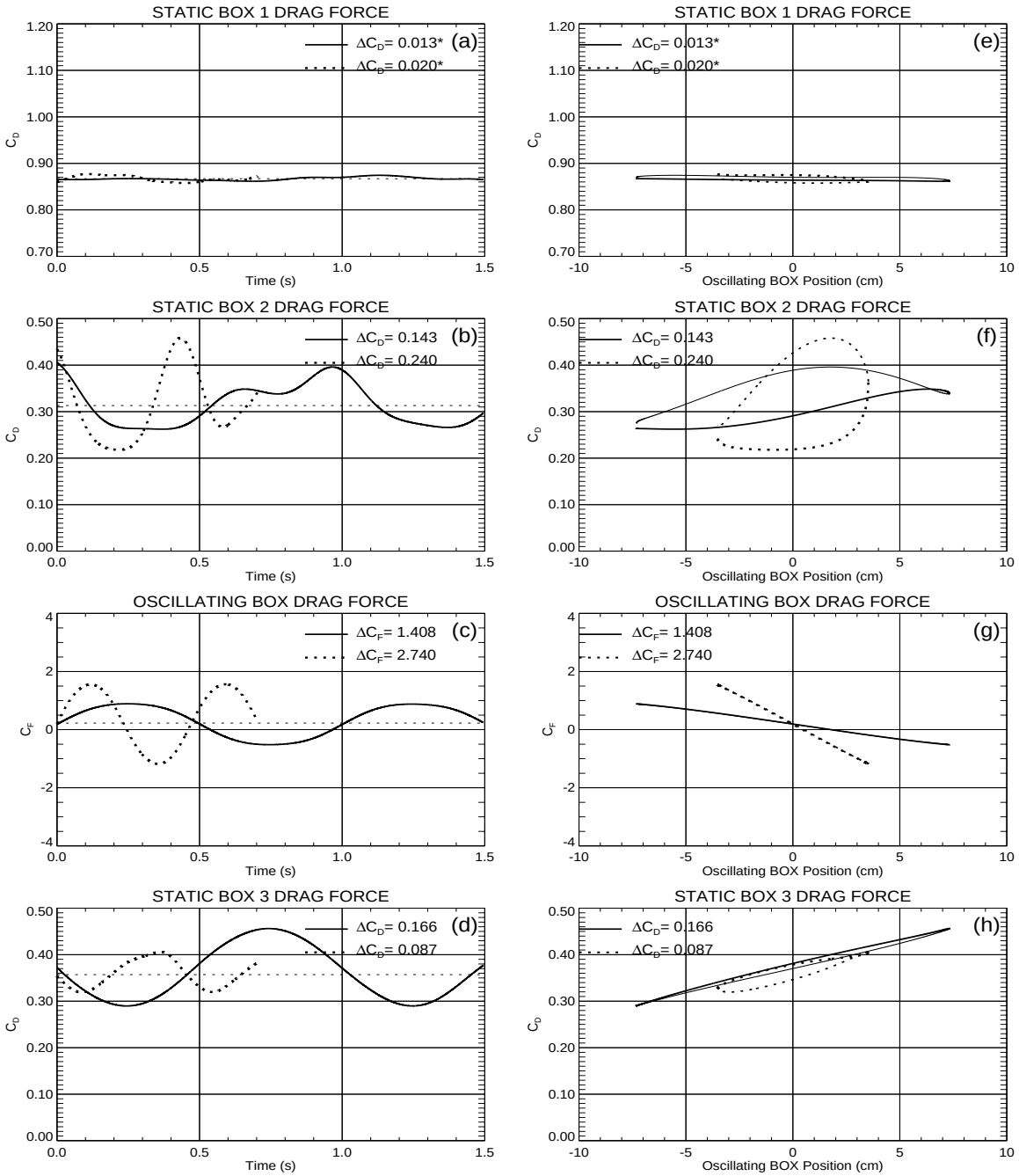

Figure 4.11: Effect of displacement amplitude — a four-box platoon ($v_{amp} = 1.0m/s$) The drag coefficient on each platoon member are shown with respect to time [frames (a)-(d)] and the oscillating box position [frames (e)-(h)].

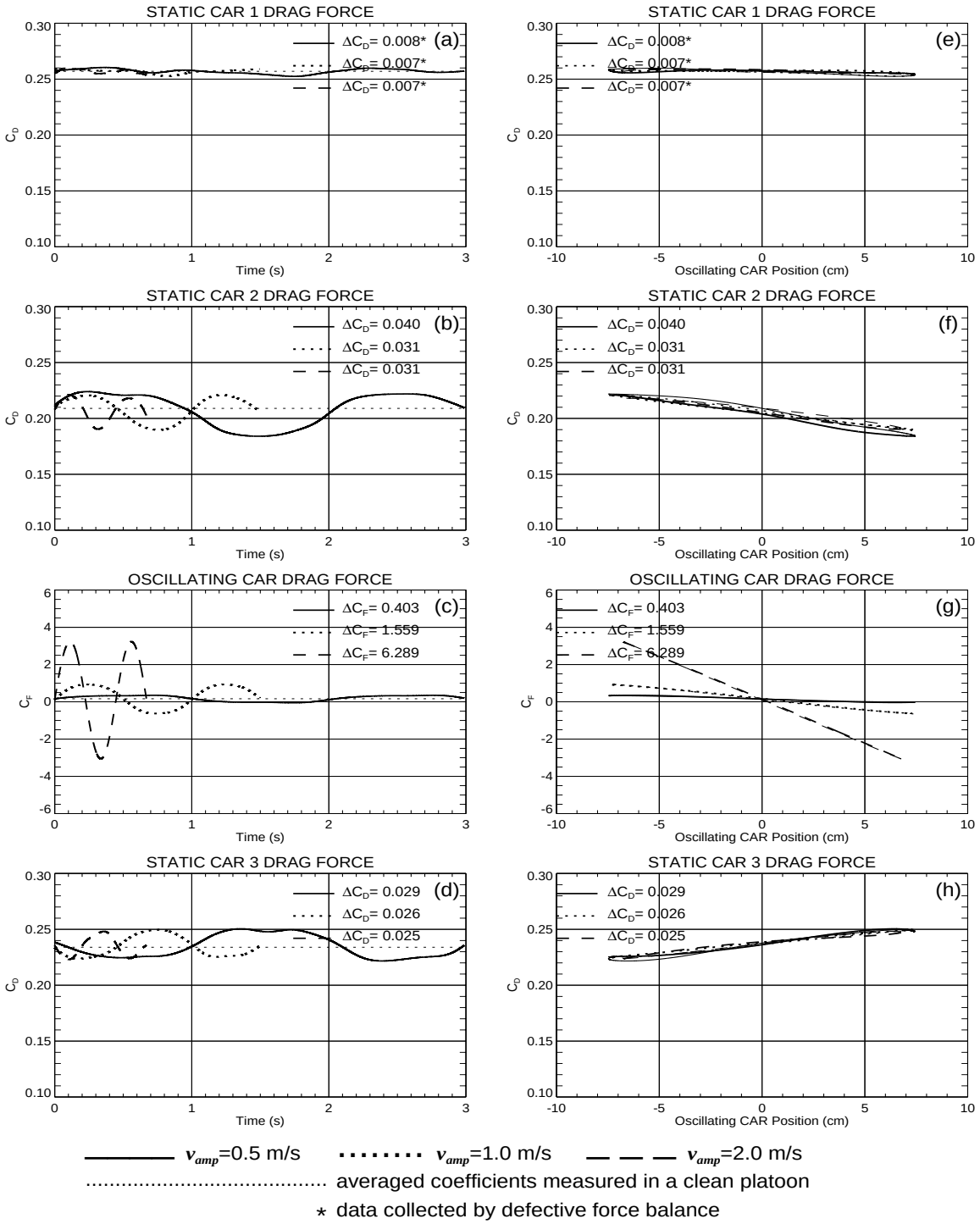

Figure 4.12: Effect of velocity amplitude — a four-car platoon ($d_{amp} = 15.2cm$)
The drag coefficient on each platoon member are shown with respect to time [frames (a)-(d)] and the oscillating car position [frames (e)-(h)].

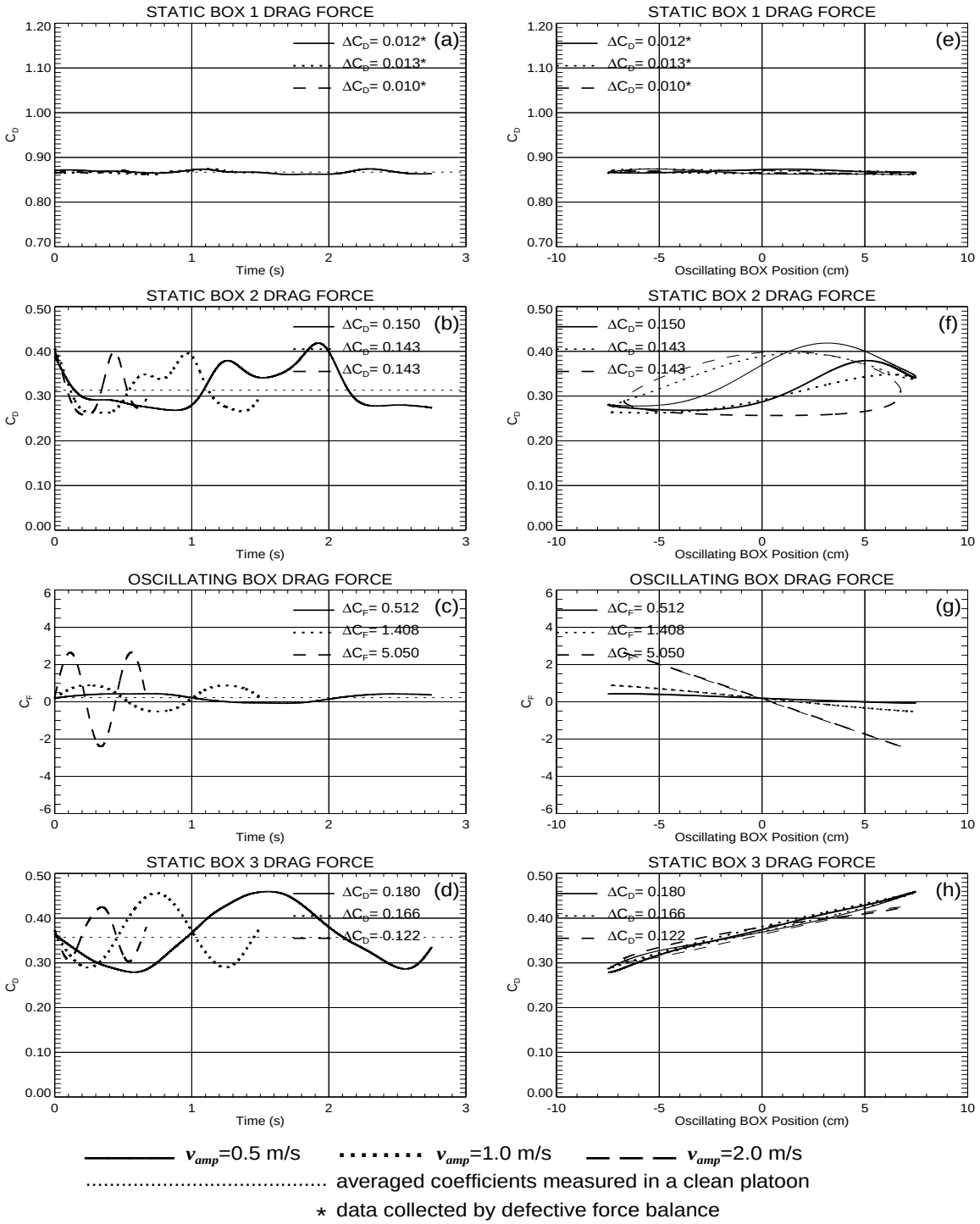

Figure 4.13: Effect of velocity amplitude — a four-box platoonn ($d_{amp} = 15.2cm$) The drag coefficient on each platoon member are shown with respect to time [frames (a)-(d)] and the oscillating box position [frames (e)-(h)].

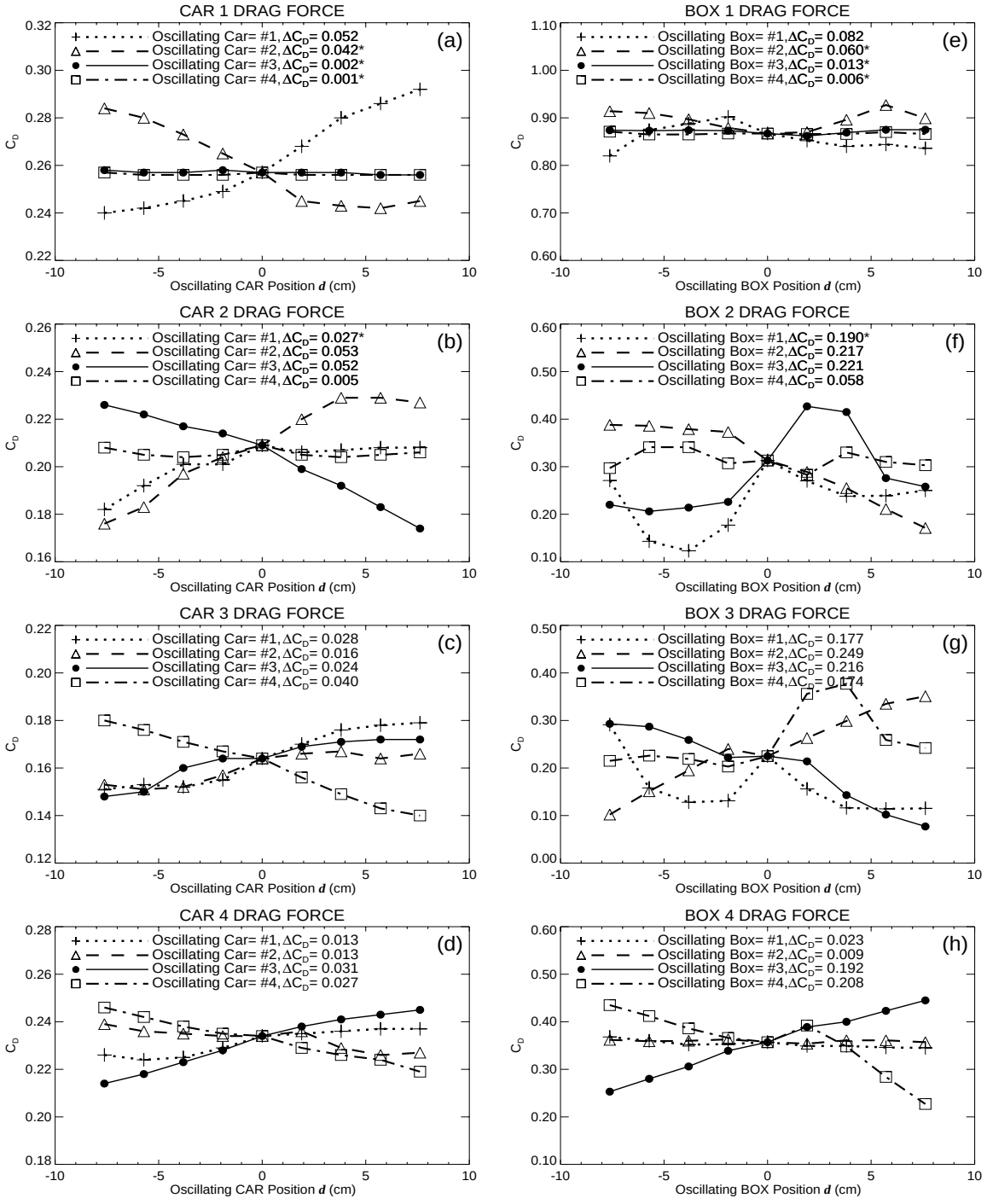

Figure 4.14: Steady results with one platoon member has position changed
The drag coefficient on each member in a four-car platoon [frames (a)-(d)] and a four-box platoon [frames (e)-(h)] are shown with respect to oscillating model's position.

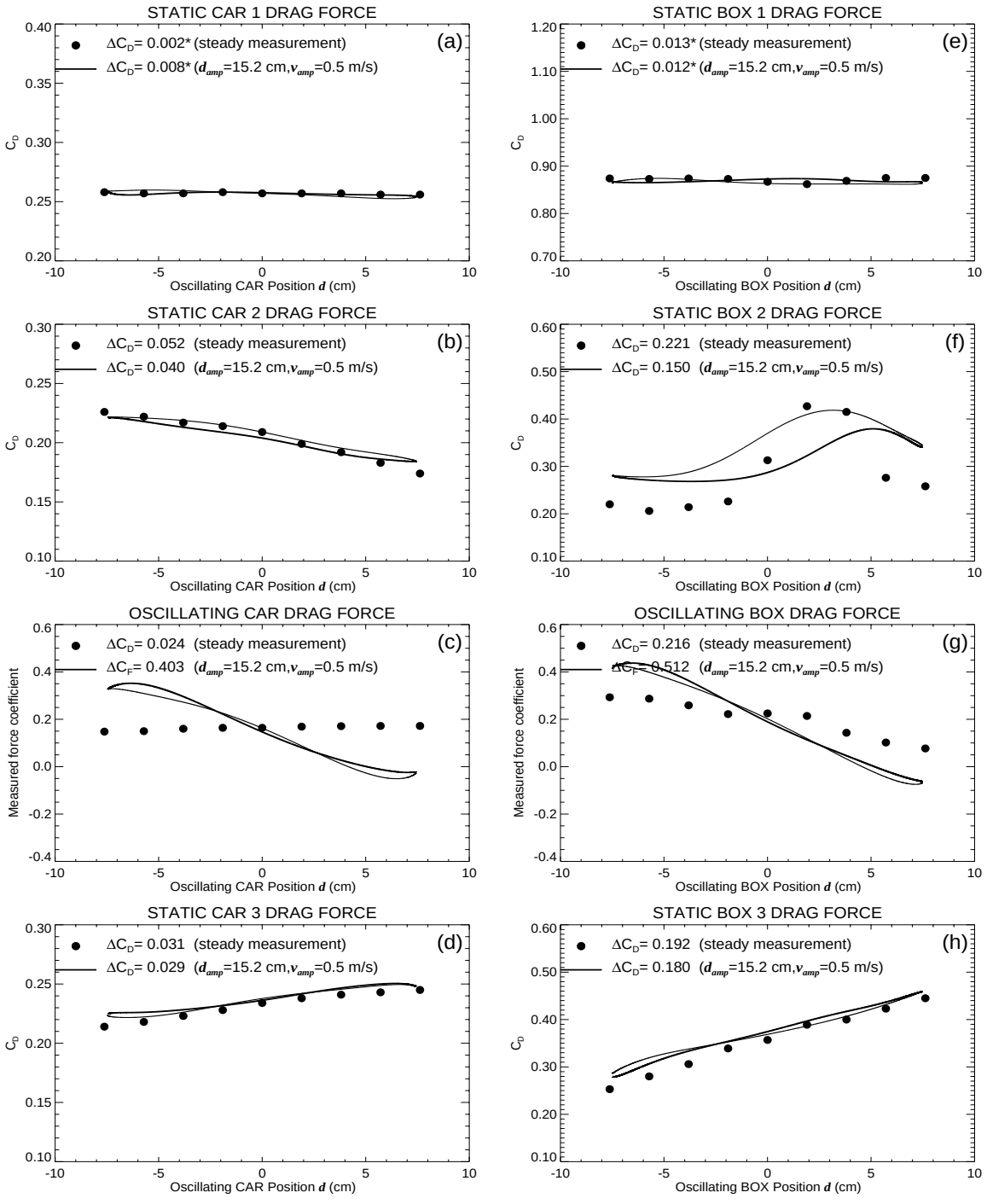

Figure 4.15: Steady measurements versus transient results ($d_{amp} = 15.2cm, v_{amp} = 0.5m/s$) The drag coefficient on each member in a four-car platoon [frames (a)-(d)] and a four-box platoon [frames (e)-(h)] are shown with respect to oscillating model's position.

4.5 Discussion

The results obtained in last section disclosed some interesting phenomena which are discussed here. The steady results are compared with data from previous work in similar topics first, and they are explained using a "cavity drag" model in this section. The transient results are then analyzed. The potential causes of errors are discussed last.

4.5.1 Steady-State Measurements

When the platoon members are all stationary in the wind tunnel, the aerodynamic drag is mainly caused by the difference between front and base pressures of each model. It has been confirmed that, for a row of bluff bodies at close spacings, the flow separating from the front body can smoothly reattach to the corner of the downstream body [29][30]. Gharib [30] studied the relation between the flow oscillations in the cavity shear layer and the cavity drag. He concluded that when the flow traveled over a cut-out, a low-drag regime was always associated with the fact that the cavity shear layer attached at the downstream corner. When the shear layer impinged on the downstream wall that was below the corner, higher cavity drag was observed.

There is an analogy between the current study and the cavity investigation. The gap between two adjacent platoon members can be considered as a cavity, especially for the box models in the present study. However, in our oscillation tests, when any platoon member had its position changed, it usually involved variation of both its front and back gaps simultaneously. The only exceptions were the cases that the first or last platoon member was the oscillating model, which provides an opportunity to examine our data by the cavity analysis.

Figure 4.16 shows the steady results of the third and fourth platoon members when the spacing between them is changed by manually moving the latter model to nine various locations. (The data of the first and second platoon members were not chosen because some of them were measured by the defective force balance.) Both results of cars and boxes were shown in this figure. Data reproduced from Zabat et al. [22] and Romberg [31], showing that the drag obtained in two tandem vehicles with various spacings, were also included in

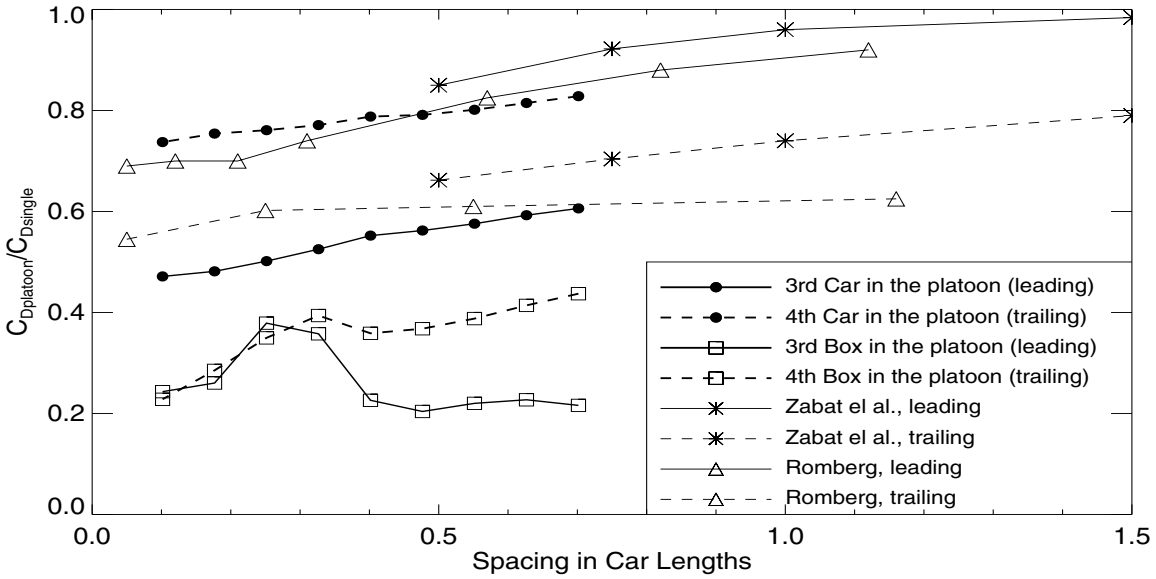

Figure 4.16: Drag variation with inter-vehicle spacing

this plot for comparison. The drag coefficients were normalized by the coefficient of a single vehicle model in isolation. They were plotted with the spacing in vehicle lengths.

It should be noted that, generally speaking, in a two-car platoon the leading model experiences higher drag than the rear one because the latter is shielded by the former. The present data in this figure showed that the fourth model (downstream) had higher drag coefficients than the third model (upstream). This was mainly because the third model experienced the lowest drag in a four-car platoon (see Chapter 2).

As can be seen in the figure, except the present data of the leading box, in general all curves indicated the drag coefficients increased with the increasing spacings. The phenomenon could be explained by the cavity analysis. The bigger the gap is, the more difficult for the flow over it to attach to the corner of the downstream model, thus results in a higher cavity drag. A higher cavity drag means a larger pressure on the downstream wall (front face of the rear model) or lower pressure on the upstream wall (base face of the front model). Therefore higher drag forces are measured by both the front and the downstream models.

The drag observed in our car data supported this conclusion. The downstream box (the fourth in the platoon) also agreed with the trend that wider gaps caused greater drags,

except a small dip was found when the spacing was about 0.4 vehicle length. However, the drag on the upstream box (the third in the platoon) first increased with the increment of the spacing, then suddenly dropped after the gap bigger than 0.25 car length. Note the descent occurred at about the same spacing that its upstream model had the dip, implying some flow structure in the cavity changed when the spacing was around this range. When the gap width was greater than 0.4 vehicle length, the drag ratio of the third box was stabilized and the values stayed around 0.2. The reason why the upstream box had a sudden drag reduction at certain range of spacings was unclear. Further investigation is required to understand this phenomenon.

The above arguments can also apply to intermediate vehicles in a multi-vehicle platoon. Figure 4.17 gives an example how the base and front pressure, and thus the drag force of each car, change due to variation in the inter-vehicle spacings.

In this figure, frame (a) demonstrates a three-car platoon with close and uniform longitudinal separations. The second car moves forward in frame (b), leaving more space behind and closing the gap in front of it at the same time. The smaller distance between car 1 and 2 causes a higher base pressure on car 1 and lower front pressure on car 2. Assuming the flow in front of car 1 is affected little, the larger base pressure helps to reduce the drag experienced by car 1. A higher cavity drag resulting from the larger gap between car 2 and 3 causes higher front pressure on car 3 and decreased base pressure on car 2. Therefore the drag of car 3 increases. The results have been observed and discussed in Section 4.4.4, where the center vehicle's drag coefficient was found to increase when it was moved forward. The higher drag experienced by car 2 is obtained because the reduction of its base pressure is larger than the decrease of its front pressure. Frame (c) in this figure shows the condition when car 2 moves behind its original position. Similar analysis can explain why the drag of car 1 becomes larger while that of car 2 and car 3 shrink.

Compared with the steady force measurements for a four-car platoon, the drag experienced by each member in a four-box platoon was much more irregular and unpredictable when one changed positions. It was observed that under certain conditions, a slight change of the cavity widths may cause wild drag variations. It also appeared that at some critical

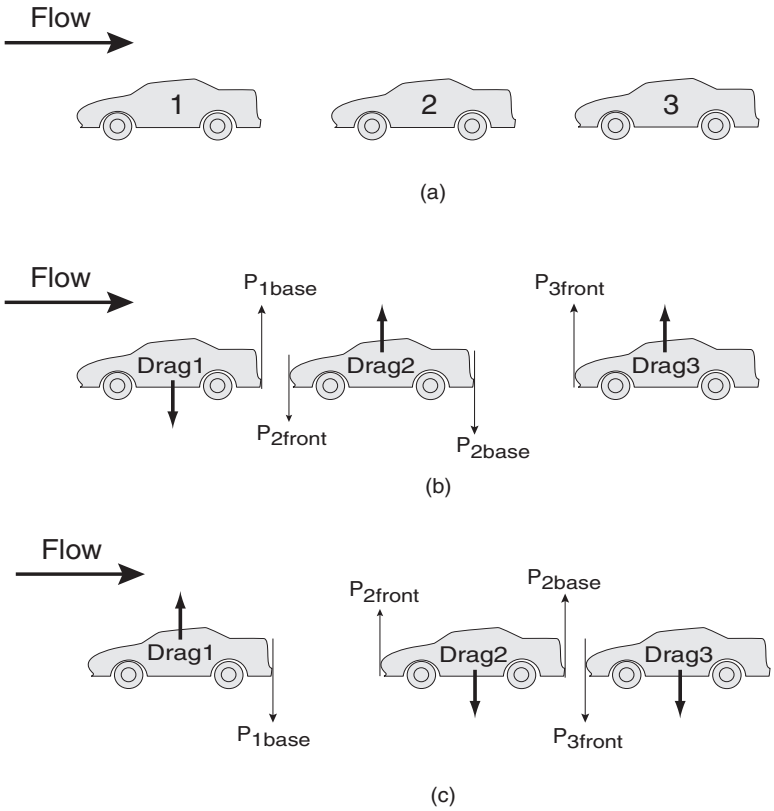

Figure 4.17: Pressure and drag variations with non-uniform inter-vehicle spacings Frame (a) shows three vehicles in a row with uniform inter-vehicle spacing; (b) and (c) show the pressure and drag change of all three cars due to non-uniform spacings

spacings around 0.3 car length, the flow structure has a dramatic change. The current study of force measurements on each box, however, were not sufficient to explain these findings. Further experiments including flow visualization are necessary to explain the phenomenon.

4.5.2 Transient Measurements

As described in Section 4.2, the oscillating model's in-line vibration induces the flow motion in the gaps between itself and its neighbors. In view of its front neighbor, the upstream model is under the influence of a time-dependent local pulsatile flow on its back and a uniform tunnel flow elsewhere. Similarly, the oscillating car's downstream neighbor experiences a local pulsatile flow on its front end. Therefore the drag force experienced by

the models next to the oscillating car is a combination of the steady aerodynamic load and the added mass effect due to the accelerating flow.

However, consider the case of a sphere in an accelerating flow, equation (4.4) suggests that the induced force is proportional to the fluid's density and the body's acceleration. It has been observed in Section 4.4.3 that the drag coefficients do not depend significantly on the oscillating model's velocity amplitudes. For fixed displacement amplitudes, it also means that the measured force changes little with the oscillating car's acceleration. Since the density of air is so small, and very little force dependence on the mobile model's acceleration is observed, the contribution to the drag coefficients from the accelerating flow may be ignored.

Figure 4.15 confirms that the transient measurements agree well with the steady forces, both qualitatively and quantitatively, suggesting that the non-equilibrium aerodynamic force only played a minor role. Owing to the consistence of the transient and steady results, cavity drag analysis can also apply to explain the drag variations experienced by each platoon member during in-line oscillations.

4.5.3 Potential Causes of Errors

Conducting this series of experiments is difficult not only because the complexity of the flow field, but also due to the difficulty in integrating all the hardware involved. Some potential causes of errors are discussed in this section.

First of all, we have experienced very high levels of electrical noise generated by the servomotor. These noises had been eliminated by a digital filter after the data collection, which only let signals within a specific range of frequencies pass through. Although it had worked very well in the passing tests (Chapter 3), the filter may still accidentally suppress some useful information here.

Second, as mentioned previously, after the experiments we discovered one of the force balance may be defective. This specific force balance may cause incorrect quantitative data which labeled "Static Car 1 Drag" and "Static Box 1 Drag" in figures in Section 4.4. The potential errors in the data collected by this specific balance resulted in an incomplete

quantitative data analysis.

Moreover, during the experiments, the speed of wind tunnel flow was gradually declining. Although all the aerodynamic forces were normalized by the dynamic head and presented as nondimensional coefficients, we did find the force coefficients affected by the non-consistent flow.

Last, the Wind Tunnel Actuator (WTA) employed in this study was constructed with relative low weight to reduce the whole system's inertia. However, when the oscillatory model traveled with a high frequency, the hard motion may bring the WTA to a slight vibration. While the WTA fitted into a slot in the wind tunnel test section, its front and rear end also touched the wind tunnel ground plane where the force balances were mounted on. Therefore the vibration of the WTA may result in some small impulses to the force balances and uncertainties to the data taking. The shake was checked carefully after the experiments. Among all six combinations of velocity and displacement amplitudes, the vibrations were barely felt by human fingers except the case at $v_{amp} = 2m/s$ and $d_{amp} = 7.6cm$. The effects of the vibration were also checked by reading the outputs from the force balance directly. The readings appeared negligible.

Despite these various uncertainties may influence the results somewhat, the experiments were basically under well control. According to the data collected in this study, the force measurements were not affected significantly by the detrimental factors.

4.6 Summary

Due to the symmetric configuration in the longitudinal oscillations, only drag force measurements were presented and discussed in this study. During the experiments, one of the four cars/boxes in the platoon was used as the oscillatory model, and the drag force experienced by all four platoon members were obtained. The factors studied include the location of the oscillating model, the shape of the model, and the displacement and velocity amplitudes of the oscillation. Both transient and static measurements were conducted.

The major observations and discoveries in this chapter are:

1. Significant force changes are observed on the platoon members which are adjacent to the oscillating model.

2. The trend of force change is more predictable for a four-car platoon than a four-box platoon. The magnitudes of force changes are larger for box models.

3. Static and transient measurements show consistent trends of force change. These results can be explained by cavity drag analysis, that bigger gap induces higher cavity drag and smaller gap causes lower cavity drag. A critical spacing of about 0.3 vehicle length is observed for the box models. The drag force experienced by the upstream box shows a dramatic drop when the gap is close to the critical spacing.

4. Regardless of the oscillation location, the transient results show that the downstream member to the oscillating model has an out-of-phase drag fluctuation by half a cycle. An in-phase drag variation with the oscillation cycle is observed for the upstream neighbor of the vibrating vehicle in a four-car platoon. In the case of a four-box platoon, the box in front to the oscillatory model experiences chaotically changed drag.

5. The oscillating model's displacement amplitudes have a strong impact to its downstream neighbor. The bigger the amplitude is, the more pronounced force is observed for the model behind it. However, for the upstream neighbor, the dependence of the force and the oscillation displacement amplitude is inconclusive.

6. Force experienced by all platoon members do not show strong dependence on the oscillation velocity amplitude.

Chapter 5

Conclusions

In this study, both the steady and transient natures of the aerodynamic forces in vehicle platoons have been investigated. By measuring the steady drag force experienced by the individual members of a multi-vehicle platoon, it has been confirmed that the more the members in the platoon, the more drag reduction found in terms of the average. Moreover, less drag forces act on the interior platoon members than the exterior ones. In both cases of a four-car and a four-box platoon, the third member from the lead vehicle has the smallest drag coefficient.

In the first transient platoon experiments, it has been discovered that the aerodynamic effects on the members of a four-car platoon during passing maneuvers are very similar to the reaction of a single car when it is overtaken by another vehicle. An overtaken car in the platoon experiences a repulsive side force when the passing vehicle is in the neighborhood of its rear half. The side force reverses its direction and becomes an attractive force when the passing vehicle moves to the proximity of its front half. In addition, the drag coefficient on the overtaken car increases when the passing vehicle is in its proximity. Both the lateral spacing and the relative velocity between the overtaking and overtaken vehicles are determined to be influential factors. When they are reduced, both the drag and the side forces experienced by the passed car are increased. The trends of force change observed in the steady and the transient measurements agree with each other. Similar trends of force changes have been observed in both cases of a vehicle passing a platoon and a vehicle overtaken by a platoon, but smaller force coefficients are recorded when the vehicle is in

backward relative motion (platoon passing). This result could not be duplicated in the steady flow measurements. The forces acting on the platoon members are increased when the passing car is replaced with a rectangular box.

The second transient experiments were conducted when one of the platoon members undergoes forced in-line oscillations. Significant drag force changes have been recorded on the platoon members which are adjacent to the oscillating vehicle. In the case of a four-car platoon, it has been found that when the oscillating car moves forward and approaches its upstream neighbor, itself and its downstream neighbor experiences an increased drag, but its upstream neighbor experiences a decreased drag. Opposite results have been obtained when the oscillating car moves backward and away from its front neighbor. In the case of a four-box platoon, a similar pattern has been observed for the downstream member to the oscillating box. However, the member in front of the oscillating box experiences a chaotically changing drag force. Steady measurements show similar results to the transient measurements, even the hysteric behavior for the upstream member to the oscillatory box.

A cavity drag model can be used to explain the force variations experienced in the four-car platoon. A bigger gap between the vehicles induces a higher cavity drag which results in the changes of the vehicles' front or base pressure. This model, however, does not apply to the box ahead of the oscillating box. A critical spacing of about 0.3 vehicle length has been observed, where the drag force experienced by the upstream box shows a dramatic drop. The drag experienced by all platoon members have not shown strong dependence on the oscillation frequency. The dependence of the drag force on the displacement amplitude of the oscillation is inconclusive.

Bibliography

[1] Hedrick, J. K., Tomizuka, M., Varaiya, P., "Control Issues in Automated Highway Systems", *IEEE Control Systems Magazine*, Vol. 14, No. 6, 21-32, 1994.

[2] Shladover, S. E., "The California PATH Program: A State Approach to IVHS Research", *Vehicle Electronics Meeting Society's Needs: Energy, Environment, Safety, Proceedings of the 1992 International Congress on Transportation Electronics*, 92C018, 329-338, 1992.

[3] *California PATH Annual Report*, 1998.

[4] Howell, J., "Catastrophic Lift Forces on Racing Cars", *J. Wind Eng. Ind. Aerodyn.*, Vol. 9, 1981.

[5] Scibor-Rylski, A. J. , *Road Vehicle Aerodynamics*, Pentech Press, London, 1975.

[6] Hucho, W. -H. (ed.), *Aerodynamics of Road Vehicles*, SAE Inc., Warrendale, 1998.

[7] Hucho, W. -H., Sovran, G., "Aerodynamics of Road Vehicles", *Annu. Rev. Fluid Mech.*, 25: 485-537, 1993.

[8] Sovran, G. ,Morel, T., Mason, W. T. Jr. (ed.), *Aerodynamic Drag Mechanisms of Bluff Bodies and Road Vehicles*, Plenum Press, New York, 1978.

[9] Abdel Azim, A. F., "An Experimental Study of the Aerodynamic Interference Between Road Vehicles", *SAE Paper*, No. 940422, 1994.

[10] Sano, M., Nagahisa, T., Kobayashi, T., "Unsteady Aerodynamical Forces by Interference of Two Bluff Bodies Moving Closely", *Bulletin of JSME*, Vol. 27, No. 226, 1984.

[11] Heffley, R. K., "Aerodynamics of Passenger Vehicles in Close Proximity to Trucks and Buses", *SAE Paper*, No. 730235, 1973.

[12] Abdel Azim, A. F., Abdel Gawad, A. F, "A Flow Visualization Study of the Aerodynamic Interference Between Passenger Cars", *SAE Paper*, No. 2000-01-0355, 2000.

[13] Zabat, M., Frascaroli, S., Browand, F., "Drag Measurements on a Platoon of Vehicles", *California PATH Research Report*, UCB-ITS-PRR-93-27, 1993.

[14] Hong, P., Marcu, B., Browand, F., Tucker, A., "Drag Forces Experienced by Two, Full-Scale Vehicles at Close Spacing", *California PATH Research Report*, UCB-ITS-PRR-98-5, 1998.

[15] Marcu, B., Browand, F., "The Aerodynamic Forces on Misaligned Platoons", *California PATH Research Report*, UCB-ITS-PRR-98-4,1998.

[16] Chen, A. L., Savaş, Ö., Hedrick, K., "Transient Vehicle Aerodynamics in Four-Car Platoons", *California PATH Research Report*, UCB-ITS-PRR-97-50, 1997.

[17] Chen, A. L., Savaş, Ö., Hedrick, K., "Transient Aerodynamics in Vehicle Interactions: Data Base Summary", *California PATH Research Report*, UCB-ITS-PWP-98-3, 1998.

[18] Snyder, P. A., "Control Implications of Platoon Aerodynamics", Master's thesis, University of California, Berkeley, 1998.

[19] Zabat, M., Stabile, N., Frascaroli, S., Browand, F., "The Aerodynamic Performance of Platoons: A Final Report", *California PATH Research Report*, UCB-ITS-PRR-95-35, 1995.

[20] Chen, A. L., "Experimental Investigation of Transient Aerodynamics in Vehicle Interactions", Ph.D. thesis, University of California, Berkeley, 1997.

[21] Press, W. H., Flannery, B. P., Teukolsky, S. A., Vetterling, W. T., *Numerical Recipes in Fortran*, Cambridge University Press, New York, 1987.

[22] Zabat, M., Stabile, N., Frascaroli, S., Browand, F., "Drag Forces Experienced by 2, 3 & 4-Vehicle Platoons at Close Spacings", *SAE Paper*, No. 940421, 1995.

[23] Tsuei, L., Hedrick, J. K., Savaş, Ö., "Transient Aerodynamic Effects on a Four-Car Platoon during Passing Maneuvers: Data Summary", *California PATH Research Report*, UCB-ITS-PRR-99-29, 1999.

[24] Tsuei, L., Savaş, Ö., "A Wind Tunnel Investigation of the Transient Aerodynamic Effects on a Four-Car Platoon during Passing Maneuvers", *SAE Paper* No. 2000-01-0875, 2000.

[25] Brown, G. J., Seemann, G. R., "An Experimental Investigation of the Unsteady Aerodynamics of Passing Highway Vehicles", *NHTSA Report*, No. DOT/HS-800 671, 1972.

[26] Beauvais, F. N., "Transient Aerodynamic Effects on a Parked Vehicle Caused by a Passing Bus", *Proceedings of the First Symposium on Road Vehicle Aerodynamics*, Paper 10, City University, London, 1969.

[27] Batchelor, G. K., *An Introduction to Fluid Dynamics*, Cambridge University Press, Cambridge, 1967.

[28] Panton, R. L., *Incompressible Flow*, John Wiley & Sons, Inc. 1993.

[29] Koenig, K., Roshko, A., "An experimental Study of Geometrical Effects on the Drag and Flow Field of Two Bluff Bodies Separated by a Gap", *J. Fluid Mech.*, 156, 167-204, 1985.

[30] Gharib, M., Roshko, A., "The Effect of Flow Oscillations on Cavity Drag", *J. Fluid Mech.*, 177, 501-530, 1987.

[31] Romberg, G. F., Chianese, F. Jr., Lajoie, R. G., "Aerodynamics of Race Cars in Drafting and Passing Situations", *SAE Paper*, No. 710213, 1971.